New Light Emitting Materials:
Synthesis, Optical Spectroscopy, Photon Upconversion and Photoionization in Ni^{2+}, Ce^{3+} and Tm^{2+} Doped Halides

Inauguraldissertation
der Philosophisch–naturwissenschaftlichen Fakultät
der Universität Bern

vorgelegt von
Judith Grimm
von Langnau i. E. BE

Leiter der Arbeit:
Prof. Dr. H. U. Güdel
Departement für Chemie und Biochemie

New Light Emitting Materials:
Synthesis, Optical Spectroscopy, Photon Upconversion and Photoionization in Ni^{2+}, Ce^{3+} and Tm^{2+} Doped Halides

Inauguraldissertation
der Philosophisch–naturwissenschaftlichen Fakultät
der Universität Bern

vorgelegt von
Judith Grimm
von Langnau i. E. BE

Leiter der Arbeit:
Prof. Dr. H. U. Güdel
Departement für Chemie und Biochemie

Von der Philosophisch–naturwissenschaftlichen Fakultät angenommen.

Der Dekan:

Bern, den 3. Februar 2006   Prof. Dr. P. Messerli

You are worthy, our Lord and God,
to receive glory and honor and power,
for you created all things,
and by your will they were created
and have their being.

Revelation 4, 11

Contents

1 Introduction

1.1   Light Emitting Materials

In our every day life we have frequent encounters with light emitting materials. Luminescent materials are present in fluorescent lamps, computer and television screens or as security features on banknotes and credit cards. More specialized applications include scintillators or laser materials. Scintillators are used to detect high-energy particles. As such they find applications in medical imaging systems like PET (positron emission tomography)-scanners and detectors in high-energy physics. Laser materials are widely used in industry, for medical applications and in fundamental research. In all the different types of applications, the light emitting material plays an important role.

The focus of this thesis is on inorganic light emitting materials. These materials consist of an inorganic host material that contains a well-defined species of light emitting ions. The light emitting ions are usually either transition metals or rare earth ions. When doped into a host material, the transition metal and rare earth ions have partially filled electronic d and f shells, respectively. These partially filled shells of d or f electrons give rise to electronic transitions that occur at wavelengths ranging from the infrared to the vacuum-ultraviolet [1].

Research on new or improved luminescent materials is of interest both from a fundamental perspective as well as an applied one. Fundamental research clarifies underlying mechanisms and may eventually lead to applications that will find their way into our every day life. Research that focuses on applications addresses for example efficiency and environmental aspects of existing luminescent materials.

The principal strategies for obtaining new luminescent materials involve: (a) variation of the host lattice and (b) variation of the luminescent ion. Changing the host lattice can have drastic influences on the radiative and nonradiative (multiphonon relaxation, energy transfer) properties. For example, multiphonon relaxation processes can be reduced by changing from a host with high phonon energies (oxide, fluoride) to one having low phonon energies (chloride, bromide, iodide). Choosing a host with specific optical and/or magnetic properties may also influence the luminescent properties of the dopant ion. To change the luminescent ion has of course a dramatic effect on the emission properties. The most obvious effect is a change in the color of the emitted light. If one is thinking in terms of applications, considerations such as the ease of synthesis and handling, stability, costs and health hazards can play an important role as well. The options available in the choice of hosts and codopant combinations open a very broad range of possibilities, leaving much to the imagination and creativity of the researcher.

In the following, a general survey is given on some important concepts that are needed for reading the thesis: An introduction into the nature of light emitting ions as well as some special processes is provided.
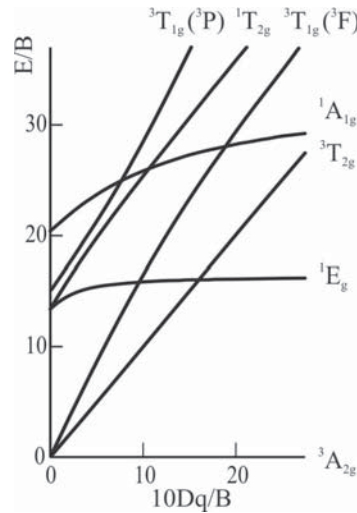
Figure 1: *Tanabe Sugano diagram for a transition metal ion with eight d electrons (d^8 electron configuration) in an octahedral crystal field.*

1.2   Transition Metal Ions

The wide color range of compounds containing transition metal ions is striking to any observer. Much of the early work for understanding the origin of these bright colors started with the work of Alfred Werner around 100 years ago [2]. Soon it was recognized that the d electrons are important for the color properties of complexes. Between 1930 and 1960 the crystal field and the ligand field theory were developed [2].

The d orbitals are the spatially outermost, and consequently the chemical environment influences the electronic transitions that involve them. The modification of the ligands or the site symmetry has dramatic consequences on the optical spectroscopic properties of d metal complexes. Upon incorporation of a transition metal ion into a crystalline environment, the d orbitals are split into two sets: the t_{2g} and the e_g (O_h symmetry). The energy difference between these levels is given by the parameter 10 Dq, which is also referred to as the ligand field strength. Discussion of the spectroscopic properties of transition metal ions is done with the help of Tanabe-Sugano diagrams [3]. An example of a Tanabe-Sugano diagram is shown in Fig. 1 for a transition metal ion with eight d electrons in a crystalline environment with octahedral coordination (O_h symmetry). The energy of the states is displayed as E/B and plotted against 10 Dq/B. The Racah parameter B is a measure for the Coulomb repulsion between the d electrons.

Upon excitation with light usually only the first excited state of a transition metal ion is emitting - if at all [4]. Rapid multiphonon relaxation usually prevents emission from higher lying excited states. Only in case of large energy gaps between excited states and/or low phonon frequencies of the host material it is possible to observe multiple emissions from one transition metal ion.

1.3 Rare Earth Ions

1.3.1 Trivalent Rare Earth Ions

The rare earth elements are usually shown at the bottom of the periodic table. The common oxidation state for rare earth ions is the trivalent one. The spectroscopic properties are mainly described for this oxidation state. In contrast to the highly colored transition metals compounds, materials containing trivalent rare earth ions are often only slightly colored. The property of the rare earth ions that sets them apart from the transition metal elements is that the $4f$ electrons are shielded from the environment by the outer filled shells of $5s$ and $5p$ electrons. As a result, the $4f$ electrons do not participate in the chemical bonding. This non-bonding characteristic is responsible for the well-known chemical similarity of the different rare earth ions. It is therefore difficult to separate different rare earth elements and as a consequence it took a long time before all rare earth ions were isolated.

The shielded character of the $4f$ electrons also influences the spectroscopic properties of the rare earth ions. The $4f$-$4f$ transitions are sharp and therefore bear strong resemblance to atomic transitions. The scientific community was puzzled over this for a long time until Bethe, Kramers and Bequerel explained the nature of the $4f$-$4f$ transitions in the early 1900's. The weak perturbation of the $4f$-$4f$ transition energies by the chemical environment allows the construction of a universal "map" of the energy level structure, widely known as the Dieke Diagram, see Fig. 2 [5]. $4f$-$4f$ transitions have low intensity because they are forbidden by the parity selection rule. The excited states can be very long lived with lifetimes in excess of 10 ms. Highly efficient luminescences with large quantum efficiencies and little energy wasted by multiphonon relaxation are typical for these transitions. This is due to the weak electron-phonon coupling [1, 6]. Thus, in contrast to the transition metal elements, the observation of emission from many states is a common phenomenon among rare earth ions.

1.3.2 Divalent Rare Earth Ions

Some lanthanides may also occur in the divalent state where one less electron is removed from the $4f$ shell. The stability of the divalent state depends on the redox potential of the lanthanide [7]. The most stable divalent lanthanide is Eu^{2+}, see Fig. 3. The spectroscopic properties of this ion have been investigated in great detail because it is easy to stabilize and also because it is used in phosphor materials for fluorescent lighting [8, 9]. Sm^{2+} and Yb^{2+} are rather stable as well, and the spectroscopic properties of these two ions are also discussed in the literature [10]. The next ion in the stability series is Tm (see Fig. 3). Much less is known about Tm^{2+} and most of the studies on Tm^{2+} originate in the 1960's. The main route to prepare Tm^{2+} was via ionization techniques starting from Tm^{3+}. The majority of materials were fluorides, where Tm^{3+} is inevitably present because Tm^{2+} is thermodynamically not stable [11, 12, 13].

Due to the additional $4f$ electron, the $4f$ radius of divalent rare earth ions is larger. As a consequence the Coulomb and spin-orbit interaction of the $4f$ electrons are reduced which moves the $4f$-$4f$ transitions down to lower energies compared to the isoelectronic trivalent ions. The energy separation between the $4f$ and $5d$ electrons is decreased as well. This fact moves the $4f$-$5d$ transitions to lower energies compared to where they are found in the isoelectronic trivalent ion [6].
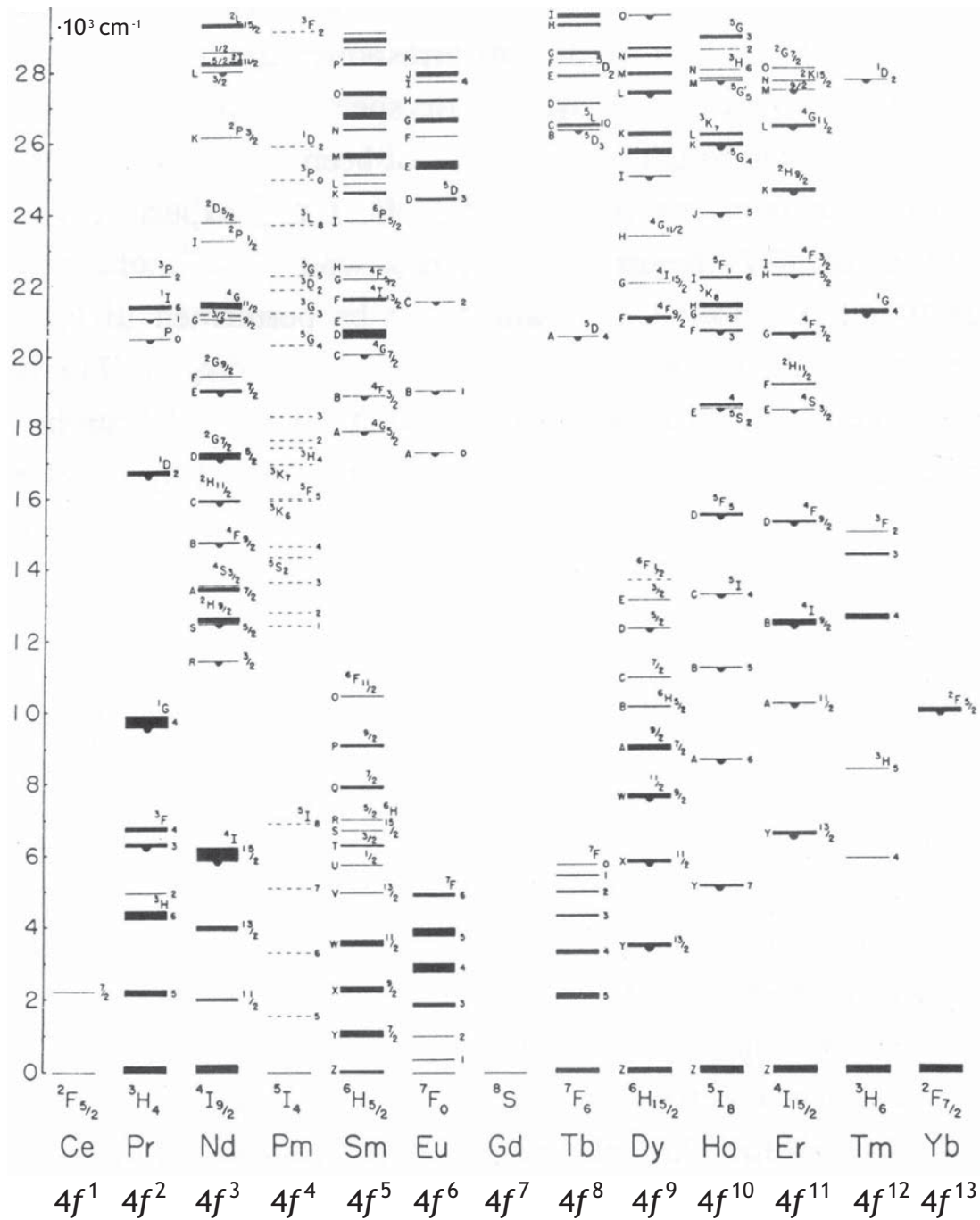
Figure 2: *Dieke diagram with the observed energy levels of the trivalent rare earth ions. The thickness of the levels is a measure for the total crystal field splitting. A pendant semicircle indicates that this level luminesces in LaCl₃. The number of 4f electrons of the rare earth ions is given at the bottom.*
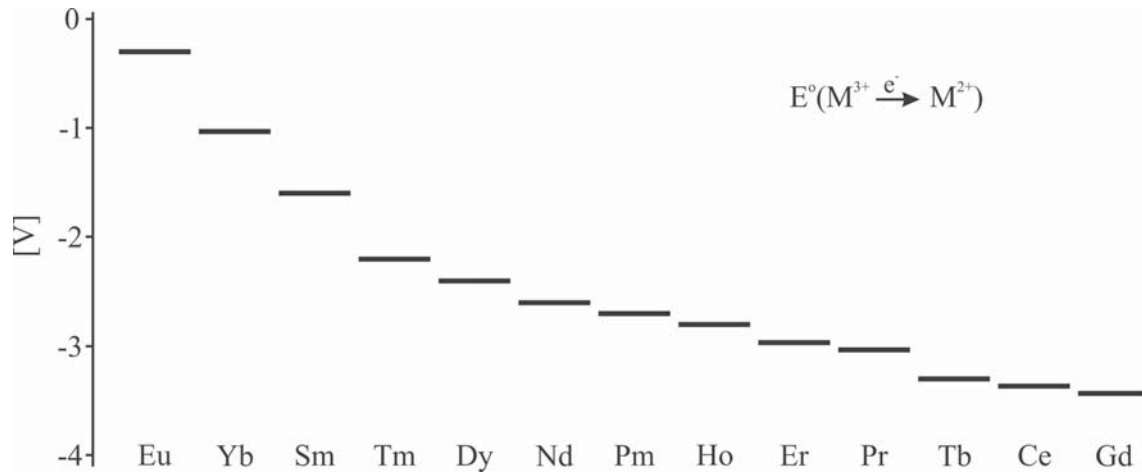
Figure 3: *Standard electrode potentials $E^0(M^{3+}/M^{2+})$ for the reduction of a trivalent rare earth ion into a divalent one [7]. The rare earth ions are shown in order of decreasing reduction potential. The more negative the reduction potential, the more difficult it is to stabilize the respective ion in the divalent oxidation state.*

1.3.3   4*f*-5*d* Transitions in Rare Earth Ions

The $(4f)^n$ to $(4f)^{n-1}(5d)^1$ transitions involve the promotion of a single electron from the $4f$ orbitals to an empty $5d$ orbital. These transitions are parity allowed (Laporte's selection rule is obeyed) resulting in high oscillator strengths [6]. Unlike the shielded intraconfigurational $4f$-$4f$ transitions, the $4f$ to $5d$ transitions are strongly affected by the host lattice, similarly as the d-d transitions of the transition metal ions. The $5d$ electron is the outermost electron of the rare earth ion and interacts with the chemical environment. Thus, $4f$-$5d$ transitions appear as broad bands in the spectrum. In trivalent lanthanides, $4f$-$5d$ transitions are usually situated in the vacuum UV and are experimentally not easily accessible [14, 15, 16]. In the divalent lanthanides, the $4f$-$5d$ transitions are observed in the near-infrared and visible spectral range [11, 17]. In contrast to the well understood $4f$-$4f$ transitions or d-d transitions, the $4f$-$5d$ transitions are less well understood.

1.3.4   Impurity-Host Transitions in Rare Earth Doped Compounds

Interactions between the localized electronic states of the rare earth ions and the delocalized states of the crystal lattice (relating to the conduction band (CB) and valence band (VB)) can strongly affect the optical properties of materials [8]. For example, the decrease of efficiency of high power laser crystals is often caused by excited state absorption to the CB [18, 19]. In contrast, ionization can be beneficial for applications such as proposed optical memories, optical processors, and frequency standards that are based on controlled ionization of the rare earth ion by photon-gated spectral hole-burning [20, 21]. The efficiency of scintillator and phosphor materials is influenced by the position of the $4f$ levels relative to the band states [22, 23].
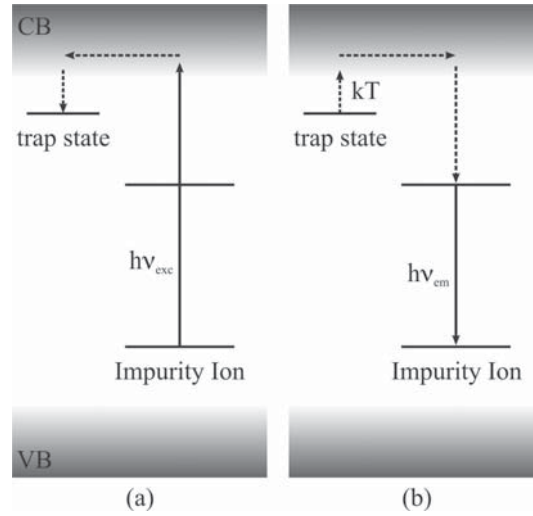
Figure 4: *Principle of thermoluminescence excitation spectroscopy: a) Trap filling process: The sample is irradiated at low temperature at a fixed photon energy $\hbar\nu_{exc}$. Electrons are promoted from the groundstate of the impurity ion into the conduction band (CB), become mobile (dotted arrows) and can get trapped. b) Trap reading process: The occupation of traps is monitored by thermally liberating the electrons (indicated by kT) and detecting the impurity specific luminescence $\hbar\nu_{em}$ when the electrons recombine with the probe ions.*

In contrast to the well-developed understanding of the electronic structure of the $4f$ states, relatively little is known about the relationships between these states and the electronic states of the crystal. An empirical model that describes the energies of the $4f$ ground states of rare earth ions relative to the host was developed recently by two independent research groups [24, 25]. The basis of their model goes back to the work of McClure and coworkers [26, 27].

Several experimental techniques have been used to explore the relationships between the localized states of a rare earth ion (also referred to as impurity) and the electronic states of the host: vacuum-ultraviolet and excited-state absorption, photoconductivity, thermoluminescence and X-ray photoelectron spectroscopy (XPS). By applying several techniques in a complementary sense, the relationships and interactions between rare earth ions and the extended electronic states of the host can be established.

1.4   Principle of Thermoluminescence

Thermoluminescence is one of many thermally stimulated processes that can be used to investigate properties of materials like the electron trap structure and photoionization mechanisms [28]. As suggested by the name, thermoluminescence entails the study of the luminescent properties of a material that result from the thermal release of stored energy. Thermoluminescence was used as experimental technique to study the photoionization threshold in rare earth doped insulators and a brief introduction into the way this techniques was applied is presented here [29].

Fig. 4 illustrates the basic principal of the thermoluminescence excitation scheme. The sample is illuminated at low temperature at a fixed energy $\hbar\nu_{exc}$ for a given period of time. If the energy of the incident light is high enough to promote electrons from the groundstate of the luminescent ion into the CB, these electrons become mobile in the CB. Some of the delocalized electrons will be trapped at sites other than the luminescent ion, see Fig. 4 (a). After illumination the sample temperature is raised in a controlled way. The trapped electrons are released into the CB due to thermal activation. They become mobile and can recombine with the ionized impurities. As a result of the recombination, the specific emission $\hbar\nu_{em}$ of the luminescent ion is observed (Fig. 4 (b)). This is the thermoluminescence signal, which can then be detected. The process is repeated over a range of excitation energies $\hbar\nu_{exc}$. At excitation energies below the photoionization threshold, no thermoluminescence signal is observed. A small thermoluminescence signal is observed at the ionization threshold. Towards higher energies, the thermoluminescence signal typically increases exponentially with excitation energy due to the increase in the density of states in the CB.

1.5   Upconversion

When a material emits light, the emission wavelength is usually longer than that of the exciting light. This means that the photon energy is reduced. However, under some circumstances one can observe the opposite effect where the wavelength of the emitted light is shorter than that of the incident light. Upconversion (UC) is such a non-linear frequency conversion process. UC is possible via excitation mechanisms which involve more than one absorbed photon per emitted photon through sequential absorption and/or energy-transfer steps involving real (metastable) excited states.

Current UC research is focused on the development of phosphors for displays and security tags, for example for bank notes and credit cards. In solar cells UC phosphors can be used to convert the lower energy part of the solar spectrum into higher energy light, which can be absorbed by the silicon semiconductor [30]. In the area of immunoassays and bio-labeling, UC phosphors are of great interest because the low energy of the exciting light will not produce autofluorescence of the cells. For such applications the observation of UC from colloidal solutions of nano-particles is of great interest [31]. In addition, fundamental research in this field is an ongoing challenge [32].

A wide variety of UC mechanisms have been proposed and observed. The majority of these involve some combination of absorption and energy-transfer steps. The two most prominent and basic mechanisms are presented in the following (see Fig. 5):

- GSA/ESA (ground state absorption/excited state absorption) is the sequential absorption of pump photons. A first absorption process populates some metastable excited level $|1\rangle$, from where further absorption can take place to even higher levels. A GSA/ESA process only occurs within the duration of the laser pulse. The time dependent luminescence after short-pulse (i.e. 10 ns) excitation leads to an immediate exponential decay of the population in level $|2\rangle$ with the intrinsic decay time of the emitting level. This is shown on the right hand side of Fig. 5 (a). Further, the UC excitation spectrum corresponds to the product of the GSA and ESA spectrum.
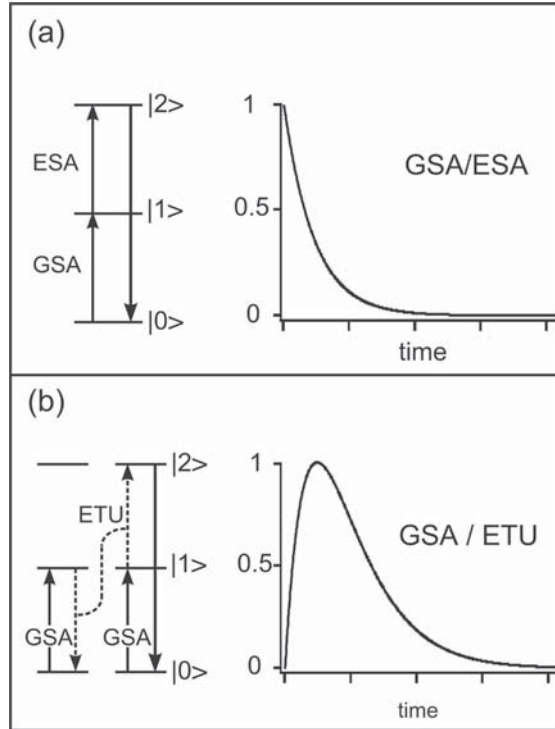
Figure 5: *Schematic representation of the GSA/ESA and GSA/ETU mechanisms for a virtual three level system. The abbreviations are: GSA: ground state absorption, ESA: excited state absorption and ETU: energy transfer upconversion. The temporal evolution of the UC luminescence after short pulse excitation is shown on the right side. Full arrows represent radiative transitions, dashed arrows are nonradiative energy transfer steps.*

- GSA/ETU (energy transfer upconversion) involves energy transfer processes between identical or different ions. Here, two ions in a metastable intermediate state $|1\rangle$ interact to generate one ion in a higher lying state while the other one gets de-excited. High doping densities are usually required to enable such energy transfers. An ETU process populates level $|2\rangle$ after the laser pulse is finished. Therefore, a rise is observed in the short pulse experiment shown on the right hand side of Fig. 5 (b). The rise time correlates with the decay time of level $|2\rangle$, while the decay rate constant is approximately twice that of level $|1\rangle$. The UC excitation spectrum corresponds to the square of the GSA spectrum.

In most cases, UC is a two photon process, which can be identified by a quadratic dependence of the number of upconverted photons on the excitation power. However, higher order processes exist when more than two metastable levels are present in a material.

The majority of compounds that are able to perform UC contain rare earth ions [33, 32, 34]. For transition metals to have more than one metastable excited state is far less common. Much work has been done in the Güdel group to explore this rare phenomenon among transition metals. Fascinating new aspects have been described for Ti^{2+} [35, 36], Ni^{2+} [37, 38], Mo^{3+}[39], Re^{4+} [40] and Os^{4+} [41, 42] doped materials. A combination of rare earth ions and transition metals into one host leads to interesting novel UC properties. Such systems have also been investigated in recent years [43, 44, 45, 46, 47].

1.6   Outline of the Thesis

Chapter two contains the main topic of this thesis, namely the investigation of the spectroscopic properties of Tm^{2+}. At the beginning of this thesis, much effort was put into the synthesis of Tm^{2+} doped fluorides by chemical methods. In a synproportionation reaction, Tm^{2+} can be prepared by adding a trivalent Tm salt and Tm metal to the synthesis mixture. The result was rather discouraging since Tm was always oxidized to the trivalent state. The only success resulted from a synthesis of the target compound $CsCaF_3$:Tm^{2+} where a large excess of Tm metal was added to the initial mixture. The synthesis yielded reproducibly a mixture of Cs metal, CaF_2:Tm^{2+}/Tm^{3+} crystals and some by-products. It is still not fully resolved how this synthesis route works. It may be related to the fact that the high temperature during the synthesis affects the properties of the elements. It is known from the literature that the synthesis of the heavier Tm^{2+} halides is possible. These materials are usually hygroscopic which is negative for possible applications. But nevertheless it opens many possibilities because a variety of compounds containing Tm solely in its divalent oxidation state can be successfully synthesized.

Very little is known about Tm^{2+} in the literature. However, the investigation of the spectroscopic properties of Tm^{2+} doped compounds turns out to be a very fruitful field. The $4f$-$4f$ and $4f$-$5d$ transitions of Tm^{2+} are the subject of a thorough investigation in chapter two. A model is proposed to explain the splittings within the $(4f)^{12}(5d)^1$ electron configuration. In all samples that are discussed in chapter two, multiple emissions are observed: sharp and long-lived $4f$-$4f$ emission in the near-infrared and up to five broad and fast decaying emission bands in the near-infrared and visible, originating from the $4f$-$5d$ states of Tm^{2+}. The dynamics of the excited states are modeled for $CsCaCl_3$:Tm^{2+}, $CsCaBr_3$:Tm^{2+} and $CsCaI_3$:Tm^{2+} using a single configurational coordinate approach. The observation of multiple emissions implies that Tm^{2+} could be a suitable ion for UC. A first upconversion investigation of $SrCl_2$:Tm^{2+} appeared in 2001 [48]. It is interesting to note, that despite the rather recent appearance of this study, Tm^{2+} was suggested for application in infrared counting devices as early as 1966 [49]. The upconverting process described involves the absorption of a first photon by the $^2F_{5/2}$ first excited state and subsequent upconversion to the $4f$-$5d$ higher excited states. This is just one of the possible upconversion schemes for Tm^{2+}. During the course of this thesis, a completely new UC process was probed which only involves the $4f$-$5d$ excited states. The UC studies were a joint project with Eva Beurer and Dr. Pascal Gerner.

In **chapter three**, the upconversion properties of Ni^{2+} in $KZnF_3$ are discussed (the respective Tanabe-Sugano diagram is displayed in Fig. 1). First upconversion studies on Ni^{2+} were performed in the Güdel group in the 1990's [50, 51]. Much effort into the elucidation of the Ni^{2+} upconversion processes was put in by Dr. Oliver Wenger. He did a thorough investigation of Ni^{2+} doped chlorides and bromides [37, 38, 52]. The work in this thesis is a continuation of his work. By changing to fluorides, the crystal field and the Racah parameters are enhanced and the Ni^{2+} transitions are shifted to higher energy. In fluorides, higher phonon energies are expected to cause higher non-radiative losses. Nevertheless, higher excited state emission has been observed in various fluorides as well as oxides [53, 54, 55].

Chapter four is about the work on Ce^{3+} doped chlorides. Ce^{3+} doped halides are investigated because they are used in scintillator materials [56, 57]. The longstanding collaboration of the Güdel group with the group of Prof. C. W. E. van Eijk at the Delft University of Technology (The Netherlands) has resulted in patents on Ce^{3+} doped scintillator crystals in the past few years [58, 59, 60]. An interesting spectroscopic aspect was found for Ce^{3+} doped Cs_3LuCl_6, $Cs_2LiLuCl_6$ and Cs_2LiYCl_6 crystals where a so-called anomalous emission is observed in the UV spectral range [61, 62, 63]. The emission was ascribed to a transition from the host conduction band to the Ce^{3+} groundstate. Experimental evidence for this assignment was missing. Due to the hygroscopicity of the samples, not all techniques to measure photoionization are readily applicable. The technique of choice is thermoluminescence because this is a very versatile technique that can be adapted to measure air-sensitive samples. The photoionization study of the Ce^{3+} doped chlorides shown in chapter four was done in collaboration with Prof. Uwe Happek from the University of Georgia (USA) and the thermoluminescence measurements were performed in his lab.

Chapter five is the final chapter of the thesis and contains a short summary and an outlook. Perspectives on future research related to the topics of chapter two through four are given.

References

[1] B. Henderson, G. F. Imbusch, Optical Spectroscopy of Inorganic Solids, Oxford Science Publication, Clarendon Press, 1989.

[2] H. L. Schläfer, G. Gliemann, Einführung in die Ligandenfeldtheorie, Akademische Verlagsgesellschaft Frankfurt am Main, 1967.

[3] S. Sugano, Y. Tanabe, H. Kamimura, Multiplets of Transition Metal Ions in Crystals, Academic Press, New York/London, 1970.

[4] M. Kasha, Discuss. Faraday Soc. 9 (1950) 14.

[5] G. H. Dieke, Spectra and Energy Levels of Rare Earth Ions in Crystals, John Wiley & Sons, 1968.

[6] S. Hüfner, Optical Spectra of Transparent Rare Earth Compounds, Academic Press, New York, 1978.

[7] G. Meyer, Chem. Rev. 88 (1988) 93.

[8] G. Blasse, B. C. Grabmeier, Luminescent materials, Springer Verlag Berlin, 1994.

[9] T. Jüstel, H. Nikol, C. R. Ronda, Angew. Chem. Int. Ed. 37 (1998) 3084.

[10] J. Rubio, J. Phys. Chem. Solids 52 (1991) 101.

[11] D. S. McClure, Z. J. Kiss, J. Chem. Phys. 39 (1963) 3251.

[12] E. Loh, Phys. Rev. 175 (1968) 533.

[13] Z. J. Kiss, Phys. Rev. 127 (1962) 718.

[14] P. Dorenbos, J. Lumin. 91 (2000) 155.

[15] L. van Pieterson, M. F. Reid, R. T. Wegh, S. Soverna, A. Meijerink, Phys. Rev. B 65 (2002) 045113.

[16] L. van Pieterson, M. F. Reid, G. W. Burdick, A. Meijerink, Phys. Rev. B 65 (2002) 045114.

[17] P. Dorenbos, J. Phys. Cond. Matt. 15 (2003) 575.

[18] C. Pedrini, F. Rogemont, D. S. McClure, J. Appl. Phys. 59 (1986) 1196.

[19] W. C. Wong, D. S. McClure, S. A. Basun, M. R. Kokta, Phys. Rev. B 51 (1995) 5682.

[20] R. M. Macfarlane, R. M. Shelby, Spectroscopy of Solids Containing Rare Earth Ions, edited by A. A. Kaplyanski and R. M. Macfarlane, North Holland Amsterdam, 1987.

[21] C. W. Thiel, Y. Sun, R. L. Cone, J. Modern Opt. 49 (2002) 2399.

[22] C. Dujardin, C. Pedrini, J. C. Gâcon, A. G. Petrosyan, A. N. Belsky, A. N. Vasil'ev, J. Phys. Cond. Matt. 9 (1997) 5229.

[23] M. Raukas, S. A. Basun, W. van Schaik, W. M. Yen, U. Happek, Appl. Phys. Lett. 69 (1996) 3300.

[24] C. W. Thiel, H. Cruegel, H. Wu, Y. Sun, G. J. Lapeyre, R. L. Cone, R. W. Equall, R. M. Macfarlane, Phys. Rev. B 64 (2001) 085107.

[25] P. Dorenbos, J. Phys. Cond. Matt. 15 (2003) 8417.

[26] C. Pedrini, D. S. McClure, C. H. Anderson, J. Phys. Chem. 70 (1979) 4959.

[27] D. S. McClure, C. Pedrini, Phys. Rev. B 32 (1985) 8465.

[28] R. Chen, S. W. S. McKeever, Theory of Thermoluminescence and Related Phenomena, World Scientific Publishing Co. Pte. Ltd, Singapore, 1997.

[29] J. Fleniken, J. Wang, J. Grimm, M. J. Weber, U. Happek, J. Lumin. 94-95 (2001) 465.

[30] A. Shalav, B. S. Richards, T. Trupke, K. W. Krämer, H. U. Güdel, Appl. Phys. Lett. 86 (2005) 013505.

[31] S. Heer, K. Kömpe, H. U. Güdel, M. Haase, Adv. Mat. 16 (2004) 2102.

[32] J. F. Suyver, A. Aebischer, D. Biner, P. Gerner, J. Grimm, S. Heer, K. W. Krämer, C. Reinhard, H. U. Güdel, Opt. Mat. 27 (2005) 1111.

[33] D. R. Gamelin, H. U. Güdel, Topics in Current Chemistry, Vol. 214, Edited by H. Yersin, Springer Verlag Berlin, 2001.

[34] F. Auzel, Chem. Rev. 104 (2004) 139.

[35] O. S. Wenger, H. U. Güdel, J. Phys. Chem. B 105 (2001) 4181.

[36] O. S. Wenger, H. U. Güdel, Inorg. Chem. 40 (2001) 5747.

[37] O. S. Wenger, R. Valiente, H. U. Güdel, Phys. Rev. B 64 (2001) 235116.

[38] O. S. Wenger, S. Bénard, H. U. Güdel, Inorg. Chem. 41 (2002) 5968.

[39] D. R. Gamelin, H. U. Güdel, J. Phys. Chem. B 104 (2000) 10222.

[40] A. Aebischer, G. M. Salley, H. U. Güdel, J. Chem. Phys. 117 (2002) 8515.

[41] M. Wermuth, H. U. Güdel, J. Am. Chem. Soc. 121 (43) (1999) 10102.

[42] M. Wermuth, H. U. Güdel, J. Lumin. 87-89 (2000) 1014.

[43] O. S. Wenger, H. U. Güdel, J. Phys. Chem. B 106 (2002) 10011.

[44] S. Heer, M. Wermuth, K. W. Krämer, H. U. Güdel, Phys. Rev. B 65 (2002) 125112.

[45] C. Reinhard, K. W. Krämer, D. A. Biner, H. U. Güdel, J. Chem. Phys. 120 (2004) 3374.

[46] P. Gerner, C. Reinhard, H. U. Güdel, Chem. Eur. J. 10 (2004) 4735.

[47] S. Garcia-Revilla, P. Gerner, H. U. Güdel, R. Valiente, Phys. Rev. B 72 (2005) 125111.

[48] O. S. Wenger, C. Wickleder, K. W. Krämer, H. U. Güdel, J. Lumin. 94-95 (2001) 101.

[49] R. C. Duncan, IEEE J. Quantum Electron. Suppl. Sec. QE 2 (1966) R52.

[50] U. Oettliker, M. J. Riley, P. S. May, H. U. Güdel, J. Lumin. 53 (1992) 553.

[51] U. Oettliker, M. J. Riley, H. U. Güdel, J. Lumin. 63 (1995) 63.

[52] O. S. Wenger, D. R. Gamelin, H. U. Güdel, Inorg. Chem. 40 (2001) 157.

[53] J. F. Ralph, M. G. Townsend, J. Phys. C: Solid State Phys. 3 (1970) 8.

[54] W. E. Vehse, K. H. Lee, S. J. Yun, W. A. Sibley, J. Lumin. 10 (1975) 149.

[55] R. Moncorgé, T. Benyattou, Phys. Rev. B 37 (1988) 9186.

[56] E. V. D. van Loef, P. Dorenbos, C. W. E. van Eijk, K. W. Krämer, H. U. Güdel, J. Phys. Cond. Matt. 14 (2002) 8481.

[57] E. V. D. van Loef, P. Dorenbos, C. W. E. van Eijk, K. W. Krämer, H. U. Güdel, Phys. Rev. B 68 (2003) 045108.

[58] P. Dorenbos, C. W. E. van Eijk, H. U. Güdel, K. W. Krämer, E. V. D. van Loef, Scintillator crystals, method for making same, use thereof, Organisation Mondiale de la Propriété Intellectuelle, Int. patent number WO 01/60944 A2, 2001.

[59] P. Dorenbos, C. W. E. van Eijk, H. U. Güdel, K. W. Krämer, E. V. D. van Loef, Scintillator crystals, method for making same, use thereof, Organisation Mondiale de la Propriété Intellectuelle, Int. patent number WO 01/60945 A2, 2001.

[60] K. W. Krämer, H. U. Güdel, A. Bessière, P. Dorenbos, C. W. E. van Eijk, High light yield thermal neutron scintillators, European Patent Office, EP 1 553 430 A1, 2005.

[61] P. Dorenbos, E. V. D. van Loef, C. W. E. van Eijk, K. W. Krämer, H. U. Güdel, Phys. Rev. B 68 (2003) 125108.

[62] A. Bessière, P. Dorenbos, C. W. E. van Eijk, L. Pidol, K. W. Krämer, H. U. Güdel, J. Phys. C 16 (2004) 1887.

[63] A. Bessière, P. Dorenbos, C. W. E. van Eijk, K. W. Krämer, H. U. Güdel, A. Galtayries, J. Lumin. 117 (2006) 187.

2 Spectroscopy of Tm^{2+} Doped Halides

Five different types of spontaneous emission simultaneously observed in Tm^{2+} doped CsCaBr$_3$

Judith Grimm *, Hans U. Güdel

University of Bern, Department of Chemistry and Biochemistry, Freiestrasse 3, CH-3012 Bern, Switzerland

Abstract

CsCaBr$_3$ doped with 1% Tm^{2+} exhibits a rich emission spectrum at 10 K. Five emission bands are identified and characterised: a sharp and long-lived 4f–4f emission at 8796 cm^{-1}. Broad 5d–4f emission bands from the lowest energy (5d)^1(4f)^{12} configurations to the groundstate at 13 640 cm^{-1} ('spin-allowed') and 12 240 cm^{-1} ('spin-forbidden'). Two broad emission bands from a higher-energy f–d state, one centered at 19 115 cm^{-1} to the ^{2}F$_{7/2}$ groundstate and the other one at 10 400 cm^{-1} to the first excited ^{2}F$_{5/2}$ state. The transitions are identified and the competition between radiative and nonradiative processes characterised from lifetime and temperature dependent measurements.
© 2005 Elsevier B.V. All rights reserved.

1. Introduction

The simultaneous observation of more than one type of spontaneous emission from the same chromophore is established in various situations. The coexistence of phosphorescence and fluorescence in organic compounds is the best known example. Also in transition metal compounds spin-forbidden and spin-allowed d–d emissions can compete and coexist. In molecular transition metal complexes d–d, charge-transfer and ligand-centered transitions can compete. In lanthanide compounds f–f and d–f emissions have been simultaneously observed. The competition between f–f and d–f emission is particularly relevant in lighting phosphors containing Eu^{2+}. In all these cases, it is usually the competition between two types of processes which leads to a dual luminescence.

In Tm^{2+} doped CsCaBr$_3$, we have the most unusual situation that five different types of emission processes can simultaneously be observed, identified and charac-terised (see Fig. 1a and b). (A) 4f–4f, (B) 'spin-forbidden' 5d–4f, (C) 'spin-allowed' 5d–4f, (D) higher excited 5d–4f state, (E) inter-excited state 5d–4f. The most important factors leading to this situation are the low vibrational energies of the host material and the fact that spin remains a reasonably good quantum number in the lowest-energy f–d excited states of Tm^{2+}.

2. Experimental

Single crystals of CsCaBr$_3$ doped with 1% Tm^{2+} (nominal concentration) were grown by the Bridgman technique as described in [1]. From the absorption and emission spectra, we can conclude that our samples contain no Tm^{3+}. Due to the hygroscopic nature of the crystals, the handling occurred under inert atmosphere at all times.

Sample cooling was achieved with a closed-cycle cryostat for absorption and with the He gas flow technique for emission measurements. Absorption spectra were recorded on a Cary 6000i spectrometer. Emission spectra were excited with the 457.9 nm (21 834 cm^{-1})

---

* Corresponding author. Fax: +41 31 631 43 99.
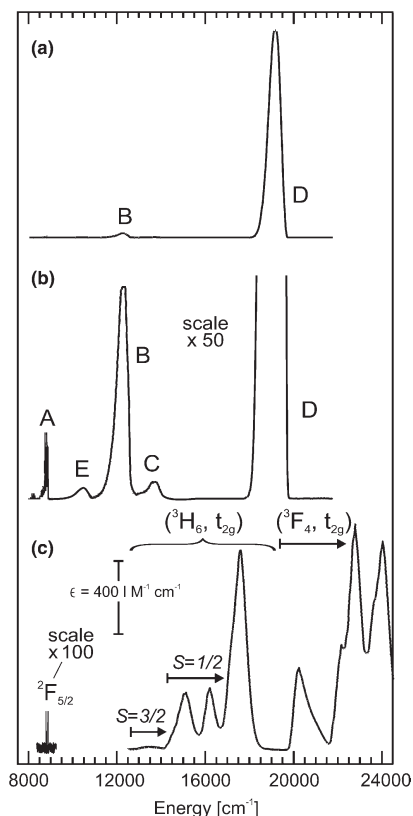 *E-mail address:* judith.grimm@iac.unibe.ch (J. Grimm).

Fig. 1. 10 K emission (a) and (b) and single crystal absorption spectra (c) of $CsCaBr_3$:1% Tm^{2+}. The emission was photoexcited at 21834 cm^{-1}. Note the different scales of (a) and (b) and the scale change in (c). The labels of the emission and absorption bands are used in the text.
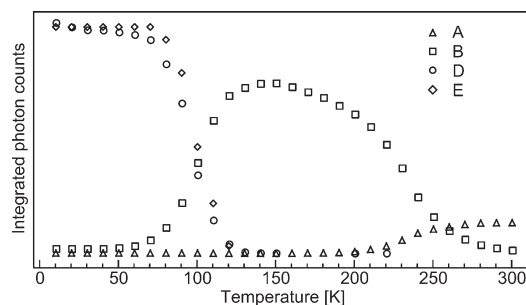

Fig. 2. Temperature dependence of the integrated emitted photons in the bands A, B, D and E. Relative intensities can be compared. The data points of E have been scaled up by a factor of 800 to make them comparable to D.

line of an Ar^+ laser. The luminescent transients were measured with either the Ar^+ laser and an acousto-optic modulator or the third harmonic of a pulsed Nd:YAG laser. The sample luminescence was dispersed either with a 0.75 m double monochromator or a 0.75 m single monochromator. A PMT or a Ge detector were used for detection of the signal in the visible and infrared range, respectively. All luminescence spectra were corrected for the sensitivity of the detection system and are displayed as photon counts versus energy.

3. Results and discussion

Fig. 1a and b shows the 10 K luminescence spectrum of $CsCaBr_3$:Tm^{2+} after 21834 cm^{-1} laser excitation. It consists of five bands labelled A through E and covers a broad spectral range from 8796 cm^{-1} (A) to 19115 cm^{-1} (D). The five bands have very distinct temperature dependencies, which are shown in Fig. 2. Below

100 K band D is dominant, between 100 and 230 K the dominating band is B and at 300 K essentially only band A has appreciable intensity. The lifetime of the emissions B and D at 10 K is 323 and 1.7 µs, respectively, and at 278 K the emission A has a lifetime of 0.1 s. Fig. 1c shows the 10 K absorption spectrum of a $CsCaBr_3$:Tm^{2+} single crystal in the relevant spectral range. Besides a very weak sharp line at 8796 cm^{-1}, there is a rich spectrum of intense broad absorption bands above 12000 cm^{-1}.

$CsCaBr_3$ is cubic at room temperature and undergoes phase transitions at 239 and 143 K according to Ref. [2]. In analogy to a similar behaviour in $CsCaCl_3$ [3] we assume that a tetragonal distortion of the octahedral Ca^{2+} site also occurs in $CsCaBr_3$. The spectroscopic properties of Tm^{2+} in an octahedral coordination are essentially unexplored. 4f–4f and 5d–4f emissions have been reported for Tm^{2+} doped SrB_4O_7 [4], $SrCl_2$ [1], $BaZnCl_4$ and $SrZnCl_4$ [5]. 4f–4f but no 5d–4f luminescence has been reported for Tm^{2+} doped CaF_2, SrF_2 and BaF_2 [6–8]. The assignment of the five emission bands A–E in $CsCaBr_3$ is straightforward on the basis of the data reported above. In the following discussion, the energy level diagram as shown in Fig. 3 will be used.

Band A: 4f–4f transition from the $^2F_{5/2}$ (Γ_8) to $^2F_{7/2}$ (Γ_6). This assignment follows from the coincidence of line A in absorption and emission at 8796 cm^{-1} and its position compared to $SrCl_2$:Tm^{2+} [1], its very long lifetime $\tau = 0.1$ s at 278 K and the very low intensity of the corresponding absorption line (see Fig. 1c). In octahedral coordination, the lowest energy crystal field component of $^2F_{5/2}$ and $^2F_{7/2}$ are Γ_8 and Γ_6, respectively [9]. Under very high resolution, the line is found to be split by 8 cm^{-1} at 10 K, which we ascribe to a splitting of $^2F_{5/2}$ (Γ_8) into two Kramer doublets in the slightly distorted O_h symmetry below the phase transition temperature. This distortion is obviously very small and we can safely ignore it in the discussion of the broad 5d–4f emissions. From Fig. 2, we see that the emission band A is very weak up to about 200 K when the
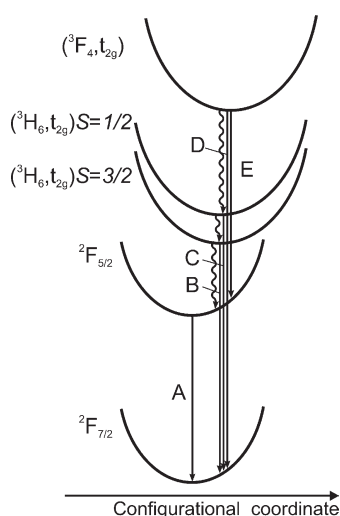
Fig. 3. Schematic configurational coordinate diagram of Tm^{2+} doped CsCaBr$_3$. Radiative and nonradiative relaxation processes are given by straight and curly arrows, respectively. The labels used for the states and emission transitions are used in the text.

excitation occurs at 21 834 cm^{-1}. This is because the higher-lying f–d states are metastable and emissive, see below. From Fig. 2, it becomes clear that band A is taking over from band B above 200 K and becomes the dominant emission at ambient temperature. This is the result of a thermally activated nonradiative feeding process of $^2F_{5/2}$ from the lowest f–d state above 200 K. In Fig. 3, the nonradiative feeding to $^2F_{5/2}$ and the radiative emission process A are indicated by curly and straight arrows, respectively.

There are no f–f excited states above 9500 cm^{-1} in Tm^{2+}, and all the broad absorption and emission bands in Fig. 1 are due to 4f–5d transitions. The (4f)^{12}(5d)^1 electron configuration is highly degenerate, and energy splittings occur as a result of various interactions. The most important is the crystal field splitting of the 5d orbital into t$_{2g}$ and e$_g$. From a comparison of the absorption spectra of Tm^{2+} doped CsCaCl$_3$ and CsCaBr$_3$, we estimate it to be of the order of 12 000 cm^{-1} in the title compound [10]. All the f–d states relevant for the present discussion derive from the (4f)^{12}(t$_{2g}$)^1 configuration. Coulomb repulsion and spin–orbit coupling split the (4f)^{12} configuration into a Tm^{3+} like pattern of terms. The isotropic exchange part of the 4f–5d Coulomb repulsion will split all of these into a high-spin ($S = 3/2$) and a low-spin ($S = 1/2$) subset [11,12]. For the present discussion, we can neglect the anisotropic exchange part and spin–orbit coupling of the 5d electron. This combined effect leads to an additional splitting in the order of 1000–2000 cm^{-1}. These simple considerations allow us to assign the bands B–E to the following 5d–4f emissions.

Band B: 'Spin-forbidden' 5d–4f transition from ($^3H_6$, t$_{2g}$)$S = 3/2$ to $^2F_{7/2}$. The lowest-energy term of the (4f)^{12} electron configuration is $^3H_6$, and the exchange splitting between the $S = 1/2$ and $S = 3/2$ components is about 1400 cm^{-1}. The ($^3H_6$, t$_{2g}$)$S = 3/2$ multiplet is the lowest-energy one deriving from this 5d–4f electron configuration, and band B at 10 K thus corresponds to a transition from the lowest state of this multiplet to the ground state. The corresponding absorption band centered at about 13 500 cm^{-1} is very weak, see Fig. 1. Emission band B is weak at 10 K but above 100 K it becomes the dominant emission, and Fig. 2 shows that it is obviously fed by band D, which loses its intensity above 100 K, see curly arrow in Fig. 3. This schematic configurational coordinate diagram also explains the observed width (FWHM) of about 520 cm^{-1} and the Stokes shift between the corresponding absorption and emission band maxima of about 1250 cm^{-1}. All the states deriving from the (4f)^{12}(t$_{2g}$)^1 configuration are displaced with respect to (4f)^{13} because the promoted electron leads to a change in the metal-ligand bond. The 10 K lifetime $\tau = 323$ μs of band B is in good agreement with the 10 K lifetime of the lowest-energy 'spin-forbidden' 5d–4f emission $\tau = 232$ μs in SrB$_4$O$_7$ [4] and $\tau = 222$ μs in SrCl$_2$ [1].

Band C: 'Spin-allowed' 5d–4f transition from ($^3H_6$, t$_{2g}$)$S = 1/2$ to $^2F_{7/2}$. The highest energy vibration in CsCaBr$_3$ has an estimated energy of about 210 cm^{-1}. This can be deduced from the phonon spectrum of CsMnBr$_3$ [13]. This very low energy and the spin-allowed character of the radiative transition to the ground state are responsible for the emission C. The photon ratio of bands C/B is less than 1/10 at 10 K and it decreases with increasing temperature. The nonradiative depopulation of ($^3H_6$, t$_{2g}$)$S = 1/2$ is thus dominant at all temperatures and a lifetime could not be determined with our equipment. This is in good agreement with an estimate using the energy gap law. From the absorption spectrum in Fig. 1c, it follows that the energy difference between the lowest state of the ($^3H_6$, t$_{2g}$)$S = 1/2$ multiplet and the highest state of the ($^3H_6$, t$_{2g}$)$S = 3/2$ multiplet is lower than 1200 cm^{-1}. Less than six quanta of the highest energy vibration are thus required to bridge the gap, and this usually favors multiphonon relaxation.

Band D: Higher excited state 5d–4f transition from ($^3F_4$, t$_{2g}$) to $^2F_{7/2}$. This band dominates the emission spectrum below 100 K, see Fig. 1a. Its sharp onset at about 19 670 cm^{-1} coincides with the sharp onset of an absorption band, which we can assign to a band of the $^2F_{7/2} \rightarrow$ ($^3F_4$, t$_{2g}$) multiplet, see Fig. 1. This assignment is based on the known $^3H_6$–$^3F_4$ energy difference of 5546 cm^{-1} in Tm^{3+} [14]. We have no unambiguous means of determining the spin state of the ($^3F_4$, t$_{2g}$) emitting state. From Fig. 1c, we see that there is an energy gap of the order of 2000 cm^{-1} between the highest component of the ($^3H_6$, t$_{2g}$) multiplet and the lowest

($^3F_4$, t_{2g}) state. Below 150 K the latter is metastable in a $CsCaBr_3$, and the radiative emission process is competitive. This is confirmed by the observation of a much weaker and faster quenching emission from this state in the corresponding $CsCaCl_3$:Tm^{2+} [10]. Above 100 K in the title compound nonradiative relaxation to ($^3H_6$, t_{2g}) becomes dominant, and the luminescence intensity shifts from band D to B. The 10 K lifetime is 1.7 µs, which is two orders of magnitude shorter than for ($^3H_6$, t_{2g})$S = 3/2$ (band B). This might indicate that the lowest state of the ($^3F_4$, t_{2g}) multiplet has $S = 1/2$ or that spin is not as well defined in this configuration as in the lowest-energy one. This is in very good agreement with recent findings for 4f–5d excited states in Tb^{3+} compounds [15].

Band E: Interexcited state 5d–4f transition from ($^3F_4$, t_{2g}) to $^2F_{5/2}$. This band has the same temperature dependence (Fig. 2) and originates from the same emitting state as band D. But the E/D ratio is only 1/800. The branching ratio for the two transitions to $^2F_{7/2}$ and $^2F_{5/2}$ is thus 800/1. This very striking observation is analogous to what has been found for the branching ratio in the 5d–4f emission of $LiYF_4$:Er^{3+} to final states with different J values where it was ascribed to the $\Delta J = 1$ selection rule [16]. In Tm^{2+}, we have a similar situation: the lowest energy state of the ($^3H_4$, t_{2g}) multiplet has dominantly $J = 9/2$ character and thus the transition to $^2F_{7/2}$ is allowed, while the $^2F_{5/2}$ transition is forbidden.

In conclusion, the title compound is an extremly rare example of a compound exhibiting five different types of spontaneous emission. The interplay of radiative and non-radiative transitions leads to a strong temperature dependence of their relative intensities. In particular, emissions from higher excited 4f–5d states can be observed at low temperatures. This is without precendence

in Tm^{2+} spectroscopy. A key factor is the low phonon energy of the host lattice, which makes multiphonon relaxation processes less competitive than in fluorides and chlorides and it and enables higher excited d–f states to become metastable at low temperature.

References

[1] O.S. Wenger, C. Wickleder, K.W. Krämer, H.U. Güdel, J. Lumin. 94–95 (2001) 101.
[2] H.-J. Seifert, D. Haberhauer, Z. Anorg. Allg. Chem. 491 (1982) 301.
[3] Y. Vaills, J.Y. Buzaré, A. Gibaud, Ch. Lunay, Solid State Commun. 60 (1986) 139.
[4] W.J. Schipper, A. Meijerink, G. Blasse, J. Lumin. 62 (1994) 55.
[5] C. Wickleder, J. Alloys Comp. 300–301 (2000) 193.
[6] Z.J. Kiss, Phys. Rev. 127 (1962) 718.
[7] E. Loh, Phys. Rev. 175 (1968) 533.
[8] H.A. Weakliem, C.H. Anderson, E.S. Sabisky, Phys. Rev. B 2 (1970) 4354.
[9] F.S. Richardson, M.F. Reid, J. Dallara, R.D. Smith, J. Chem. Phys. 83 (1985) 3813.
[10] J. Grimm, unpublished results.
[11] D.S. McClure, Z.J. Kiss, J. Chem. Phys. 39 (1963) 3251.
[12] C.K. Duan, M.F. Reid, J. Solid State Chem. 171 (2003) 299.
[13] G.L. McPherson, J.R. Chang, Inorg. Chem. 12 (1973) 1196.
[14] G.H. Dieke, Spectra and Energy Levels of Rare Earth Ions in Crystals, Wiley, 1968.
[15] P. Dorenbos, J. Phys. Cond. Matter 15 (2003) 6249.
[16] P.S. Pijzel, Ph.D. Thesis, Utrecht University, The Netherlands, 2004.

Light Emission and Excited State Dynamics in Tm^{2+} Doped CsCaCl$_3$, CsCaBr$_3$ and CsCaI$_3$

J. Grimm, J. F. Suyver, E. Beurer, G. Carver, and H. U. Güdel*

Department of Chemistry and Biochemistry, University of Bern, Freiestrasse 3, 3012 Bern, Switzerland

The light emission and photophysical properties of CsCaCl$_3$:Tm^{2+} (1.04%), CsCaBr$_3$:Tm^{2+} (0.48%) and CsCaI$_3$:Tm^{2+} (0.76%) are presented. We find that Tm^{2+} is a multiple emitter under 21834 cm^{-1} laser excitation at low temperatures in all three compounds. Several distinct types of emission are observed and characterized: sharp and long-lived 4f-4f emission in the infrared and up to four broad and fast decaying emission bands in the near-infrared and visible, originating from the 4f-5d states of Tm^{2+}. The optical spectroscopic properties of the samples are compared, and we find that the measured differences in the relative intensities and the shifts in the position of the emissions can be related to the chemical influence on the absorption and emission properties of Tm^{2+}. Thus, it nicely illustrates the principle of chemical variation on the optical spectroscopic properties. An investigation of the temperature dependence of the luminescence yields important information about the dynamics of the excited states. The interplay and competition between radiative and nonradiative pathways is explained and modeled using a single configurational coordinate approach.

I.   INTRODUCTION

The most common valence state of lanthanides in solids is the trivalent one. The basic features of the optical spectra of trivalent lanthanide ions in solids are well understood, and an enormous amount of studies describing the light emission properties can be found in the literature. Some rare earth ions may also occur in the divalent state. Eu^{2+}, Yb^{2+}, and Sm^{2+} have received most attention among them [1]. These are the lanthanides that are most easily stabilized in their divalent oxidation state. In some lattices, Tm^{2+} can also be stabilized in its divalent state, but most Tm^{2+} compounds are air sensitive [2], and they have received considerably less attention in the past.

Several aspects of the optical spectroscopic properties of Tm^{2+} in alkaline earth halides (mainly fluorides) have been described and interpreted already in the 1960s by McClure, Kiss and Loh [3–5]. An early research highlight was the demonstration of laser oscillation on the intra-configurational ^{2}F$_{5/2} \rightarrow$ ^{2}F$_{7/2}$ transition in CaF$_2$:Tm^{2+} at low temperatures at the dawn of the invention of optical lasers [6]. It has also been known for decades that, in addition to the ^{2}F$_{5/2} \rightarrow$ ^{2}F$_{7/2}$ emission, the lowest 4f-5d state is spontaneously emitting [7]. Due to this, Tm^{2+} has been suggested for application in infrared counting devices as early as 1966 [7]. Spontaneous 5d-4f emission from the lowest 4f-5d excited state was since reported for Tm^{2+} doped SrB$_4$O$_7$ [8], SrCl$_2$ [9], BaZnCl$_4$, SrZnCl$_4$ [10] and CsCaBr$_3$ [11], whereas this emission was not reported for Tm^{2+} in alkaline earth fluorides [12]. Recently, we described the light emission properties of Tm^{2+} in CsCaBr$_3$, where we have the most unusual situation of five different types of spontaneous emission

processes [11]. In particular, emission from higher lying 5d-4f states in Tm^{2+} was observed and characterized.

The 4f-5d states are affected by changes in the ligand field, whereas a change in the host lattice will have only a small effect on the 4f-4f excited states as these are essentially ligand-field independent. This prompted us to extend our studies of Tm^{2+} doped compounds. In the present contribution we give a detailed account of the light emission properties of the Tm^{2+} doped cubic perovskites CsCaBr$_3$ and CsCaCl$_3$. For a comparative discussion of the excited state dynamics we include the results of the isostructural CsCaI$_3$:Tm^{2+}. An account of the spectroscopic properties of CsCaI$_3$:Tm^{2+} together with RbCaI$_3$:Tm^{2+} will be provided separately [13]. The chemical variation along the perovskite series CsCaCl$_3$, CsCaBr$_3$ and CsCaI$_3$ leads to a systematic variation of the light emission properties. These can be understood from the competition between radiative and nonradiative relaxation processes in the photophysics of Tm^{2+}. In Section IV D we provide a simple model based on rate equations, which nicely reproduces the observed trends.

II.   EXPERIMENTAL SECTION

A.   Synthesis and Crystal Growth

Single crystals of CsCaCl$_3$, CsCaBr$_3$ and CsCaI$_3$ doped with Tm^{2+} were grown by the Bridgman technique. For the synthesis, stoichiometric amounts of CsX (X=Cl, Br, I) and CaX$_2$ were mixed and Tm^{2+} was prepared in situ by synproportionation of TmX$_3$ (prepared via the ammonium halide route [14] from 99.999% pure Tm$_2$O$_3$ from Johnson Matthey) and Tm metal (Alfa Aesar 99.9%). All starting materials are hygroscopic and were handled in a glovebox under N$_2$ atmosphere. Dark green crystals of good optical quality with diameters up to 2 mm×2 mm×2 mm were obtained. The crystals were

---

*Electronic address: `hans-ulrich.guedel@iac.unibe.ch`

checked for purity by X-ray powder diffraction. The absolute concentrations of Tm in the crystals were determined with ICP-OES and are 1.04%, 0.48% and 0.76% in CsCaCl$_3$, CsCaBr$_3$ and CsCaI$_3$, respectively. The use of tantalum rather than the more commonly used silica ampules was found to be indispensable for obtaining crystals which contain no Tm^{3+}. Crystals grown from silica ampules contain trace amounts of Tm^{3+} because under such crystal growth conditions Tm^{2+} is easily oxidized by silica. Due to the hygroscopic nature of the crystals, the handling occurred under inert atmosphere at all times. For absorption measurements the samples were polished in a drybox and enclosed in an air-tight copper cell equipped with a quartz window. Thermal contact of the crystal with the sample holder was provided through the application of copper grease (Lake Shore Cryotronics Inc.). For luminescence measurements, the samples were sealed into quartz ampules under partial pressure of He, which serves as an inert atmosphere as well as a heat transmitter.

B.   Spectroscopic Measurements

Sample cooling was achieved with a closed-cycle cryostat (Air Products) for absorption and with the He gas flow technique for emission measurements. Absorption spectra were recorded on a Cary 6000i spectrometer (Varian). Emission spectra were excited with the 457.9 nm (21834 cm^{-1}) line of an Ar$^+$ laser (Spectra Physics 2060-10 SA). The sample luminescence was dispersed either with a 0.85 m double monochromator (Spex 1402) or a 0.75 m single monochromator (Spex 1702). A PMT (Hamamatsu P3310-01) and a photon counting system (Stanford Research 400) or a Ge detector (ADC 403L and 403HS) interfaced to a lock-in amplifier (Stanford Research 830) were used for detection of the signal in the visible and infrared ranges, respectively. The luminescence transients were measured with either the Ar$^+$ laser and an acousto-optic modulator (Coherent 305, Stanford Research DS 345 function generator) or the fundamental (1064 nm = 9398 cm^{-1}) or the third harmonic (355 nm = 28169 cm^{-1}) of a pulsed Nd:YAG laser (Quanta Ray DCR 3, 20 Hz). Transient signals were detected as described above using a multichannel scaler (Stanford Research 430) or an oscilloscope (Tektronix TDS 540a). All luminescence spectra were corrected for the sensitivity of the detection system and are displayed as photon counts versus energy.

III.   RESULTS

Parts (a) and (b) of Fig. 1 show the 10 K emission spectra of CsCaCl$_3$:Tm^{2+} and CsCaBr$_3$:Tm^{2+} along with the corresponding absorption spectra (c) and (d), respectively. Laser excitation for the emission spectra occurred at 21834 cm^{-1} for both samples. The observed emission
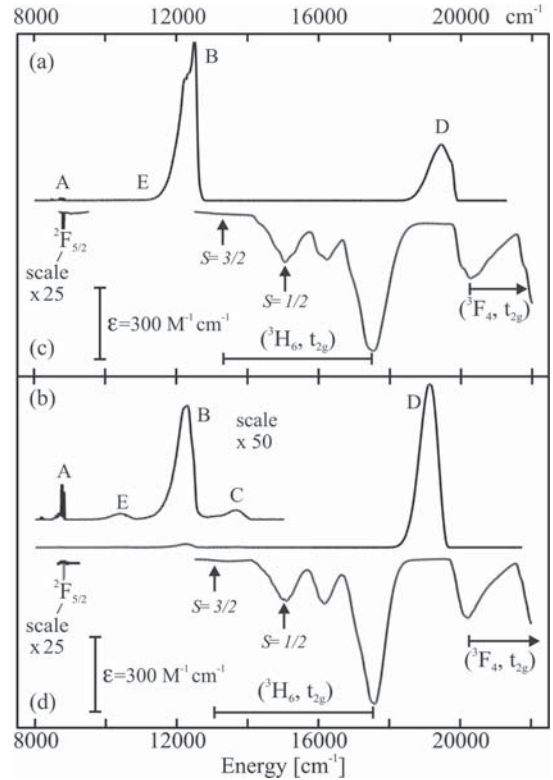

FIG. 1: Survey emission (a) and onset of single crystal absorption spectrum (c) of CsCaCl$_3$:1.04% Tm^{2+} recorded at 10 K. In (b) and (d), the analogous data are presented for CsCaBr$_3$:0.48% Tm^{2+}. Both emissions were photoexcited at 21834 cm^{-1}. Note the scale changes in (b), (c), and (d). The labels of the emission bands are used in the text. The range of (^{3}H$_6$, t$_{2g}$) and the onset of (^{3}F$_4$, t$_{2g}$) absorptions are indicated. The first $S = 3/2$ and $S = 1/2$ absorption bands within are marked by arrows.

bands are labeled A through E, and the electronic transitions to which they refer will be discussed in Section IV. The same notation is used for both samples. The band positions and the partition of the emitted photons at 10 K among the five bands A to E are given in Table I including the results of CsCaI$_3$:Tm^{2+}. The positions of the broad emission bands B through E all undergo a redshift of about 300-350 cm^{-1} as the host lattice is changed from the chloride to the bromide and about 900 cm^{-1} from the bromide to the iodide. The sharp emission A, in contrast, is shifted to lower energy by only about 15 cm^{-1} from chloride to bromide and about 11 cm^{-1} from bromide to iodide. The partition of photons among the bands at 10 K is very different for the three samples. While D is absolutely dominant in the bromide and iodide, both B and D have sizable intensity in the chloride. All the transitions A to E are observable at 10

TABLE I: Positions in cm^{-1} of emission bands A to E at 10 K and integrated photon counts as a percentage of the total photon flux at 10 K in Tm^{2+} doped CsCaCl$_3$, CsCaBr$_3$ and CsCaI$_3$. Laser excitation occurred at 21834 cm^{-1}.

Compound	Emission	Position [cm^{-1}]	Integrated Photon Counts [%]
CsCaCl$_3$	D	19450	36.5
	B	12497	63
	E	10647	0.2
	A	8810	0.3
CsCaBr$_3$	D	19152	97.6
	C	13676	0.2
	B	12237	2
	E	10370	0.1
	A	8796	0.1
CsCaI$_3$	D	18344	92.7
	C	12703	2.3
	B	11348	4.6
	E	9503	0.1
	A	8785	0.3

K in the bromide and iodide, whereas C could not be detected in the chloride.

Parts (a) and (b) of Fig. 2 show the high resolution 10 K emission spectra of bandsystem A in CsCaCl$_3$:Tm^{2+} and CsCaBr$_3$:Tm^{2+}, along with the corresponding 10 K absorption spectra (c) and (d), respectively. Laser excitation for the emission spectra occurred at 21834 cm^{-1} for both samples. Disregarding the lines marked with an asterisk, which we assign to nonregular crystal sites, the sharp-line spectra of the chloride and bromide resemble each other and will be analyzed in Section IV C .

In Figs. 3 (a) and (b) the emission spectra of CsCaCl$_3$:Tm^{2+} and CsCaBr$_3$:Tm^{2+}, respectively, are shown at three different temperatures: 10 K, 130 K and 300 K. The spectra are scaled within (a) and (b), therefore intensities at different temperatures can be compared. There is a general shift of photons from high energy to low energy bands in both samples as the temperature is raised. The temperature dependence of the integrated photon counts of the three dominant emissions A, B (+ C in CsCaI$_3$:Tm^{2+}) and D under 21834 cm^{-1} excitation is shown in Figs. 4 (a), (b) and (c) for CsCaCl$_3$:Tm^{2+}, CsCaBr$_3$:Tm^{2+} and CsCaI$_3$:Tm^{2+}, respectively. The data will be analyzed in Section IV D. In Fig. 5, the temperature dependences of the integrated photon counts and the lifetime of emission B in (a) CsCaCl$_3$:Tm^{2+} and (b) CsCaBr$_3$:Tm^{2+} are compared. For both compounds, the lifetime is constant below 100 K, whereas the intensity shows an increase with increasing temperature. Above 100 K in the chloride and 150 K in the bromide, the lifetime decreases along with the integrated photon counts. The lifetimes of the emission bands A, B, and D of Tm^{2+} are given in Table II for CsCaCl$_3$, CsCaBr$_3$, and CsCaI$_3$. They will be used to determine the decay rate constants in the rate equation modeling in Section IV D.
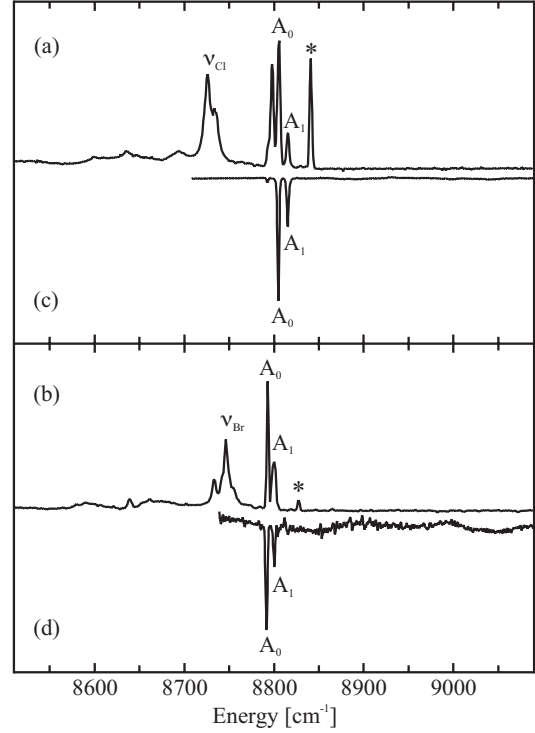

FIG. 2: The 10 K emission spectrum of the $^2F_{5/2} \rightarrow ^2F_{7/2}$ transition (band A) of Tm^{2+} is shown in (a) for CsCaCl$_3$ and (b) for CsCaBr$_3$. Both emissions were photoexcited at 21834 cm^{-1}. The 10 K single crystal absorption spectrum of the $^2F_{7/2} \rightarrow ^2F_{5/2}$ transition of Tm^{2+} is shown in (c) for CsCaCl$_3$ and (d) for CsCaBr$_3$. The emission lines that are labeled with an asterisk are attributed to Tm^{2+} on nonregular sites (see text). The bands labeled ν_{Cl} and ν_{Br} are vibronic sidebands of the $^2F_{5/2} \rightarrow ^2F_{7/2}$ transition in CsCaCl$_3$:Tm^{2+} and CsCaBr$_3$:Tm^{2+}, respectively.

TABLE II: Measured lifetimes τ of the emission bands D, B and A of Tm^{2+} in CsCaCl$_3$, CsCaBr$_3$, and CsCaI$_3$. The radiative lifetime τ_{calc} of emission D is calculated from Eq. 7 (see Section IV D)

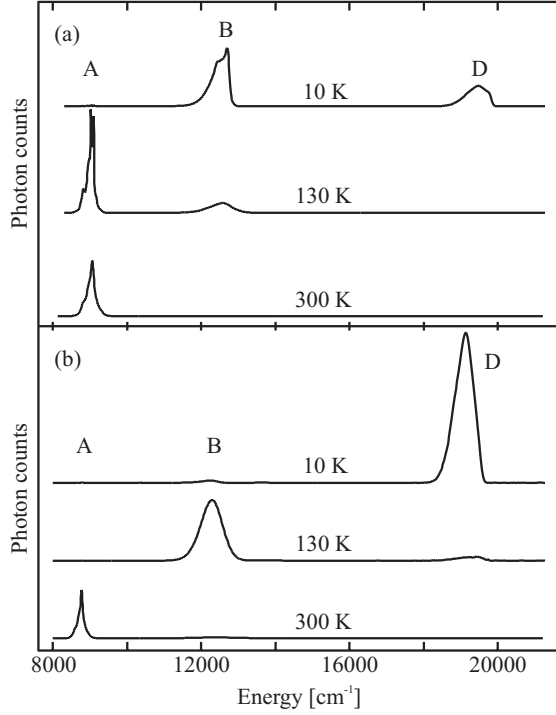| Emission	T		CsCaCl$_3$	CsCaBr$_3$	CsCaI$_3$
D	10 K	τ	904 ns	1.7 μs	1 μs
		τ_{calc}	1.7 μs	1.8 μs	2 μs
B	10 K	τ	296 μs	323 μs	391 μs
A	300 K	τ	501	534	650

FIG. 3: Emission spectra of Tm^{2+} in (a) CsCaCl$_3$ and (b) CsCaBr$_3$ at three temperatures: 10, 130, and 300 K. The emission was photoexcited at 21834 cm^{-1}. The spectra are shifted arbitrarily along the vertical axis. The spectra within (a) or (b) have the same scale, therefore intensities at different temperatures can be compared. Only the prominent emissions A, B, and D are labeled.

IV. ANALYSIS

A. Structures and Site Symmetries

CsCaCl$_3$ and CsCaBr$_3$ are cubic perovskites at room temperature, crystallizing in the space group $Pm3m$ [15, 16]. The Tm^{2+} ions replace Ca^{2+} on site $1(b)$ with O_h point symmetry. Both samples undergo phase transitions upon cooling , which is common for cubic perovskites. The cubic to tetragonal phase change at $T= 95$ K in CsCaCl$_3$ is well documented in the literature [17, 18]. The site symmetry of Ca^{2+} below the phase change is C_{4h} [17]. The distortion from octahedral symmetry at the Ca^{2+} site is small [18]. CsCaBr$_3$ undergoes two phase changes at 237 and 145 K, respectively [16].

CsCaI$_3$ crystallizes in the orthorhombic $Pnma$ phase at 300 K [19]. The Ca^{2+} in the orthorhombic $Pnma$ phase has site symmetry C_i. Regardless of the phase changes, the Tm^{2+} ion is always coordinated by six X^- (X^-=Cl, Br, I). From the spectroscopic data of the three samples, we conclude that the only band splitting
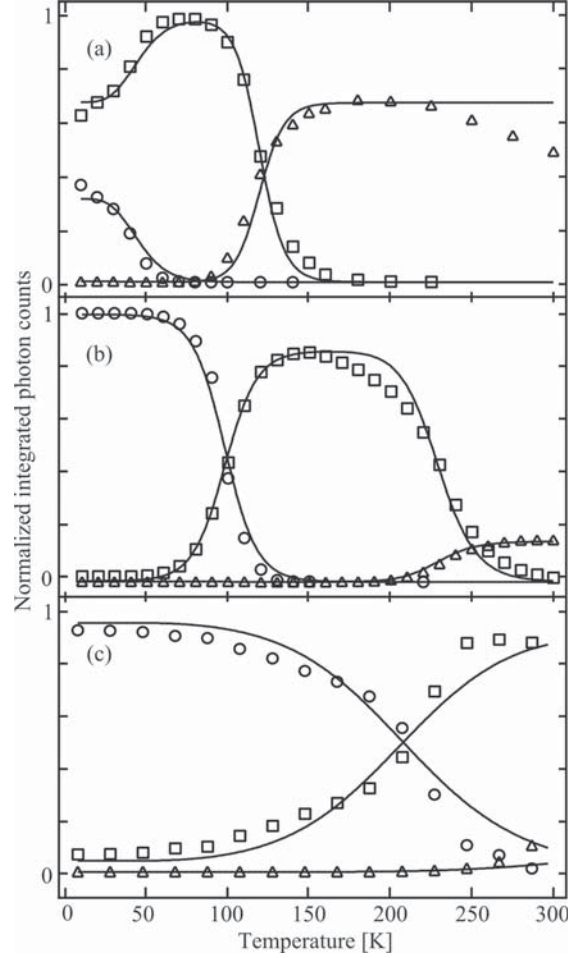

FIG. 4: Temperature dependence of the integrated photon counts (normalized to 1 for the most intense band) of the three dominant emissions △: A, □: B (+ C in CsCaI$_3$:Tm^{2+}) and ◯: D in (a) CsCaCl$_3$:Tm^{2+}, (b) CsCaBr$_3$:Tm^{2+}, and (c) CsCaI$_3$:Tm^{2+}. The photon counts were corrected for the decreasing absorption cross section with increasing temperature at the excitation energy of 21834 cm^{-1}. The solid lines represent simulations of the data using the model in Section IV D (Eq. (2)). The input and fit parameters are listed in Tables III and IV, respectively.

due to symmetry reduction is observable in bandsystem A and is in the order of a few wavenumbers (vide infra). The data interpretation of the 4f-5d states is therefore done in the octahedral approximation.
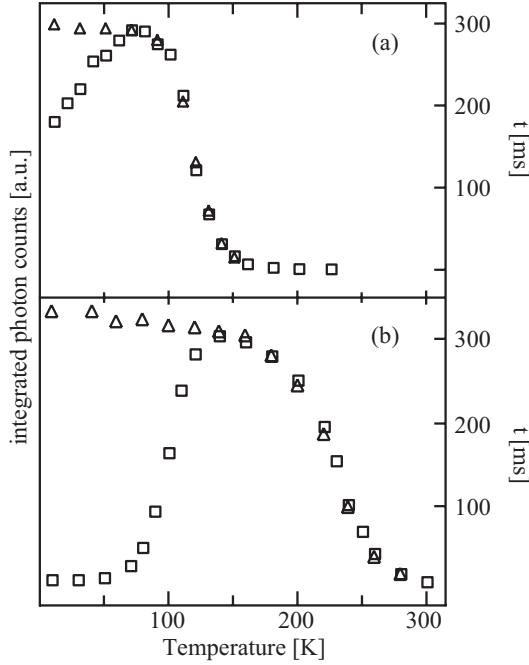
FIG. 5: Temperature dependence of emission lifetimes ($\triangle$) and intensities ($\square$) of band B in (a) CsCaCl$_3$:Tm^{2+} and (b) in CsCaBr$_3$:Tm^{2+}. of band B.

FIG. 6: (a) Schematic single configurational coordinate (SCC) diagram of Tm^{2+} assuming harmonic potentials and equal force constants for all states. The emitting excited states are schematically displayed in (b) with the radiative and nonradiative processes indicated as straight and curly arrows, respectively. The labeling of the transitions corresponds to Fig. 1 and Tables I and II.

B.   Emitting States and Spectral Assignments

The assignment of the emission bands has already been discussed for CsCaBr$_3$:Tm^{2+} in Ref. [11]. Fig. 6 (a) shows a schematic single configurational coordinate (SCC) diagram of the lowest excited states of Tm^{2+} assuming harmonic potentials and equal force constants for all states. The relevant radiative and nonradiative relaxation processes are indicated in Fig. 6 (b) as straight and curly arrows, respectively.

Tm^{2+} has a $(4f)^{13}$ ground state electron configuration, that is, it is isoelectronic with Yb^{3+}. The two multiplets arising from the $(4f)^{13}$ electron configuration are ^{2}F$_{7/2}$ and ^{2}F$_{5/2}$. The energy of the ^{2}F$_{5/2}$ multiplet is about 1200 cm^{-1} lower in Tm^{2+} than in Yb^{3+}, reflecting the smaller spin-orbit coupling in Tm^{2+} [20]. As seen in Fig. 2, the sharp $4f$-$4f$ bands are observed in absorption and emission around 8800 cm^{-1} in both CsCaCl$_3$:Tm^{2+} and CsCaBr$_3$:Tm^{2+} at 10 K. The fine structure will be analyzed in Section IV C. For the modeling in Section IV D, the total $4f$-$4f$ emission intensity (transition A in Fig. 6) will be considered.

In the absorption spectra in Figs. 1 (c) and (d), all the bands above 10000 cm^{-1} are due to $4f$-$5d$ transitions, in which one electron is promoted from the $4f$-orbitals to the $5d$-orbitals. These absorption transitions are between 1 and 4 orders of magnitude more intense than the
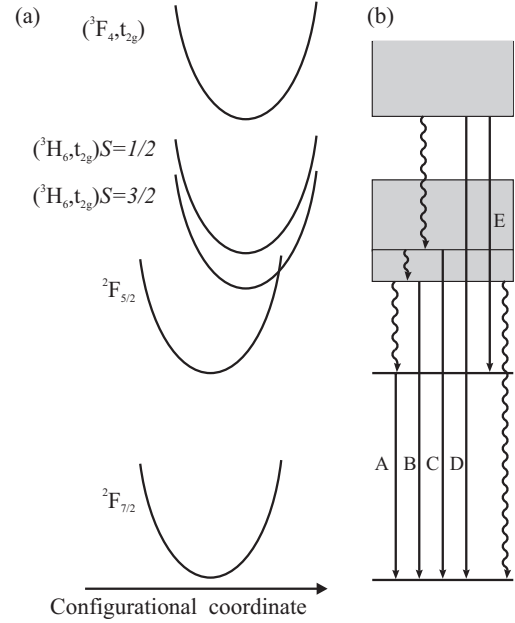
intraconfigurational $4f$-$4f$ transitions. In contrast to the latter, the $4f$-$5d$ transitions are parity-allowed, which can result in a huge increase in the oscillator strength. The states resulting from the $(4f)^{12}(5d)^1$ electron configuration are represented with a displacement along the configurational coordinate in Fig. 6, in agreement with the observed broad absorption and emission bands. The displacement results from the different chemical bonding in the $(4f)^{13}$ and $(4f)^{12}(5d)^1$ configurations. The $(4f)^{12}(5d)^1$ electron configuration has a total degeneracy of 910, and energy splittings occur as a result of various interactions.

An important interaction in the $(4f)^{12}(5d)^1$ configuration is the ligand field interaction of the $5d$ electron. The octahedral ligand field splits the $5d$ orbitals into t_{2g} and e_g sets, separated by $10Dq$. All bands below 25000 cm^{-1} that are shown in the absorption spectra (Fig. 1 (a) and (b)) can be attributed to excited states with the $5d$ electron in the t_{2g} set. The $(4f)^{12}$ part of the configuration is split into the $^{2S+1}L_J$ terms of Tm^{3+} by the Coulomb repulsion and the spin-orbit coupling of the f electrons. Thus, the energy multiplets of the Tm^{2+} $(4f)^{12}(5d)^1$ configuration can be roughly characterized as $(^{2S+1}L_J, t_{2g})$ and $(^{2S+1}L_J, e_g)$. For Tm^{2+}, we expect each of these multiplets to be split into a set of lower energy high-spin $S = 3/2$ and a set of higher energy low-

spin $S = 1/2$ states due to the isotropic exchange part of the Coulomb interaction between the $4f$ and $5d$ electrons [11]. As a consequence, the lowest energy $(4f)^{12}(5d)^1$ bands are expected to have formally "spin-forbidden" character, which will manifest itself in weaker oscillator strengths compared to the formally "spin-allowed" bands [3].

The emission band B (Figs. 1 and 6) originates from the lowest energy $4f$-$5d$ state. The corresponding weak absorption band is shown in Fig. 1 (c) for CsCaCl$_3$:Tm^{2+} and (d) for CsCaBr$_3$:Tm^{2+}. Band B is thus assigned as a "spin-forbidden" $5d$-$4f$ transition from $(^3H_6, t_{2g})S = 3/2$ to $^2F_{7/2}$. Band C is correlated with the first intense $4f$-$5d$ absorption band and is therefore assigned as "spin-allowed" $5d$-$4f$ transition from $(^3H_6, t_{2g})S = 1/2$ to $^2F_{7/2}$. Quite to our surprise, we observed emission from an even higher lying $4f$-$5d$ state: band D is assigned to a transition from the lowest excited state of the $(^3F_4, t_{2g})$ multiplet to the $^2F_{7/2}$ groundstate. Finally, band E is the interexcited state transition from $(^3F_4, t_{2g})$ to $^2F_{5/2}$. The spin of the emitting $(^3F_4, t_{2g})$ state cannot be specified. Apparently, spin is not as well defined in the $(^3F_4, t_{2g})$ multiplet as it is in $(^3H_6, t_{2g})$ [11, 21].

C. $4f$-$4f$ Emission A and Crystal Field Splitting of the $^2F_{7/2}$ and $^2F_{5/2}$

The high resolution absorption and emission data obtained at 10 K in the region of the $4f$-$4f$ transitions (Fig. 2) exhibit considerable fine structure. Some lines around 8800 cm^{-1} in both compounds coincide in absorption and emission. They are labeled A$_0$ and A$_1$, and they can be assigned to electronic origins as shown in the diagram of Fig. 7. Since the intensity ratio of A$_1$ and A$_0$ was found to increase with temperature between 10 and 30 K, the splitting between A$_0$ and A$_1$ is necessarily an excited state splitting. Fig. 7 is a schematic representation of the splitting of $^2F_{7/2}$ and $^2F_{5/2}$ in an O_h (first step) and then C_{4h} or C_i (small distortion from O_h) crystal field. The octahedral splittings are of the order of several hundred cm^{-1} [22], and an unambiguous assignment of absorption or emission features outside the 8800 cm^{-1} region to electronic origins is not possible. The situation is very similar to Yb^{3+} in many host lattices. Unlike $4f$-$4f$ transitions in most other lanthanides, the $^2F_{7/2} \leftrightarrow {}^2F_{5/2}$ bands in $(4f)^{13}$ are characterized by the presence of strong vibronic sidebands. The bands labeled ν_{Cl} and ν_{Br} in the emission spectra of Fig. 2 are such bands. Their identity as vibronic sidebands is confirmed by the reduced energy difference to the strong A$_0$ and A$_1$ origins in the bromide, a result of the smaller vibrational energies in the bromide. At the phase transitions of the host lattice, the site symmetry of Tm^{2+} is reduced from O_h to C_{4h} and C_i in the chloride and bromide, respectively. The degree of the distortion from O_h must
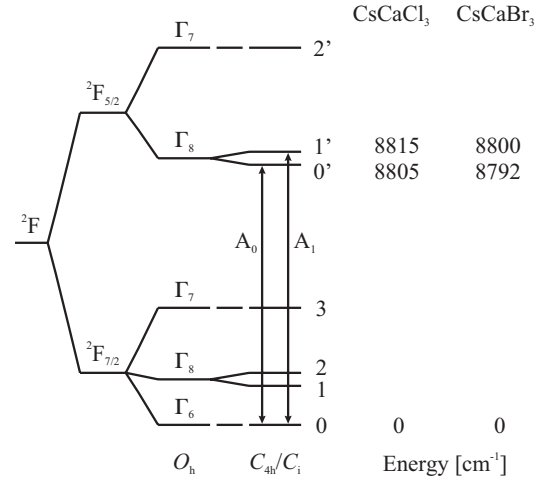

FIG. 7: Schematic representation of the crystal field splitting of the $^2F_{7/2}$ and $^2F_{5/2}$ states of Tm^{2+} in CsCaCl$_3$ and CsCaBr$_3$. The energies of the CF levels are determined from Fig. 2.

be relatively small, however, since the splitting of $^2F_{5/2}$ (Γ_8) into the two Kramer's doublets $0'$ and $1'$ is only 10 cm^{-1} and 8 cm^{-1}. respectively. The bands marked with asterisks in the emission spectra of Fig. 2 are assigned to other species due to their different excitation spectrum. Tm^{2+} ions on some defect sites or Tm^{2+} pair transitions are possibilities.

D.   Modeling the Excited State Dynamics

The very pronounced redistribution of intensity with temperature among the three major emissions A, B and D (Figs. 3 and 4) provides clear evidence for thermally activated nonradiative relaxation processes. A simple model to treat such nonradiative processes is based on the single configurational coordinate (SCC) model [23]. The SCC diagram for Tm^{2+} doped halides is shown in Fig. 6 (a) where the configurational coordinate represents an effective accepting mode for the relaxation process. To model the temperature dependence of emissions A, B, and D, we simplified the SCC diagram. Since emission C is absent in CsCaCl$_3$ and very weak at all temperatures in the bromide we left emission C out of the calculations. In the iodide emission C is not negligible and therefore the integrated photon counts of emission B and C were added together in order to keep the model simple. Emission E shows the same temperature dependence as emission D, because the initial state is the same. The simplified SCC diagram that contains all the relevant radiative (straight arrows) and nonradiative processes (curly arrows) that are considered is shown in Fig. 8. The state $|0\rangle$ corre-
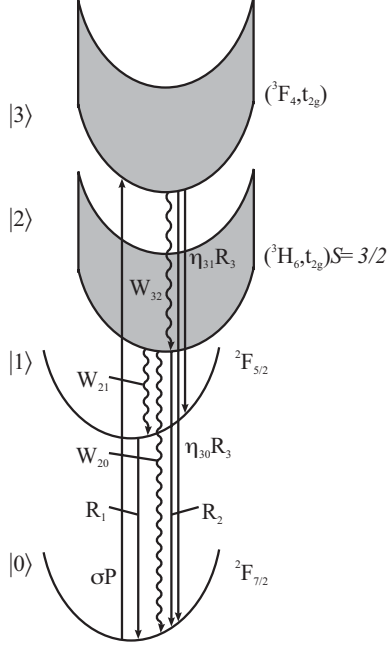
FIG. 8: Simplified SCC diagram of Tm^{2+} to model the temperature dependence of the three major emissions A, B and D. The four emissions in the SCC diagram correspond to the following transitions: A: $|1\rangle \rightarrow |0\rangle$, B: $|2\rangle \rightarrow |0\rangle$, D: $|3\rangle \rightarrow |0\rangle$, E: $|3\rangle \rightarrow |1\rangle$. Curly arrows are used to indicate nonradiative processes (W_{ij}) and straight arrows for radiative transitions (R_i). The branching ratios η_{30} and η_{31} determine the ratio of photons in the emission bands D and E, with $\eta_{30} + \eta_{31} = 1$. P is the laser power and σ the absorption cross section at the excitation energy.

sponds to the ^{2}F$_{7/2}$ ground state of Tm^{2+}, $|1\rangle$ to ^{2}F$_{5/2}$, $|2\rangle$ to (^{3}H$_6$, t$_{2g}$)$S = 3/2$ and $|3\rangle$ to (^{3}F$_4$, t$_{2g}$). The radiative and nonradiative rate constants are labeled R_i and W_{ij}, respectively. Subscript i stands for the initial state and subscript j for the final state. The ratio of photons in the emission bands D and E is given by the branching ratios η_{30} and η_{31}, with $\eta_{30} + \eta_{31} = 1$. P is the laser power and σ the absorption cross section at the excitation energy.

For the laser powers used in our experiments, we can assume that the ground state population N$_0$ is not affected by the excitation. We further assume that multiphonon relaxation from $|1\rangle$ to $|0\rangle$ is negligible. The following rate equations then describe the evolution of the excited state populations N$_i$ ($i = 1, ..., 3$) upon excitation:

$$\frac{\mathrm{d}N_3}{\mathrm{d}t} = \sigma P N_0 - W_{32}N_3 - (\eta_{30} + \eta_{31})R_3 N_3, \quad \text{(1a)}$$

$$\frac{\mathrm{d}N_2}{\mathrm{d}t} = W_{32}N_3 - (W_{21} + W_{20} + R_2)N_2, \quad \text{(1b)}$$

$$\frac{\mathrm{d}N_1}{\mathrm{d}t} = W_{21}N_2 + \eta_{31}R_3 N_3 - R_1 N_1. \quad \text{(1c)}$$

The steady state solutions are:

$$N_3 = \frac{\sigma P N_0}{W_{32} + R_3}, \quad \text{(2a)}$$

$$N_2 = \frac{\sigma P N_0 W_{32}}{(W_{21} + W_{20} + R_2)(W_{32} + R_3)}, \quad \text{(2b)}$$

$$N_1 = \frac{\sigma P N_0 (\eta_{31}R_3(W_{21} + W_{20} + R_2) + W_{32}W_{21})}{R_1(W_{21} + W_{20} + R_2)(W_{32} + R_3)} \quad \text{(2c)}$$

The temperature dependence of the nonradiative decay rate constants W_{ij} is calculated within the framework of the SCC model [24]. We assume linear coupling and harmonic potentials. W_{ij} can be written as [25]:

$$W_{ij} = C_{ij}F_{ij}. \quad \text{(3)}$$

where C_{ij} is the electronic factor and F_{ij} the thermal Franck-Condon factor. The temperature dependent Franck-Condon factor F_{ij} can be written as [25]:

$$F_{ij}(T) = \exp\left(-S_{ij}(1 + 2m)\right)\left(\frac{1+m}{m}\right)^{\frac{p_{ij}}{2}} \times$$
$$I_{p_{ij}}\left(2S_{ij}\sqrt{m(m+1)}\right). \quad \text{(4)}$$

where S_{ij} is the Huang-Rhys factor for the $|i\rangle \rightarrow |j\rangle$ transition, $I_{p_{ij}}$ is the modified Bessel function of the first kind, and m is the thermal population of the effective vibrational mode:

$$m = \frac{1}{\exp\left(\frac{\hbar\omega_{eff}}{kT}\right) - 1}. \quad \text{(5)}$$

with k the Boltzman constant and $\hbar\omega_{eff}$ the energy of the effective accepting mode in the SCC model. p_{ij} is the number of effective phonons required to bridge an energy gap:

$$p_{ij} = \frac{E_{ij}}{\hbar\omega_{eff}}. \quad \text{(6)}$$

E_{ij} is the adiabatic energy difference between the minima of the potential energy curves of states $|i\rangle$ and $|j\rangle$. For a detailed derivation of these equations, we refer the reader to Refs. [24, 25].

TABLE III: Input parameters from the experimental data for the rate equation model discussed in Section IV C.

	CsCaCl$_3$:Tm^{2+}	CsCaBr$_3$:Tm^{2+}	CsCaI$_3$:Tm^{2+}
E_{32}	2700 cm^{-1}	2700 cm^{-1}	2700 cm^{-1}
E_{21}	3929 cm^{-1}	3906 cm^{-1}	2995 cm^{-1}
S_{32}	0.1	0.1	0.1
S_{21}	2	2	2
R_3	1106195 - W_{32}^{a} s^{-1}	588235 s^{-1}	954000 s^{-1}
R_2	3378 s^{-1}	3096 s^{-1}	2555 s^{-1}
R_1	1996 s^{-1}	1873 s^{-1}	1538 s^{-1}
η_{31}	0.00816	0.00125	0.00123

^{a}At T=10 K

We use Eqs. (2) and (3) to model the temperature dependence of the relative photon counts of the emissions A, B, and D shown in Fig. 4. All W_{ij} values are defined as in Eq. (3) except for W_{20} which is defined as $W_{20} = C_{20} W_{21}$ so as to introduce a "branching ratio" that describes the competition between the nonradiative processes $|2\rangle \rightarrow |1\rangle$ and $|2\rangle \rightarrow |0\rangle$. The fitting parameters are then the three electronic factors C_{32}, C_{21} and C_{20} as well as $\hbar\omega_{eff}$.

All the other parameters are deduced from the spectroscopic data and fixed to the values given in Table III. We include the data obtained for CsCaI$_3$:Tm^{2+} in this comparative study. The radiative rate constants R_i are assumed temperature independent and determined from the lifetimes (Table II). The high radiative rate constants R_3 of emission D are notable. It might be possible that the (^{3}F$_4$, t$_{2g}$) multiplet is located inside the conduction band and that a mixing of states occurs. States located inside the conduction band can have high radiative decay rate constants [26]. The radiative decay rate constant R_3 can be calculated from the oscillator strength f of the first (^{3}F$_4$, t$_{2g}$) absorption band assuming equal degeneracies in the ground and excited state [25]:

$$R = f \frac{n[(n^2 + 2)/3]^2}{\alpha\lambda^2}. \tag{7}$$

n is the index of refraction and is estimated to be 1.58, 1.64 and 1.73 for CsCaCl$_3$, CsCaBr$_3$, and CsCaI$_3$, respectively. α is a constant (1.5·10^4 m·s^{-2}) and λ is the emission wavelength. We find good agreement of the calculated and measured radiative lifetimes of emission D in all three materials (see Table 2). It is thus unlikely that mixing with the conduction band states of the host affects the luminescent properties of our samples. Luminescence D in CsCaCl$_3$:Tm^{2+} has a nonradiative contribution already at 10 K. In this case, R_3 is given by (at 10 K):

$$R_3 = k_3 - W_{32}. \tag{8}$$

k_3 is the measured decay rate constant of emission D at 10 K (Table II). The branching ratio η_{31} is the experimental photon ratio of bands E/D. The energy gaps

TABLE IV: Parameters that are obtained in the fit: W_{ij} (calculated from Eq. (3) using the fitted C_{ij} and $\hbar w_{eff}$.

	CsCaCl$_3$:Tm^{2+}	CsCaBr$_3$:Tm^{2+}	CsCaI$_3$:Tm^{2+}
W_{32} at 10 K	757217 s^{-1}	2532 s^{-1}	43761 s^{-1}
W_{21} at 10 K	0.05 s^{-1}	3.2 10^{-7} s^{-1}	1.6 s^{-1}
W_{20} at 10 K	0.02 s^{-1}	1.8 10^{-6} s^{-1}	-^{a}
$\hbar w_{eff}$	106 cm^{-1}	109 cm^{-1}	212 cm^{-1}

^{a}The process W_{20} is not active in the iodide up to 300 K.

E_{ij} are estimated from the absorption and luminescence data. While E_{21} can be accurately determined, there is considerable uncertainty in the value of E_{32}. We use the same value of 2700 cm^{-1} for all three compounds. Similarly, the Huang-Rhys factors S_{21} and S_{32} are set to 2 and 0.1, respectively, for all three compounds. This is a rather crude approximation, since S_{21} is expected to vary across the series. But we have no experimental means of determining this variation, and we want to keep the model as simple as possible. The pump rate constant $\sigma P N_0$ is normalized to 1 s^{-1}. This means that we are in the linear regime and we are ignoring groundstate bleaching.

The integrated photon counts of all three emissions A, B, and D are simultaneously fit (simple minimalization of chi-squared over the parameter space) for a given compound, and the solid lines in Fig. 4 represent the best fits. Overall, the model is able to reproduce the data of CsCaCl$_3$:Tm^{2+} and CsCaBr$_3$:Tm^{2+} very well. The deviations are larger for CsCaI$_3$:Tm^{2+}. The observed drop of emission A in CsCaCl$_3$:Tm^{2+} above 200 K is the result of energy transfer, see Section VI, and thus not within the realm of our photophysical model.

The parameter values obtained in the least-squares fits are listed in Table IV for the three compounds. A graphical representation of the competition between radiative and nonradiative processes is provided in Fig. 9, where the relevant rate constants are logarithmically plotted as a function of temperature for all three systems. It provides insight into the changes that occur along our chemical coordinate.

We are confident that the fits for CsCaCl$_3$:Tm^{2+} and CsCaBr$_3$:Tm^{2+} and the resulting parameter values represent reasonable approximations of the physical reality in these systems. The fitted effective phonon energies for CsCaCl$_3$:Tm^{2+} and CsCaBr$_3$:Tm^{2+} are lower than the highest energy vibrational energies and are comparable with literature data [27–29]. The effective phonon energy for such nonradiative processes is often lower than the highest energy vibrations [27, 30]. For CsCaI$_3$:Tm^{2+}, however, the simple model is a poor approximation of the complex photophysical processes. The best evidence for this is the value of $\hbar\omega_{eff} = 212$ cm^{-1} obtained for the effective accepting mode. This is higher than any vibrational energy in CsCaI$_3$ and thus not physical. Evidence for much more complex photophysics in iodide hosts is also provided by the behavior of Tm^{2+} in

RbCaI$_3$, in which the $4f$-$4f$ emission A already dominates at 10 K [13]. Since our model is extremely simple, there are many possible reasons why it is no longer fully adequate in CsCaI$_3$:Tm^{2+}. The necessary caution will therefore be used in the interpretation of the iodide fit in Section VI. But it must be noted that an analysis of the type provided in Figure 4 with the parameters in Tables III and IV is extremely ambitious and has not been reported so far. Fits of the temperature dependence of emission intensities or lifetimes are usually done for just one transition in one compounds [27, 28, 30, 31]. We extend this by including three competing transitions in each of three related compounds, and we do this without adjusting the model. We thus gain considerably more insight into the photophysics and their dependence on the chemical variable in these systems. But we do reach the limit of applicability of the model.

V.   DISCUSSION

Each of the five emissions A to E will be discussed separately, with the main emphasis on its variation with temperature for a given compound and its variation along the series of Tm^{2+} doped halides.

Emission D is the highest energy emission in the chloride and bromide. In the iodide, we observe a weak emission below 200 K, which lies at even higher energy. This is discussed in Ref. [13]. In all three compounds, emission D appears bright green to the eye. It is a broad $5d$-$4f$ emission band and has its origin in the lowest states of the (^{3}F$_4$, t$_{2g}$) multiplet. With the exception of $4f$-$4f$ emissions in lanthanides and actinides, Kasha's rule is a guiding principle for light emitting materials [32]. It states that, if at all, spontaneous emission occurs from the lowest energy excited state. Our emission D is an exception to this rule, and to our knowledge, emission from higher than the lowest energy "spin-allowed" and "spin-forbidden" $4f$-$5d$ states has not been reported in lanthanide systems [12].

On the basis of Fig. 9, we can understand how this exceptional behavior comes about. First, we note that emission D has the highest radiative rate constant (R_3) of all the observed emissions. R_3 is the dominant relaxation path in the iodide up to 220 K, in the bromide up to 100 K. At these temperatures, the crossing of W_{32} with R_3 occurs in the two samples and thus nonradiative relaxation to (^{3}H$_6$, t$_{2g}$) becomes the dominant relaxation process at elevated temperatures. These crossover points are highlighted and connected with a dashed line in Fig. 9. In the chloride, R_3 has a strong competition already at 10 K from the nonradiative W_{32}, and above 50 K R_3 loses out completely; see also data in Fig. 4. The comparison of the three samples shows the strong dependence of W_{32} on the chemistry. W_{32} decreases by two orders of magnitude at 10 K in the bromide compared to the chloride, but for CsCaI$_3$:Tm^{2+}, the values lie between
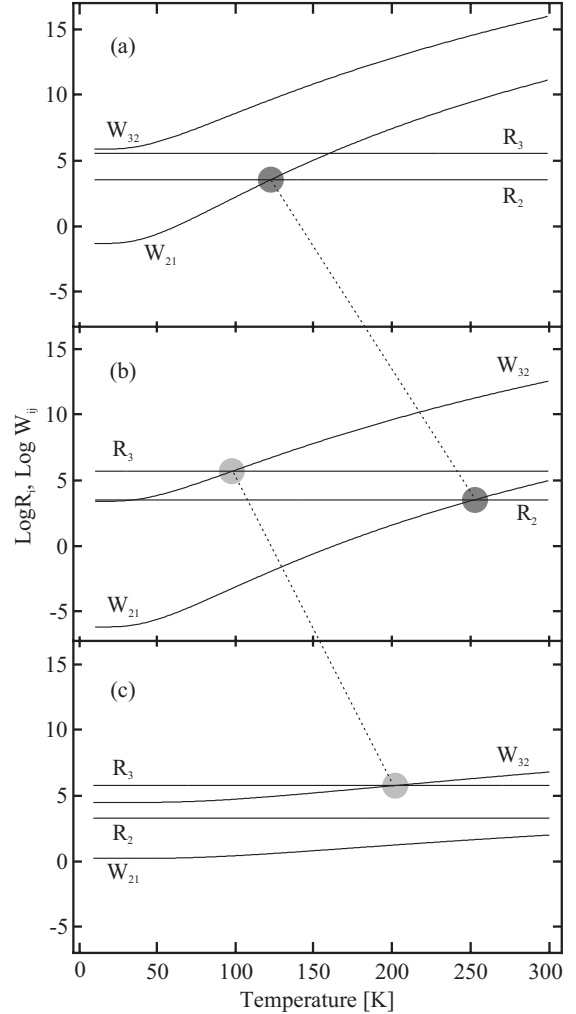

FIG. 9: Semilog plot of the radiative R_i and nonradiative W_{ij} rate constants as a function of temperature for Tm^{2+} doped CsCaCl$_3$ (a), CsCaBr$_3$ (b), and CsCaI$_3$ (c). The radiative rate constants R_i are given in Table III. The nonradiative rate constants W_{ij} are calculated from Eq. (3) using the parameter values in Tables III and IV. The crossover points of W_{32} with R_3 and W_{21} with R_2 are highlighted and connected with dashed lines for better illustration of the influence of the chemical variable on the photophysics of Tm^{2+}.

the two others. Within our model, a decrease of W_{32} (10 K) along the halide series is expected on the basis of decreasing phonon energies. The observed increase in the iodide clearly shows the limits of our model. The evolution of W_{32} with temperature is similar in the chloride and bromide, whereas in the iodide the increase with temperature is much less steep. The chemical variation thus affects not only the 10 K value of W_{32} but also its

temperature dependence, with a significant difference in the iodide.

Emission E has the same temperature dependence and originates from the same state as D, but the final state is ^{2}F$_{5/2}$ instead of the ground state. It is extremely weak, with D/E photon ratios of 123:1, 800:1, and 806:1 in the chloride, bromide, and iodide, respectively. We ascribe this extreme branching ratio to a selection rule $\Delta J = 1$ [33]. The lowest-energy component of (^{3}F$_4$, t$_{2g}$) has, according to Hund's rule, a $J = 9/2$ value, if we only consider the spin angular momentum of the d electron. Thus, a transition to ^{2}F$_{7/2}$ is allowed, whereas ^{2}F$_{5/2}$ is not accessible in this rough approximation.

Emission B is a broad $5d$-$4f$ band in the near IR around 12000 cm^{-1}. It is assigned to a transition from the lowest-energy (^{3}H$_6$, t$_{2g}$)$S = 3/2$ to ^{2}F$_{7/2}$. It is the dominant feature in the emission spectrum of the chloride up to 120 K, of the bromide between 100 and 250 K, and of the iodide above 220 K; see also Figs. 3 and 4. (^{3}H$_6$, t$_{2g}$)$S = 3/2$ is being populated by multiphonon relaxation (W_{32}) from the higher (^{3}F$_4$, t$_{2g}$) metastable state. Since the decrease of emission D with increasing temperature is also determined by W_{32}, we can immediately understand that the observed rise with the temperature of B is correlated with the decline of D, nicely seen in Fig. 4 for all three samples. The lifetime of emission B is constant up to 70 and 160 K in CsCaCl$_3$:Tm^{2+} and CsCaBr$_3$:Tm^{2+}, respectively (see Fig. 5), which proves the radiative nature of the decay up to these temperatures. Above 120 K in the chloride and 250 K in the bromide, emission B is taken over by emission A. Their correlated rise and decline is again nicely observed in Fig. 4. The nonradiative relaxation process from (^{3}H$_6$, t$_{2g}$)$S = 3/2$ to ^{2}F$_{5/2}$ (W_{21}) is responsible for this, see the crossing of log[W_{21}] with log[R_2] at 120 and 250 K in the chloride and bromide, respectively, in Fig. 9. This onset of nonradiative relaxation is also confirmed by the simultaneous decrease of the respective lifetimes in Fig. 5. In the iodide, the W_{21} process is not competitive up to room temperature, that is, we observe no crossing point of W_{21} with R_2.

Emission C is a weak emission only observed in the bromide and iodide, which originates in a higher excited state within the (^{3}H$_6$, t$_{2g}$) multiplet. We assign it to the (^{3}H$_6$, t$_{2g}$)$S = 1/2 \rightarrow$ ^{2}F$_{7/2}$ transition. This is a formally "spin-allowed" transition with a high oscillator strength. The energy difference between the lowest level of (^{3}H$_6$, t$_{2g}$)$S = 1/2$ and the highest level of (^{3}H$_6$, t$_{2g}$)$S = 3/2$ is difficult to estimate from the absorption and luminescence spectra: A range of 600 to 1200 cm^{-1} is compatible with the data. This is a very small gap, and in all compounds studied here, relaxation by multiphonon processes is active down to the lowest temperatures. In the chloride, multiphonon relaxation is too efficient for C to be observed. In the bromide, the intensity of C compared to B is small, whereas in the iodide C has gained considerable intensity. The observation of emission C in the bromide and iodide is surprising considering the small

energy gaps involved. In Ce^{3+} doped compounds, energy gaps of up to several thousand cm^{-1} are observed between the states deriving from the $(4f)^0(5d)^1$ electron configuration [34, 35]. Generally, only emission from the lowest state is observed. Multiphonon relaxation among states of the same spin multiplicity appears to be efficient. In contrast, the multiphonon relaxation process from (^{3}H$_6$, t$_{2g}$)$S = 1/2$ to $S = 3/2$ requires a reorientation of the spin, which slows it down. This is considered a key to the observation of emission from low-spin states [36]. Among the lanthanides having a more than half-filled $4f$ shell, "spin-forbidden" and "spin-allowed" emissions have been reported for Yb^{2+} [12], Er^{3+}, and Tm^{3+} doped compounds [36, 37]. The ratio of "spin-forbidden" and "spin-allowed" emission was found to depend on the host and the temperature.

Emission A (^{2}F$_{5/2} \rightarrow$ ^{2}F$_{7/2}$) is the strongest emission at 300 K in the chloride and bromide. The emitting state ^{2}F$_{5/2}$ is populated from (^{3}H$_6$, t$_{2g}$)$S = 3/2$ by the multiphonon relaxation process with rate constant W_{21}. A takes over from B as the most intense emission at about 120 and 250 K, respectively; in the two lattices, see Fig. 4 and the crossing points of R_2 with W_{21} in Fig. 9. In the iodide, this crossing is not reached below 300 K, because W_{21} is not competitive. It is interesting to note that a very small A emission of the order of 0.1% is observed even at 10 K in all three samples; see Table I. In the bromide, the ^{2}F$_{5/2}$ population occurs purely radiatively by process E, whereas in chloride and iodide there is an additional nonradiative contribution to the ^{2}F$_{5/2}$ feeding. In CsCaCl$_3$:Tm^{2+}, the intensity of emission A decreases above 200 K. This is not due to multiphonon relaxation to the ground state, for which the energy gap of 8800 cm^{-1} is too large. We ascribe it nonradiative losses by energy migration to unidentified killer traps.

VI. CONCLUSIONS AND OUTLOOK

The temperature dependent study of the emission properties of Tm^{2+} doped into a series of isostructural halide lattices provides insights into the photophysics of this ion. The interplay and the competition of the various radiative and nonradiative relaxation processes are elucidated, and the rate constants of the relevant processes are quantified. The observation and characterization of up to five different types of light emission from a given compound, which is without precedent, provide the basis for such a detailed analysis. It turns out that the chemical variation along the series of CsCaCl$_3$, CsCaBr$_3$, and CsCaCl$_3$ host lattices and its significant consequences on the light emission behavior are essential for the relatively detailed picture obtained. The pronounced temperature dependence of the nonradiative processes is an important factor, which we are reproducing with an approximate model in the present paper, whereas the radiative

decay constants are essentially temperature independent. In the iodide, we reach the limit of the applicability of the simple model. But it does allow a discussion of the relevant processes and their temperature dependence.

The choice of Tm^{2+} as the active ion turns out to be fortunate for both chemical and physical reasons. It is possible to stabilize the divalent Tm in all the halides (chloride, bromide, and iodide). Physically, a big advantage of the $(4f)^{13}$ electron configuration of Tm^{2+} lies in the fact that ^{2}F$_{5/2}$ is the only $4f$-$4f$ excited state, and above 9000 cm^{-1}, the properties of the states arising from the $(4f)^{12}(5d)^1$ configuration can be probed without any interference from the $(4f)^{13}$ configuration. The observation of emissions from higher excited $4f$-$5d$ states is facilitated by the fact that we are dealing with divalent host lattices with heavy anions. A practical advantage of the systems studied here is the energy range of the emissions studies, from the near IR to the green, which is experimentally more easily accessible than the vacuum UV, where the $5d$-$4f$ emissions of the trivalent lanthanides are often found.

Let us finally briefly compare the light emission properties reported and analyzed here in chloride, bromide, and iodide lattices with literature studies of Tm^{2+} doped fluorides. All these studies deal with the $4f$-$4f$ emission in the near IR, and we found no report of $5d$-$4f$ emission in a fluoride, even at cryogenic temperatures. This may simply be a reflection of a very efficient (^{3}H$_6$, t$_{2g}$)$S = 3/2$ to ^{2}F$_{5/2}$ nonradiative relaxation rate constant W_{21}. However, there are chemical considerations that have to be taken into account. Tm^{2+} is harder to stabilize in a fluoride than in the heavier halides. As a consequence, Tm^{3+} is invariably present in Tm^{2+} doped fluorides, and this might quench the emission B of Tm^{2+} by energy transfer. We have found some preliminary evidence of emission B in a CaF$_2$:Tm^{2+} sample, in which Tm^{2+} was chemically incorporated and not created by irradiation as in some of the other investigations.

Acknowledgments

[1] Rubio, J. *J. Phys. Chem. Solids* **1991**, *52*, 101.
[2] Meyer, G. *Chem. Rev.* **1988**, *88*, 93.
[3] McClure; D. S.; Kiss, Z. J. *J. Chem Phys.* **1963**, *39*, 3251.
[4] Kiss, Z. J. *Phys. Rev.* **1962**, *127*, 718.
[5] Loh, E. *Phys. Rev.* **1968**, *175*, 533.
[6] Duncan, R. C.; Kiss, Z. J. *Appl. Phys. Lett.* **1963**, *3*, 23.
[7] Duncan, R. C. *IEEE J. Quantum Electron.* **1966**, *2*, R52.
[8] Schipper, W. J.; Meijerink, A.; Blasse, G. *J. Lumin.* **1994**, *62*, 55.
[9] Wenger, O. S.; Wickleder, C.; Krämer, K.; Güdel, H. U. *J. Lumin.* **2001**, *94-95*, 101.
[10] Wickleder, C. *J. Alloys Compd.* **2000**, *300-301*, 193.
[11] Grimm, J.; Güdel, H. U. *Chem. Phys. Lett.* **2005**, *404*, 40.
[12] Dorenbos, P. *J. Phys. Condens. Matter* **2003**, *15*, 575.
[13] Beurer, E.; Grimm, J.; Güdel, H. U. *to be submitted for publication.*
[14] Meyer, G. *Adv. Synth. React. Solids* **1994**, *2*, 1.
[15] Seifert, H.-J.; Langenbach, U. *Z. Anorg. Allg. Chem.* **1969**, *368*, 36.
[16] Seifert, H.-J.; Haberhauer, D. *Z. Anorg. Allg. Chem.* **1982**, *491*, 301.
[17] Vaills, Y.; Buzaré, J. Y.; Gibaud, A.; Launay, C. *Solid State Comm.* **1986**, *60*, 139.
[18] Lucas, M. C. M.; Rodriguez, F.; Prieto, C.; Verdaguer, M.; Güdel, H. U. *J. Phys. Chem. Solids* **1995**, *56*, 995.
[19] Schilling, G.; Meyer, G. *Z. Anorg. Allg. Chem.* **1996**, *622*, 759.
[20] Hüfner, S. *Optical Spectra of Transparent Rare Earth Compounds*, Academic Press: New York, 1978.
[21] Dorenbos, P. *J. Phys. Condens. Matter* **2003**, *15*, 6249.
[22] Richardson; F. S., Reid, M. F.; Dallara, J. J.; Smith, R. D. *J. Chem Phys.* **1985**, *83*, 3813.
[23] Struck, C. W.; Fonger, W. H. *J. Lumin.* **1975**, *10*, 1.
[24] Donnelly, C. J.; Imbusch, G. F. In *Advances in Nonradiative Processes in Solids*, di Bartolo, B., Ed.; NATO ASI Series, Plenum Press: New York, 1991; pp 175-195.
[25] Henderson, B.; Imbusch, G. F., *Optical Spectroscopy of Inorganic Solids*, Oxford University Press: New York, 1989.
[26] Dorenbos, P. *J. Phys. Condens. Matter* **2003**, *15*, 2645.
[27] Reber, C.; Güdel, H. U. *J. Lumin.* **1988**, *42*, 1.
[28] May, P. S.; Güdel, H. U. *J. Lumin.* **1990**, *46*, 277.
[29] Gamelin, D. R.; Güdel, H. U. *J. Phys. Chem. B* **2000**, *104*, 10222.
[30] Sturge, M. D. *Phys. Rev. B* **1973**, *8*, 6.
[31] Donegan, J. F.; Bergin, J. F.; Glynn, T. J.; Imbusch, G. F. *J. Lumin.* **1986**, *35*, 57.
[32] Kasha, M. *Discuss. Faraday Soc.* **1950**, *9*, 14.
[33] Peijzel, P. S., Vergeer, P.; Meijerink, A.; Reid, M. F.; Boatner, L. A.; Burdick, G. W. *Phys. Rev. B* **2005**, *71*, 045116.
[34] Dorenbos, P. *Phys. Rev. B* **2000**, *62*, 15640.
[35] Dorenbos, P. *Phys. Rev. B* **2000**, *62*, 15650.
[36] Wegh, R. T.; Meijerink, A. *Phys. Rev. B* **1999**, *60*, 10820.
[37] van Pieterson, L.; Wegh, R. T.; Meijerink, A.; Reid, M. F. *J. Chem. Phys.* **2001**, *115*, 9382.

Crystal Absorption Spectra in the Region of 4*f*-4*f* and 4*f*-5*d* Excitations in Tm^{2+} Doped CsCaCl$_3$, CsCaBr$_3$ and CsCaI$_3$

Judith Grimm, Eva Beurer, and Hans U. Güdel*

Department of Chemistry and Biochemistry, University of Bern, Freiestrasse 3, 3012 Bern, Switzerland

Low-temperature absorption spectra of single crystals of Tm^{2+} doped CsCaCl$_3$, CsCaBr$_3$ and CsCaI$_3$ in the spectral range from 8700 cm^{-1} to 47000 cm^{-1} are presented. Weak sharp-line 4*f*-4*f* absorptions around 8800 cm^{-1} are essentially independent on the nature of the halide. More intense broad absorptions cover the region between 12000 cm^{-1} and 47000 cm^{-1}. They are assigned to 4*f*-5*d* excitations and interpreted in terms of a simple qualitative picture taking into account the most important interactions. As a result of two counterbalancing effects, the onsets of the 4*f*-5*d* spectra are almost coincident in the three materials: The blueshift of about 3000 cm^{-1} between chloride and iodide resulting from the decreasing crystal field splitting of 5*d* is roughly balanced by the redshift resulting from the reduced energy gap between 5*d* and 4*f* orbitals. The absorption helps to understand the most unusual light emission properties of these materials.

I. INTRODUCTION

Studies on the optical spectroscopic properties of divalent lanthanides have mainly concentrated on Eu^{2+}, Yb^{2+} and Sm^{2+}, as these are readily stabilized in the divalent oxidation state [1]. By far the most comprehensive literature is found for Eu^{2+}. The luminescence of Eu^{2+} has been intensively studied, as this ion plays an important role in phosphor materials for fluorescent lighting [2]. In Sm^{2+} doped crystals, room temperature persistent spectral hole burning was demonstrated for the first time [3]. The 5*d* to 4*f* transitions of Yb^{2+} are of interest for possible laser applications [4]. In contrast, spectroscopic studies of Tm^{2+} are rather scarce. This mainly reflects the greater difficulties that are encountered when trying to stabilize this ion in its divalent state in an oxide or fluoride environment. In the heavier halides the situation is thermodynamically more favorable, and we have recently presented the light emission properties of Tm^{2+} doped into CsCaBr$_3$ [5]. An unusually rich variety of light emissions was discovered in this system. Five different types of transitions were found to coexist and compete as a function of temperature. We are extending these studies to include other host lattices and find that the Tm^{2+} light emission properties exhibit a great deal of variation depending on the host [6]. Besides the light emission, the absorption properties are of great interest because they are essentially unexplored.

In the present contribution we offer a comparative study of the absorption spectra from the near-infrared (NIR) to the ultraviolet (UV) of Tm^{2+} in the perovskite host lattices CsCaCl$_3$, CsCaBr$_3$ and CsCaI$_3$. Both 4*f*-4*f* and 4*f*-5*d* excitations are observed from the NIR to the UV, and the chemical variation mainly affects the latter through the direct exposure of the 5*d* electron to the octahedral halide coordination. The experimental results are discussed semiquantitatively by identifying the dom-

inant interactions but without an attempt to model the data quantitatively. This is the first systematic study of the 4*f*-4*f* and 4*f*-5*d* excitations of Tm^{2+} in a series of related host lattices.

II. EXPERIMENTAL

Single crystals of CsCaCl$_3$, CsCaBr$_3$ and CsCaI$_3$ doped with Tm^{2+} were grown by the Bridgman technique. For the synthesis, stoichiometric amounts of CsX (X=Cl, Br, I) and CaX$_2$ were mixed. Tm^{2+} was prepared in situ by synproportionation of TmX$_3$ and Tm metal. The use of Ta ampoules is indispensable for the success of the synthesis. The absolute concentration of Tm is 1.04%, 0.48% and 0.76% in CsCaCl$_3$, CsCaBr$_3$ and CsCaI$_3$, respectively, and was determined by ICP-OES. Due to their hygroscopic nature, the handling of the starting materials as well as the crystals occurred under inert atmosphere at all times. For absorption measurements the samples were polished in a dry box and enclosed in an air-tight copper cell. Absorption spectra were recorded on a Cary 6000i spectrometer (Varian). Sample cooling was achieved with a closed-cycle cryostat (Air Products).

III. RESULTS

CsCaCl$_3$:1.04% Tm^{2+}, CsCaBr$_3$:0.48% Tm^{2+} and CsCaI$_3$:0.76% Tm^{2+} are dark green crystals. Figure 1 a) shows sections of the 10 K crystal absorption spectra of finely polished crystals in the region of the 4*f*-4*f* excitations between 8700 and 9100 cm^{-1} in the NIR. Except for a very slight redshift within the series from chloride to iodide there is little variation in these sharp-line spectra.

Figure 2 shows the absorption spectra extending from 13000 cm^{-1} in the NIR to 47000 cm^{-1} in the UV. This is the region of 4*f*-5*d* excitations, and it is most unusual that absorption spectra of allowed transitions can be measured over such a broad spectral range. Usually,
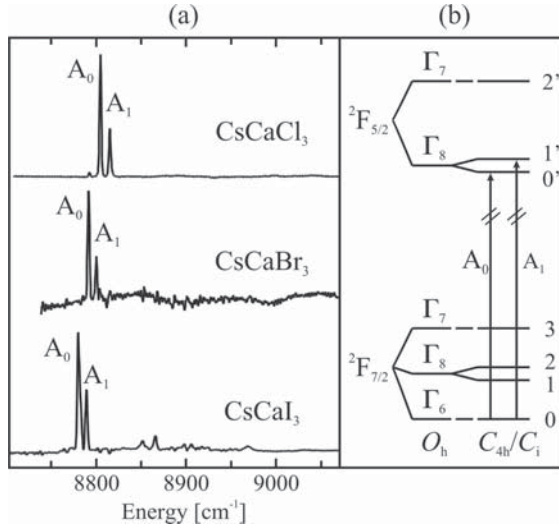
*Electronic address: `guedel@iac.unibe.ch`

FIG. 1: (a) 10 K absorption spectrum of CsCaCl$_3$:1.04% Tm^{2+}, CsCaBr$_3$:0.48% Tm^{2+} and CsCaI$_3$:0.76% Tm^{2+} in the region of the 4f-4f excitations. (b) Schematic energy level diagram of the ^{2}F$_{7/2}$→^{2}F$_{5/2}$ transition. The arrows indicate the transitions that are observed in (a).

big variations in absorption intensities prevent this. The spectra in Figure 2 show a rich structure with bands of similar widths and intensities. A first-sight comparison of the three spectra reveals both similarities and differences. The first, and perhaps surprising, observation is that the onset of the 4f-5d bands in the NIR does not differ by more than about 1000 cm^{-1} in the three systems. The low-energy part of the spectra is shown on an expanded scale in Figure 3 for better comparison. It shows that not only the onset but also the appearance of the spectra up to about 23000 cm^{-1} is similar for the three compounds. Above 23000 cm^{-1} the similarity becomes less pronounced, and in particular the shape of the CsCaI$_3$:Tm^{2+} spectrum deviates from the other two.

IV. DISCUSSION

A. Host Materials

CsCaCl$_3$ and CsCaBr$_3$ are cubic perovskites at room temperature (space group $Pm3m$) with Ca^{2+} on a site with O_h symmetry. Both samples undergo phase transitions at lower temperatures [7, 8]. At 10 K CsCaCl$_3$ and CsCaBr$_3$ crystallize as tetragonal (space group P4/mbm) and orthorhombic (space group $Pnma$) phases, respectively. CsCaI$_3$ is stable in the orthorhombic $Pnma$ space group at all temperatures between 10 and 300 K. At 10 K the Ca^{2+} site symmetry is C_{4h} in CsCaCl$_3$ and C_i in CsCaBr$_3$ and CsCaI$_3$. In all cases the distortions of the octahedral CaX$_6$ coordination are very small, and in the

crystal spectra their effect only shows up in the highly resolved 4f-4f absorptions of the Tm^{2+} doped materials, in which Tm^{2+} substitutes for Ca^{2+}. O_h notation will therefore be used in the discussion of the 4f-5d excitation.

B. 4f-4f Excitations

Tm^{2+} has a (4f)^{13} ground state electron configuration, resulting in a ^{2}F$_{7/2}$ ground term and a ^{2}F$_{5/2}$ excited term, see Figure 1 b). This is in exact analogy to the situation in Yb^{3+}, whose spectroscopic properties have been well explored in a variety of chemical environments. Since the spin-orbit coupling is smaller in Tm^{2+}, the ^{2}F$_{7/2}$↔^{2}F$_{5/2}$ transitions, both in absorption and emission and independent of the chemical environment, are shifted from about 10000 cm^{-1} in Yb^{3+} to about 8800 cm^{-1} in Tm^{2+} [9, 10]. This is seen in Figure 1 a).

The absorption spectra in Figure 1 a) are dominated by the sharp lines A$_0$ and A$_1$, which show a redshift of 16 cm^{-1} between the chloride and iodide. Both A$_0$ and A$_1$ are assigned to electronic origins as shown in Figure 1 b) from their coincidence with corresponding cold emission lines. The redshift along the halide series is a result of the decreasing spin-orbit coupling strength, caused by the increasing covalency. Since Tm^{2+} occupies a centrosymmetric site in all the lattices, the transition A$_0$ and A$_1$ arise by a magnetic dipole (MD) mechanism. Γ$_6$ to Γ$_8$ (O_h notation) is MD allowed, while Γ$_6$ to Γ$_7$ is forbidden. This explains the dominance of A$_0$ and A$_1$ in the spectra. It is not possible to unambiguously assign any other features to the Γ$_6$ to Γ$_7$ origin. The small splitting of 8 or 9 cm^{-1} between A$_0$ and A$_1$ results from the splitting of Γ$_8$ into the two Kramers doublets $0'$ and $1'$ and thus reflects the small distortion of the TmX$_6$ octahedron below the phase transitions.

C. 4f-5d Excitations

Yb^{3+} doped oxides, fluorides, chlorides and bromides are completely transparent between about 10000 cm^{-1} and 30000 cm^{-1}. This property makes Yb^{3+} an important sensitizer ion for photon upconversion in Er^{3+} and Tm^{3+} doped systems [11, 12]. The first allowed optical excitations of Yb^{3+} in the UV are of the ligand-to-metal charge transfer (LMCT) type, and only at higher energies 4f-5d absorptions occur [13]. In contrast, Tm^{2+} shows intense absorptions with ϵ values of the order of 1000 M^{-1}cm^{-1} throughout the visible (VIS) and UV region, see Fig. 2 [14, 15]. These are due to 4f-5d excitations, which are shifted to lower energies by about 50000 cm^{-1} compared to Yb^{3+}. LMCT transitions, on the other hand, are expected to shift to higher energies in Tm^{2+}, and we do not consider them in our discussion of Fig. 2.

A redshift of 30000 cm^{-1} to 50000 cm^{-1} in the 4f-5d excitations of divalent lanthanides compared to their
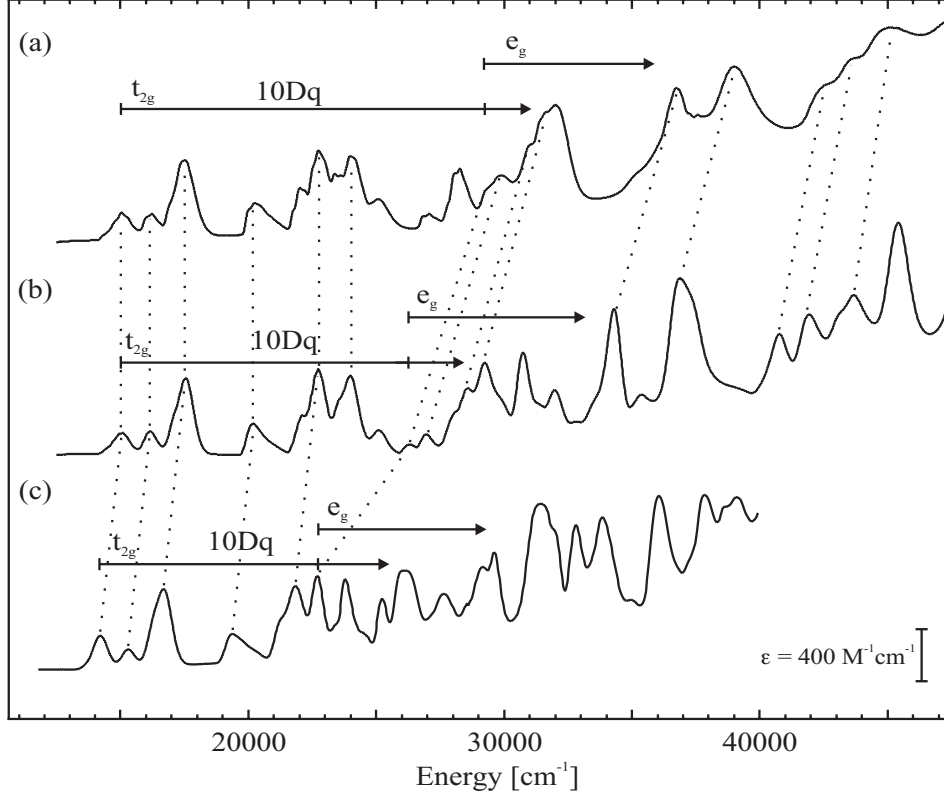
FIG. 2: Single crystal absorption spectra of in the region of the 4f-5d transitions of CsCaCl$_3$:1.04% Tm^{2+} (a), CsCaBr$_3$:0.48% Tm^{2+} (b) and CsCaI$_3$:0.76% Tm^{2+} (c) recorded at 10 K. The spectra are corrected for the Tm^{2+} concentration to have the same ϵ scales, see bottom right. Corresponding bands are connected by dotted lines, and the onset of absorption bands corresponding to the (^{3}H$_6$, t$_{2g}$) and (^{3}H$_6$, e$_g$) multiplets are marked with t$_{2g}$ and e$_g$ arrows.

isoelectronic trivalent counterparts is observed throughout the lanthanide series [16, 17]. This is a result of the reduced Coulomb attraction of the 5d electron by the nucleus in the divalent ions, which leads to a reduced energy separation of 5d and 4f. All the absorption bands shown in Figure 2 between 13000 cm^{-1} and 47000 cm^{-1} can thus be assigned to 4f-5d excitations.

The $(4f)^{12}(5d)^1$ electron configuration has a total degeneracy of 910. This is split by a variety of interactions, the four most important of which are

$$H = H_{CF}(d) + H_{Coul+SO}(f) + H_{Coul}(fd) + H_{SO}(d).$$

- H$_{CF}(d)$: Crystal field interaction of the 5d electron

- H$_{Coul+SO}(f)$: Combined Coulomb repulsion and spin-orbit coupling within the $(4f)^{12}$ configuration

- H$_{Coul}(fd)$: Coulomb repulsion of the 4f and 5d electrons

- H$_{SO}(d)$: Spin-orbit interaction of the 5d electron

H$_{CF}(d)$ splits the 5d orbital into t$_{2g}$ and e$_g$ sets of octahedral orbitals separated by 10 Dq. The effect of H$_{Coul+SO}(f)$ is to split the $(4f)^{12}$ configuration into $^{2S+1}$L$_J$ terms very similar to the situation in Tm^{3+}, represented in the well-known Dieke diagram [18]. This leads to a situation as depicted schematically in Figure 4. The multiplets in Figure 4 will then be further split by H$_{Coul}(fd)$ and H$_{SO}(d)$.

With this relatively simple picture in mind we are able to interpret the low-energy part of the spectra in Figure 2. The spectra of CsCaCl$_3$:Tm^{2+} and CsCaBr$_3$:Tm^{2+} are very similar up to 26200 cm^{-1}, where a new band appears in the bromide spectrum. And in CsCaI$_3$:Tm^{2+} the first new band appears at 22800 cm^{-1}. All the bands at lower energies can be assigned to excited states deriving from the $(4f)^{12}(t_{2g})^1$ electron configuration, and we take the appearance of the first new band as the onset of the $(4f)^{12}(e_g)^1$ ladder, see right-hand side of Figure 4. This assignment is confirmed by the correspondence between equivalent bands connected by dotted lines for the chloride and bromide in Figure 2. For the iodide, the
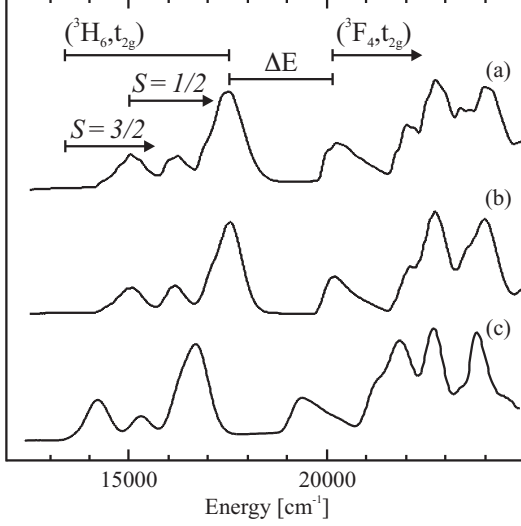
FIG. 3: 10 K absorption spectrum of CsCaCl$_3$:1.04% Tm^{2+} (a), CsCaBr$_3$:0.48% Tm^{2+} (b) and CsCaI$_3$:0.76% Tm^{2+} (c) in the region of the onset of the $4f$-$5d$ absorption transitions. The assignment of the bands is given on top of the CsCaCl$_3$:Tm^{2+} spectrum.
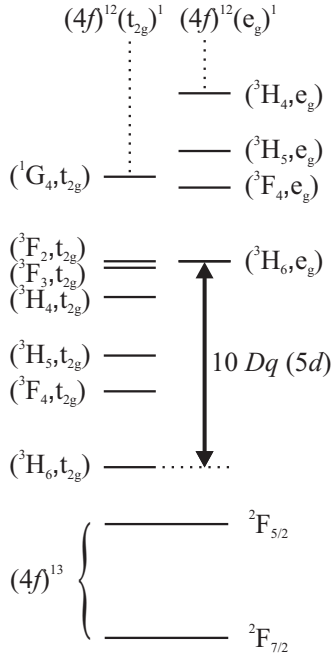

FIG. 4: Schematic energy splittings of the $(4f)^{13}$ and $(4f)^{12}(5d)^1$ electron configurations in Tm^{2+}. For the $(4f)^{12}(5d)^1$ only the interactions H$_{CF}(d)$ and H$_{Coul+SO}(f)$, as defined in the text, are considered. The levels derived from $(4f)^{12}(t_{2g})^1$ and $(4f)^{12}(e_g)^1$ are displayed separately for better distinction.

TABLE I: The 10 Dq values of Tm^{2+} doped CsCaCl$_3$, CsCaBr$_3$ and CsCaI$_3$ as determined from Fig. 2.

	CsCaCl$_3$	CsCaBr$_3$	CsCaI$_3$
10 Dq [cm^{-1}]	14200	11200	8500

analogy to the chloride and bromide spectra ends above 23000 cm^{-1}.

The decrease of 10 Dq from chloride to iodide of 40% would predict a corresponding blueshift of the $4f$-$5d$ bands of about 3000 cm^{-1}. However, we observe slight redshifts of less than 1000 cm^{-1} in the low-energy part of the absorption spectrum (see Figure 3). The CsCaCl$_3$:Tm^{2+} and CsCaBr$_3$:Tm^{2+} absorption spectra are essentially superimposable between 13000 cm^{-1} and 25000 cm^{-1}. It clearly demonstrates that the decrease of 10 Dq is counterbalanced by a decrease of the energy separation between $5d$ and $4f$ orbitals. This is a result of the decreasing Coulomb attraction of the $5d$ electron by the nucleus due to the increased covalency. As a consequence we observe a redshift of the total $4f$-$5d$ spectrum along the halide series. Between the chloride and the bromide the two effects happen to cancel exactly at the onset of the $4f$-$5d$ absorption spectrum.

In the low energy part of the spectra in Figure 3 we can push the interpretation of the observed bands a bit further. The effect of H$_{Coul+SO}(f)$ can be identified. The lowest terms arising from $(4f)^{12}(t_{2g})^1$ under the action of H$_{Coul+SO}(f)$ are (^{3}H$_6$,t$_{2g}$) and (^{3}F$_4$,t$_{2g}$), see the left column in Figure 4. In Tm^{3+}, ^{3}F$_4$ lies about 5550 cm^{-1} above ^{3}H$_6$, and thus we expect the onset of (^{3}F$_4$,t$_{2g}$) at about 19700 cm^{-1} in the chloride and bromide and at about 18700 cm^{-1} in the iodide in our absorption spectra. This is nicely borne out, as shown in Figure 3, where the assignment is given for the chloride. (^{3}H$_6$,t$_{2g}$) consists of numerous absorption bands and covers an energy range of about 4000 cm^{-1}. An energy gap ΔE of about 2700 cm^{-1} separates the lowest component of (^{3}F$_4$,t$_{2g}$) from the highest component of (^{3}H$_6$,t$_{2g}$) in all three samples, see Figure 3. This gap, by the way, is large enough for the lowest component of (^{3}F$_4$,t$_{2g}$) to become metastable and emissive, particularly in the bromide and iodide [6]. At higher energies there is no energy gap of this order of magnitude. Increasing overlap of bands towards higher energies makes an unambiguous assignment of ($^{2S+1}$L$_J$,t$_{2g}$) and ($^{2S+1}$L$_J$,e$_g$) terms impossible.

The energy splittings within the (^{3}H$_6$,t$_{2g}$) multiplet arise from the interactions H$_{Coul}(fd)$ and H$_{SO}(d)$. The isotropic part of H$_{Coul}(fd)$ causes a splitting into a set of states with spin $S=1/2$ and another with $S=3/2$. From the absorption and emission spectra we conclude that S is still a reasonably good quantum number within (^{3}H$_6$,t$_{2g}$): The lowest-energy $4f$-$5d$ absorption band is very weak in all the three spectra and we assign it to a spin-forbidden ^{2}F$_{7/2} \rightarrow$(^{3}H$_6$,t$_{2g}$)$S=3/2$ transition. This lowest excited $4f$-$5d$ state is emissive in all three compounds. As shown in Figure 3, the first intense

absorption band lies about 2000 cm^{-1} higher in energy and is assigned to the lowest energy spin-allowed $^2F_{7/2}\rightarrow(^3H_6,t_{2g})S=1/2$ excitation. This state is also metastable up to room temperature in the bromide and iodide and shows a very weak short-lived emission. From the experiment based distinctions between spin-forbidden and spin-allowed transitions within the multiplet we conclude that the effect of H$_{SO}(d)$ is weaker than that of H$_{Coul}(fd)$. In the higher energy multiplet $(^3F_4,t_{2g})$ such a distinction is no longer possible, as the lowest energy absorption band is intense [19].

V. CONCLUSIONS

This study shows that in contrast to oxide and fluoride lattices, Tm^{2+} is easily incorporated into crystal lattices of the heavier halides. The synthesis of sizeable crystals of Tm^{2+} doped CsCaCl$_3$, CsCaBr$_3$ and CsCaI$_3$ perovskites allows a systematic study of the 4f-4f and 4f-5d excited state properties by absorption spectroscopy. This is an essentially unexplored area. By their location in the VIS and near UV part of the spectrum, the 4f-5d excitations are experimentally easily accessible. This is in contrast to trivalent lanthanides, in which 4f-5d absorptions are usually in the vacuum UV and thus more difficult to explore. Tm^{2+} offers another significant advantage for the study of 4f-5d excitations. There is only one 4f-4f excited state within the $(4f)^{13}$ electron configuration, $^2F_{5/2}$, and it lies around 8800 cm^{-1}, so that the whole spectral range between 12000 and 47000 cm^{-1} covered in the present study consists of pure 4f-5d excitations, without any interference from higher 4f-4f excited states. In Refs. [6] we show that the light-emission properties of the title materials are unusual and interesting, possibly also with respect to future applications. A particularly interesting feature is the unprecedented observation of light-emission from higher-excited 4f-5d states and the resulting occurrence of upconversion processes [20]. The present study helps to clarify the excited state situation. It also shows that a reasonable level of understanding can be achieved using a very simple picture, without trying to model all the excited state splittings quantitatively.

[1] J. Rubio, J. Phys. Chem. Solids **52**, 101 (1991).
[2] G. Blasse and B. C. Grabmeier, *Luminescent materials* (Springer Verlag Berlin, 1994).
[3] K. Holliday, C. Wei, M. Croci, and U. P. Wild, J. Lumin. **53**, 227 (1992).
[4] S. Kück, Appl. Phys. B **72**, 515 (2001).
[5] J. Grimm and H. U. Güdel, Chem. Phys. Lett. **404**, 40 (2005).
[6] J. Grimm, J. F. Suyver, E. Beurer, G. Carver, and H. U. Güdel, J. Phys. Chem. B (2005), accepted.
[7] H.-J. Seifert and U. Langenbach, Z. anorg. allg. Chem. **368**, 36 (1969).
[8] H.-J. Seifert and D. Haberhauer, Z. anorg. allg. Chem. **491**, 301 (1982).
[9] Z. J. Kiss, Phys. Rev. **127**, 718 (1962).
[10] O. S. Wenger, C. Wickleder, K. W. Krämer, and H. U. Güdel, J. Lumin. **94-95**, 101 (2001).
[11] J. F. Suyver, A. Aebischer, D. Biner, P. Gerner, J. Grimm, S. Heer, K. W. Krämer, C. Reinhard, and H. U. Güdel, Opt. Mat. **27**, 1111 (2005).
[12] F. Auzel, Chem. Rev. **104**, 139 (2004).
[13] L. van Pieterson, M. Heeroma, E. de Heer, and A. Meijerink, J. Lumin. **91**, 177 (2000).
[14] E. Loh, Phys. Rev. **175**, 533 (1968).
[15] R. C. Alig, R. C. Duncan, and B. J. Mokross, J. Chem. Phys **59**, 5837 (1973).
[16] P. Dorenbos, J. Phys. Cond. Matter **15**, 575 (2003).
[17] P. Dorenbos, J. Lumin. **91**, 155 (2000).
[18] G. H. Dieke, *Spectra and Energy Levels of Rare Earth Ions in Crystals* (John Wiley & Sons, 1968).
[19] P. Dorenbos, J. Phys. Cond. Matter **15**, 6249 (2003).
[20] E. Beurer, J. Grimm, P. Gerner, and H. U. Güdel, submitted to J. Am. Chem. Soc.

Upconversion Between 4*f*-5*d* Excited States in Tm^{2+} Doped CsCaCl$_3$, CsCaBr$_3$ and CsCaI$_3$

J. Grimm, E. Beurer, and P. Gerner

Department of Chemistry and Biochemistry, University of Bern, Freiestrasse 3, 3012 Bern, Switzerland

Near-infrared to visible upconversion luminescence in CsCaCl$_3$:Tm^{2+}, CsCaBr$_3$:Tm^{2+} and CsCaI$_3$:Tm^{2+} is presented and analyzed. The upconversion process involves exclusively the 4*f*-5*d* excited states of Tm^{2+}, which is a novelty among upconversion materials. The presence of more than one long-lived 4*f*-5*d* excited state is the prerequisite for this. Multiple emissions from Tm^{2+} are observed in the title compounds. This is made possible by the favorable energy structure within the 4*f*-5*d* states and the low phonon energies of the materials. The energy positions of the relevant 4*f*-5*d* states and thus the photophysical and light emission properties are affected by the chemical variation along the series. The UC efficiency increases from chloride to iodide and the upconversion mechanism is found to be a combination of absorption and energy transfer steps.

I. INTRODUCTION

Light emitting inorganic materials that are able to emit visible (VIS) light upon excitation in the near-infrared (NIR) in a so-called upconversion (UC) process have received considerable attention in the past [1, 2]. UC is a well-established and efficient non-linear optical process. It does not require coherent pump radiation in contrast to other non-linear optical processes like second-harmonic generation (SHG) or two-photon-absorption (TPA). Since nowadays light emitting diodes with extremely high energy efficiencies are available as pump sources in the NIR, UC processes are attractive for future technologies. As a consequence, UC materials are investigated for use as lasing media [3], for application in displays [4], for use in immunoassays and bio-labeling [5] as well as for improving the efficiency of solar cells [6].

A second fundamental difference of UC compared to SHG and TPA is that the former process requires at least two metastable excited states. This basic prerequisite reduces the number of potential upconversion systems because the majority of light emitting materials has just one emissive state, usually the first excited state. Exceptions are most trivalent lanthanides. Thus, it is not surprising that the vast majority of UC studies involve the 4*f*-4*f* transitions of lanthanide doped materials. In addition, a few upconversion systems based on *d*-*d* transitions in transition metal doped materials exist. But they usually suffer from low efficiencies. However, UC is not restricted to transitions within the 4*f* states of lanthanides, the *d* states of transition metals or a combination of both. Any luminescent material that exhibits multiple emissions is a potential candidate for UC.

Recent investigations of the optical spectroscopic properties of Tm^{2+} revealed that this ion is capable of emitting light from more than one excited state. The number of observed Tm^{2+} transitions is highly dependent on the host lattice [7–10]. In all lattices sharp and long-lived 4*f*-4*f* emission is found in the NIR. At higher energies, broad and fast decaying emission bands are observed that originate from the 4*f*-5*d* states of Tm^{2+}. UC between 4*f*-4*f* and 4*f*-5*d* states was demonstrated a few years ago in

SrCl$_2$:Tm^{2+} [9]. A new type of UC process involving exclusively the 4*f*-5*d* states of Tm^{2+} was reported recently for CsCaI$_3$:Tm^{2+} [11]. In the present contribution, an extended study on the entire CsCaX$_3$ (X = Cl, Br, I) series is presented. The spectroscopic properties of Tm^{2+} are affected by the chemical variation of the compounds. This is ideal to achieve a more thorough understanding of the 4*f*-5*d* UC properties of this ion. The samples were studied under the same experimental conditions and we find that the UC efficiency increases along the halide series. The UC mechanism is found to be a combination of the two most prominent UC processes, which involve absorption and energy transfer steps.

II. EXPERIMENTAL SECTION

A. Synthesis and Crystal Growth

Single crystals of CsCaCl$_3$, CsCaBr$_3$ and CsCaI$_3$ doped with Tm^{2+} were grown by the Bridgman technique. For the synthesis, stoichiometric amounts of CsX (X=Cl, Br, I) and CaX$_2$ were mixed. Tm^{2+} was prepared in situ by synproportionation of TmX$_3$ (prepared via the ammonium halide route from 99.999% pure Tm$_2$O$_3$ from Johnson Matthey) and Tm metal (Alfa Aesar 99.9%). The absolute concentration of Tm in the crystals was determined with ICP-OES and is 1.04%, 0.48% and 0.76% in CsCaCl$_3$, CsCaBr$_3$ and CsCaI$_3$, respectively. The use of tantalum rather than the more commonly used silica ampoules is indispensable for obtaining crystals that contain no Tm^{3+}. Crystals grown from silica ampoules contain trace amounts of Tm^{3+} because under such crystal growth conditions Tm^{2+} is easily oxidized by silica. Due to the hygroscopic nature of the starting materials as well as the crystals, the handling occurred under inert atmosphere at all times. For absorption measurements the samples were polished in a dry box and enclosed in an air-tight copper cell. Thermal contact of the crystal with the sample holder was provided through application of copper grease (Lake Shore Cryotronics Inc.). For luminescence measurements the samples were sealed

into quartz ampoules under partial pressure of He, which serves as an inert atmosphere as well as a heat transmitter.

B.   Spectroscopic Measurements

Sample cooling was achieved with a closed-cycle cryostat (Air Products) for absorption and with the He gas flow technique for emission measurements. Absorption spectra were recorded on a Cary 6000i spectrometer (Varian).

For upconversion measurements, the samples were excited with one or two multimode standing wave Ti:sapphire lasers (Spectra Physics 3900S), pumped by the second harmonic of a Nd:YVO$_4$ laser (Spectra Physics Millennia Xs) or by an argon-ion laser in all-lines mode (Spectra Physics 2045-15/4S). The wavelength control of the Ti:sapphire laser was achieved by an inchworm-driven (Burleigh PZ-501) birefringent filter and a wavemeter (Burleigh WA2100). The sample luminescence was dispersed either with a 0.85 m double monochromator (Spex 1402) or a 0.75 m single monochromator (Spex 1702). A cooled PMT (Hamamatsu P3310-01) and a photon counting system (Stanford Research 400) or a Ge detector (ADC 403L) interfaced to a lock-in amplifier (Stanford Research 830) were used for detection of the signal in the visible and infrared range, respectively. The laser power was measured with a power meter (Coherent Labmaster Ultima) and the laser beam was focused using a $f = 53$ mm lens. The typical excitation density was 4.7 kW/cm^2 for the one-color upconversion experiments. The excitation densities used for the two-color upconversion experiments were of the order of 0.34 kW/cm^2 for laser 1 and about 8.3 kW/cm^2 for laser 2. To measure the power dependence, the beam was attenuated with a series of neutral density filters (Balzers). For time resolved measurements 10 ns pulses of the second harmonic of a Nd:YAG (Quanta Ray DCR 3, 20 Hz) pumped dye laser (Lambda Physik FL 3002; pyridine 1 in methanol) were used. Transient signals were detected as described above using a multichannel scaler (Stanford Research 430).

All luminescence spectra are corrected for the sensitivity of the detection system and are displayed as photon counts versus energy [12].

III.   RESULTS

In Fig. 1 the 10 K absorption spectra of CsCaCl$_3$:Tm^{2+} (a), CsCaBr$_3$:Tm^{2+} (b) and CsCaI$_3$:Tm^{2+} (c) are displayed. A weak and sharp 4f-4f absorption transition is observed around 8800 cm^{-1} in all three samples. Note the scaling factor for this transition. The position as well as the band shape does not vary much along the series. The energy range extending from 12000 cm^{-1} in the NIR up to the UV is the region of the 4f-5d transitions of
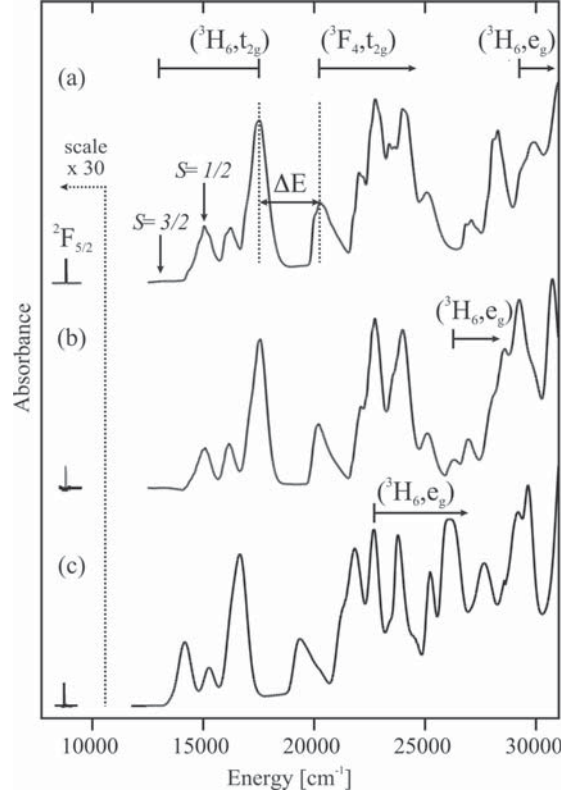
FIG. 1: 10 K absorption spectrum of (a) CsCaCl$_3$:1.04% Tm^{2+}, (b) CsCaBr$_3$:0.48% Tm^{2+} and (c) CsCaI$_3$:0.76% Tm^{2+}. The observed absorption transitions in this region are due to the Tm^{2+} 4f-4f and 4f-5d transitions from the ^{2}F$_{7/2}$ groundstate. The assignment of the absorption bands is given on top of the CsCaCl$_3$:Tm^{2+} spectrum. Note the scaling factor for the ^{2}F$_{5/2}$ transition. (^{3}H$_6$,e$_g$) is indicated for all three compounds because the onset of the e$_g$ shifts to lower energies along the series. The energy gap ΔE is relevant for the emission properties of the three samples.

Tm^{2+}. 4f-5d transitions are parity allowed and thus high absorption intensities are observed. The energy gap ΔE between the (^{3}H$_6$,t$_{2g}$) and (^{3}F$_4$,t$_{2g}$) multiplets, which is indicated in Fig. 1, is relevant for the emission properties and its exact value is given in Table I for the three compounds.

Fig. 2 shows the 10 K UC emission spectra of the three samples (full lines) and the UC excitation scans (dotted lines). All the samples are excited with the same laser power density of approximately 4.7 kW/cm^2. The number of observed emissions depends on the host lattice. Up to five distinct emission band systems are observed. Emissions C, D and F are the UC emissions, whereas B and A correspond to downconversion emissions. The 10 K maxima of emissions B, C, D and F as well as the origin of emission A are given in Table I. The assignment of the
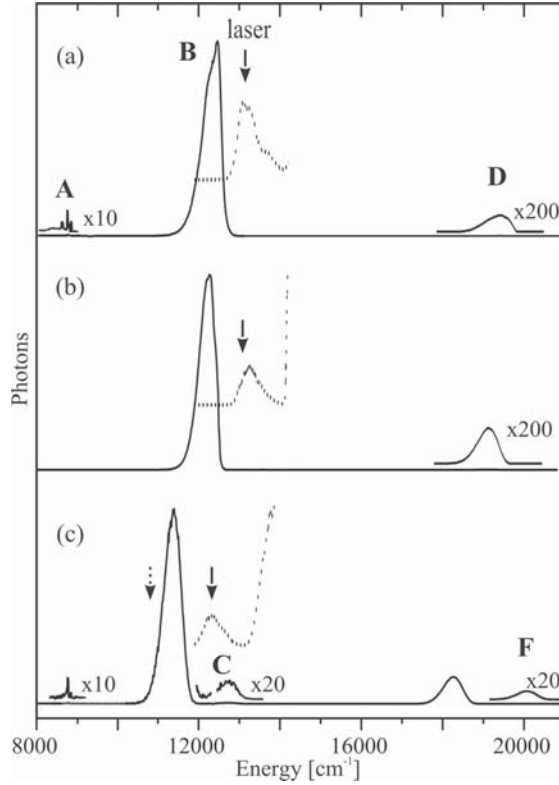
FIG. 2: Overview UC emission spectra at 10 K of (a) CsCaCl$_3$:1.04% Tm^{2+}, (b) CsCaBr$_3$:0.48% Tm^{2+} and (c) CsCaI$_3$:0.76% Tm^{2+} photoexcited at 13150 cm^{-1}, 13100 cm^{-1} and 12350 cm^{-1}, respectively, see full arrows. The labeling of the emission bands is given on top of the CsCaCl$_3$:Tm^{2+} and CsCaI$_3$:Tm^{2+} spectra, respectively. Note the scaling factors for the various emission bands. The insets (dotted lines) correspond to the 10 K UC excitation scans of (a) CsCaCl$_3$:Tm^{2+} monitored at 19450 cm^{-1}, (b) CsCaBr$_3$:Tm^{2+} monitored at 19070 cm^{-1} and (c) CsCaI$_3$:Tm^{2+} monitored at 18250 cm^{-1}. The dotted arrow in (c) corresponds to the excitation energy of laser 2 in the two-color experiment.

bands will be discussed in Section IV B. The UC excitation scans were obtained by monitoring at the maximum of emission D while the laser was scanned in the region of the low-energy tail of the (^{3}H$_6$,t$_{2g}$) absorption (see Fig. 1). The dotted arrow in Fig. 2 (c) corresponds to the excitation energy of laser 2 in the two-color experiment (see below).

In Fig. 3 the intensity of emissions D and B of CsCaI$_3$:Tm^{2+} is shown in a double logarithmic representation as a function of the exciting laser power in an UC experiment. Emission D depends quadratically on the laser power as evidenced by the slope of 1.93 obtained from a fit of the data (Fig. 3 (a)). In contrast, emission B shows a linear dependence on the laser power, with a
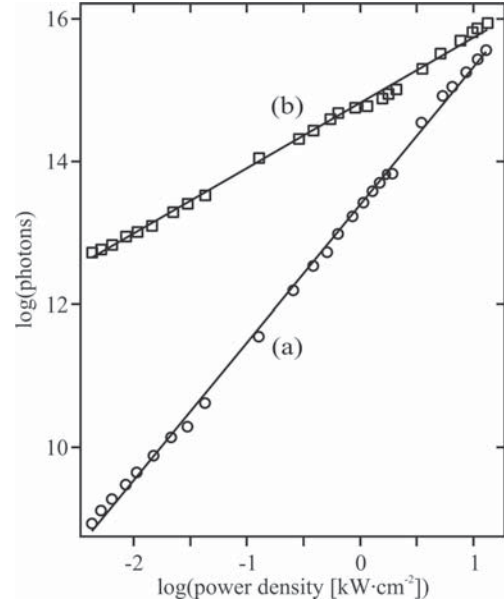
FIG. 3: 10 K power dependence of the photons emitted of (a) the VIS UC emission band D and (b) the NIR emission band B of CsCaI$_3$:Tm^{2+} in a double-logarithmic representation. Laser excitation of the sample occurred at 12350 cm^{-1}. The straight lines correspond to linear fits to the logarithmic data with slopes of (a) 1.93 and (b) 0.92.

slope of 0.92 (Fig. 3 (b)). The same experiment yields slopes of 1.8 and 1.7 for emission D in CsCaCl$_3$:Tm^{2+} and CsCaBr$_3$:Tm^{2+}, respectively, and 1.1 for emission B in CsCaBr$_3$:Tm^{2+} (data not shown).

Fig. 4 shows the temporal evolution of the 10 K luminescence intensity of emission D in the three samples after 10 ns excitation pulses at 14450 cm^{-1} into the (^{3}H$_6$,t$_{2g}$) multiplet. All three curves can be fitted by double exponential decay functions. The decay times found are: 19 μs and 101 μs in CsCaCl$_3$:Tm^{2+}, 1.7 μs and 26 μs in CsCaBr$_3$:Tm^{2+} and 3.9 μs and 13.1 μs in CsCaI$_3$:Tm^{2+}. The decay curves are relevant for the identification of the upconversion mechanism and will be discussed later.

In Fig. 5 the intensity of the UC emission D of CsCaI$_3$:Tm^{2+}, monitored at 18250 cm^{-1}, is shown for various combinations of two exciting lasers. In this two-color experiment, a Ti-sapphire laser (laser 1) was used with a typical excitation power density of 0.34 kW/cm^2 to pump at 12350 cm^{-1} (full arrow in Fig. 2 (c)). At this energy Tm^{2+} ground-state absorption occurs into the (^{3}H$_6$,t$_{2g}$) and thus Tm^{2+} UC is induced (Fig. 5 (b)). Laser 2 was used to pump at 10800 cm^{-1}, which is below the onset of the (^{3}H$_6$,t$_{2g}$) absorption (dotted arrow in Fig. 2 (c)). This laser had a high power density (typically 8.3 kW/cm^2). This laser alone induces no upconversion emission D as can be seen from a comparison of Fig. 5

TABLE I: Compiled data of the spectroscopic properties of the title compounds. $\hbar\omega_{max}$ is the highest vibrational frequency in the three lattices. ΔE is the energy difference between the ($^3F_4$,t_{2g}) and the ($^3H_6$,t_{2g}) absorption multiplets at 10 K, see Fig. 1. Em A denotes the origin of emission A whereas Em B, Em C, Em D and Em F correspond to the maxima of the respective emissions at 10 K. UC Exc. is the excitation energy for the UC process. η_{UC} is a measure for the upconversion efficiency at 10 K and is defined in the text. The quenching temperature T_Q (Em D) is the temperature at which the intensity of the UC emission D drops below 10% of the intensity at 10 K.

Compound	$\hbar\omega_{max}$[a] [cm^{-1}]	ΔE [cm^{-1}]	Em A [cm^{-1}]	Em B [cm^{-1}]	Em C [cm^{-1}]	Em D [cm^{-1}]	Em F [cm^{-1}]	UC Exc. [cm^{-1}]	η_{UC}[b] [%]	T_Q (Em D) [K]
CsCaCl$_3$:Tm^{2+}	310	2760	8810	12497	–	19450	–	13150	0.1	75
CsCaBr$_3$:Tm^{2+}	210	2620	–	12237	–	19152	–	13100	0.2	125
CsCaI$_3$:Tm^{2+}	170	2700	8785	11348	12703	18344	20110	12350	11	275

[a] taken from Ref. [10].
[b] Excitation power density: 4.7 kW/cm^2.
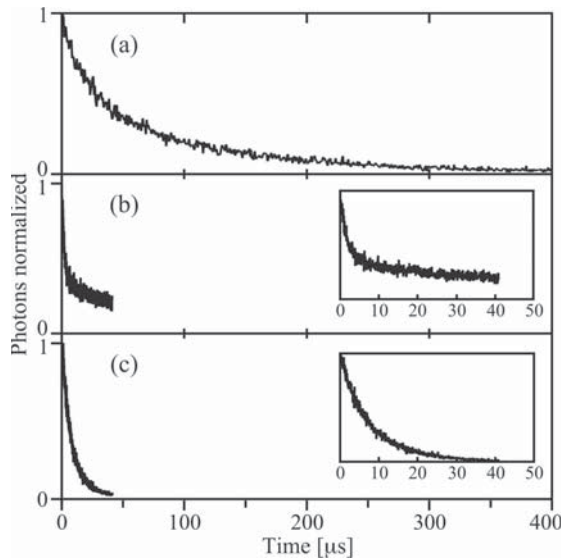
FIG. 4: Time evolution of emission D at 10 K after 10 ns pulsed excitation at 14450 cm^{-1} in (a) CsCaCl$_3$:Tm^{2+}, (b) CsCaBr$_3$:Tm^{2+} and (c) CsCaI$_3$:Tm^{2+}. The insets in (b) and (c) show the same data on an expanded time scale.

FIG. 5: Intensity of emission D in the two-color laser UC experiment in CsCaI$_3$:Tm^{2+} with laser 1 at 12350 cm^{-1} (0.34 kW/cm^2), see full arrow in Fig. 2 (c), and laser 2 at 10800 cm^{-1} (8.3 kW/cm^2), see dotted arrow in Fig. 2 (c). The time sequence corresponds to the following combinations of the lasers: (a) lasers 1 and 2, (b) only laser 1, (c) only laser 2, (d) both lasers blocked.

IV. ANALYSIS AND DISCUSSION

A. Materials and Site Symmetries

CsCaCl$_3$ and CsCaBr$_3$ are cubic perovskites at room temperature that crystallize in the $Pm3m$ space group [13, 14]. Tm^{2+} replaces Ca^{2+} on a crystallographic site with O_h point symmetry. Upon cooling both samples undergo phase transitions. The site symmetry of Ca^{2+} below the phase change is C_{4h} in CsCaCl$_3$ [15]. At 10 K CsCaBr$_3$ crystallizes in the orthorhombic $Pnma$ phase which is the phase that is also found for CsCaI$_3$ in the temperature range between 10 and 300 K [16]. The Ca^{2+} in the orthorhombic $Pnma$ phase has site symmetry C_i. Regardless of the phase changes, the Tm^{2+} ion is always
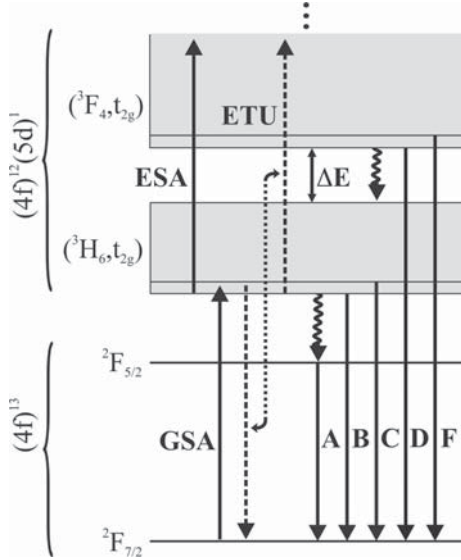
(c) and (d), where the intensity of emission D is at the dark-count level. The combination of the two lasers results in a more than twofold increase of the UC emission compared to the sum of the UC intensity of the two individual lasers, see Fig. 5 (a) and (b). This result will be discussed together with the transients (Fig. 4) in connection with the upconversion mechanism.

FIG. 6: Schematic energy level diagram for Tm^{2+} doped CsCaCl$_3$, CsCaBr$_3$ and CsCaI$_3$ with the relevant radiative (straight arrows) and non-radiative processes (curly and dotted arrows, respectively). GSA, ESA and ETU stand for groundstate absorption, excited state absorption and energy transfer upconversion, respectively. They are the relevant processes in UC. The energy gap ΔE is indicated in Fig. 1. The labeling of the emission bands corresponds to Fig. 2 and the electronic transitions to which they refer are explained in Section IV B.

coordinated by six X$^-$–ions (X$^-$=Cl, Br, I). From the spectroscopic data of the three samples we conclude that the only band splitting due to symmetry reduction is observable in the 4f-4f transitions and is in the order of a few wavenumbers [10]. The data interpretation is therefore done in the octahedral approximation.

B. Assignment of States

The assignment of the excited states and the emission bands has already been discussed for the three compounds in Refs. [10, 17]. A brief recapitulation is given here. Fig. 6 shows the energy level diagram of the spectroscopically relevant excited states of Tm^{2+} as well as the observed transitions.

Tm^{2+} has a (4f)^{13} ground state electron configuration, i. e. it corresponds to a one-hole system and is isoelectronic with Yb^{3+}. There are only two multiplets arising from the (4f)^{13} electron configuration which are the ^{2}F$_{7/2}$ groundstate and the ^{2}F$_{5/2}$ first excited state. The sharp 4f-4f transitions are observed in absorption and emission (labeled A) around 8800 cm^{-1}, see Figs. 1 and 2.

In the absorption spectra of Fig. 1 all bands above 10000 cm^{-1} are due to 4f-5d transitions. They are be-

tween 1 and 4 orders of magnitude more intense than the intraconfigurational 4f-4f transitions because they are parity-allowed [18–20]. The excited states arise from the (4f)^{12}(5d)^1 configuration. This has a total degeneracy of 910, and energy splittings occur as a result of various interactions.

An important interaction in the (4f)^{12}(5d)^1 configuration is the ligand field interaction of the 5d electron. The octahedral ligand field splits the 5d orbitals into t$_{2g}$ and e$_g$ sets, separated by 10Dq. The octahedral (O_h) coordination of Tm^{2+} in all three samples causes the t$_{2g}$ to be lower in energy than the e$_g$. The (4f)^{12} part is split into the $^{2S+1}L_J$ terms of Tm^{3+} by the Coulomb repulsion and the spin-orbit coupling of the 4f electrons. Thus, the energy multiplets of the Tm^{2+} (4f)^{12}(5d)^1 configuration can be roughly characterized as ($^{2S+1}$L$_J$,t$_{2g}$) and ($^{2S+1}$L$_J$,e$_g$), see Fig. 1. For Tm^{2+} we expect each of these multiplets to be split into a set of high-spin $S = 3/2$ and a set of low-spin $S = 1/2$ states due to the isotropic exchange part of the Coulomb interaction between the 4f and 5d electrons. Due to Hund's rule, the former lie lower in energy. As a consequence, transitions from the ^{2}F$_{7/2}$ groundstate to the lowest energy 4f-5d bands are expected to have formally spin-forbidden character. This is expressed in weaker oscillator strengths compared to the spin-allowed bands [18, 20, 21]. The first spin-forbidden and spin-allowed bands are marked with arrows in Fig. 1.

The 5d-4f emission bands in Fig. 2 are assigned to the following transitions: Band B is a spin-forbidden 5d-4f transition from (^{3}H$_6$,t$_{2g}$)$S = 3/2$ to ^{2}F$_{7/2}$. The corresponding weak absorption band is hardly seen in Fig. 1, but clearly observable in the UC excitation scans in Fig. 2. In CsCaI$_3$:Tm^{2+} a spin-allowed emission from the first (^{3}H$_6$,t$_{2g}$)$S = 1/2$ state to the groundstate is observed and labeled emission C. Band D is assigned to a transition from the lowest excited state of the (^{3}F$_4$,t$_{2g}$) multiplet to the ^{2}F$_{7/2}$ groundstate. The spin of the emitting (^{3}F$_4$, t$_{2g}$) state is not specified because spin ceases to be a good quantum number in the higher multiplets [10, 22]. In CsCaI$_3$:Tm^{2+}, a very weak emission F at energies higher than emission D is observed, originating in a higher excited state of the (^{3}F$_4$,t$_{2g}$) multiplet. A schematic picture of these radiative transitions is given in Fig. 6.

C. 4f-5d to 4f-5d Upconversion in Tm^{2+}

Excitation into the spin-forbidden component of the (^{3}H$_6$,t$_{2g}$) leads to the observation of multiple luminescences in the title compounds at 10 K, see Fig. 2. Emission D is the dominant UC luminescence in all three samples. The intensity of emission D depends quadratically on the excitation power, see Fig. 3 (a). This confirms that it is created in a two-photon type excitation. At 10 K the large size of the energy gap ΔE prevents efficient multiphonon relaxation from (^{3}F$_4$,t$_{2g}$) to (^{3}H$_6$,t$_{2g}$), espe-

cially in the bromide and iodide, see also Ref. [10]. Most of the energy in (^{3}F$_{4}$, t$_{2g}$) is therefore emitted radiatively in emission band D in a bromide and iodide environment.

For excitation into the (^{3}H$_{6}$,t$_{2g}$)S = 1/2 multiplet, emission B dominates the emission spectrum in all samples at 10 K. This is not surprising, because direct pumping in the (^{3}H$_{6}$,t$_{2g}$)S = 3/2 absorption band occurs. The intensity of emission B depends linearly on power (Fig. 3 (b)). Multiphonon relaxation from (^{3}H$_{6}$, t$_{2g}$)S = 3/2 to ^{2}F$_{5/2}$ populates the ^{2}F$_{5/2}$ multiplet (see curly arrow in Fig. 6). Emission A, which originates in this state, is not observed at 10 K in the bromide. It does come up with temperature, but only above 130 K.

The emission properties were also studied as a function of temperature under UC excitation. The intensity of emission D decreases with increasing temperature in all samples. However, the quenching temperatures T$_{Q}$ (Em D) are different for the three samples as can be seen from Table I. We define T$_{Q}$ (Em D) as the temperature where the intensity drops below 10% of the intensity at 10 K. T$_{Q}$ (Em D) increases along the series. This trend is also observed in downconversion where the quenching of emission D occurs at similar temperatures [10]. The shift of T$_{Q}$ (Em D) is ascribed to the decreased phonon energies along the series, see Table I.

D. Upconversion Mechanisms

The temporal behavior of the UC luminescence is used to distinguish between potential UC mechanisms. The two most prominent mechanisms are a sequence of ground state absorption (GSA) and excited state absorption (ESA) or GSA and energy transfer upconversion (ETU) steps [23]. GSA/ESA is usually a one-ion process whereas GSA/ETU is a two-ion process. The signature of the former is immediate decay of the UC emission with the intrinsic decay time of the upper excited state. The signature of the latter is the observation of a rise from zero that is correlated with the decay of upper excited state and a subsequent decay with half the lifetime of the intermediate excited state. A combination of the two mechanisms leads to a more complicated picture: When a higher percentage of the UC ions proceeds via GSA/ESA an immediate decay is expected, whereas in case of a higher GSA/ETU percentage a rise (not from zero) is observed.

The transients of emission D measured in UC are shown in Fig. 4 and the decay times are given in Section III. Direct excitation into the 4f-5d absorption bands above (^{3}F$_{4}$, t$_{2g}$) with short pulses yields single exponential decay curves of emission D with lifetimes of 904 ns, 1.7 μs and 1.1 μs for CsCaCl$_{3}$:Tm^{2+}, CsCaBr$_{3}$:Tm^{2+} and CsCaI$_{3}$:Tm^{2+}, respectively. The lifetime of emission B is 296 μs, 323 μs and 391 μs for CsCaCl$_{3}$:Tm^{2+}, CsCaBr$_{3}$:Tm^{2+} and CsCaI$_{3}$:Tm^{2+}, respectively [10]. The immediate fast decay of emission D in the bromide is a clear signature of a GSA/ESA

process whereas the long decay in the chloride points to GSA/ETU. The UC transients thus bear no clear signature of either the GSA/ESA or the GSA/ETU mechanism. The two-color experiment shown in Fig. 5 provides evidence that some GSA/ESA is present. One would not expect to see a difference between Fig. 5 (a) and (b) if the mechanism was exclusively GSA/ETU. The transients indicate that the situation complicated, and they point to the existence of several UC species in the samples. Very often a subset of the luminescent ions participates in UC that may be different from the main species observed in downconversion [24]. This is especially true for a GSA/ETU, as these ions need to be in close proximity to each other because of the inherent two-ion process. For GSA/ETU it is generally not straightforward to interpret the measured transients in an unambiguous way. We conclude that we observe a combination of the two mechanisms in the three samples with various ratios of GSA/ESA and GSA/ETU. This is schematically shown in Fig. 6.

E. Upconversion Efficiency

The intensity distribution among the observed emission bands is very different in the title compounds. This leads to very different efficiencies for the UC process. The efficiency of the UC process is defined as:

$$\eta_{UC} = \frac{\text{Photons}_{\text{VIS}}}{\text{Photons}_{\text{NIR}} + 2 \cdot \text{Photons}_{\text{VIS}}}.$$

The efficiency of the UC process was determined from spectra that were measured under identical conditions. The efficiencies for the three systems under 4.7 kW/cm^{2} excitation density at 10 K are: 0.1% in CsCaCl$_{3}$:Tm^{2+}, 0.2% in CsCaBr$_{3}$:Tm^{2+} and 11% in CsCaI$_{3}$:Tm^{2+}, see also Table I. As a general trend, the efficiency increases along the series. The difference in the efficiency between the chloride and the bromide can be caused by the increased multiphonon relaxation processes in the chloride and/or by the different UC mechanisms. In CsCaCl$_{3}$ the highest phonon energy is higher than in CsCaBr$_{3}$, see Table I. Increased multiphonon relaxation in CsCaCl$_{3}$:Tm^{2+} quenches the intensity of emission D in downconversion already at 10 K [10]. Therefore it is possible that the increased multiphonon processes will also reduce the UC efficiency in CsCaCl$_{3}$:Tm^{2+} relative to CsCaBr$_{3}$:Tm^{2+}. As discussed in the previous section, the UC process in the title compounds is a combination of GSA/ESA and GSA/ETU. This potentially causes differences in the UC efficiency since the two processes might involve different sets of ions. Surprisingly, the efficiency in the iodide is increased by almost two orders of magnitude compared to the two other samples. Reduced loss processes due to hindered multiphonon relaxation cannot account for this difference. In downconversion, the relative percentage of emission D in the bromide and iodide is

comparable at 10 K [10]. It is unlikely that the UC mechanism will cause this increase of efficiency of about two orders of magnitude. However, the energy level structure of the iodide is such that the second UC step occurs into the e_g levels. In the bromide the second step ends just below the onset of e_g and in the chloride it is far from reaching the e_g, see Fig. 1. The high efficiency in the iodide might thus be ascribed to the more favorable energy structure for UC because it enables a much more efficient second step in the process.

V. CONCLUSIONS AND OUTLOOK

The experimental findings clearly show the existence of upconversion processes between the $4f$-$5d$ states of Tm^{2+} in the title compounds. This type of UC is without precedent. Usually rapid multiphonon relaxation between the $4f$-$5d$ states prevents emission from higher excited $4f$-$5d$ states. In the title compounds the observation of more than one $5d$-$4f$ emission is made possible due to the favorable energy structure of the $4f$-$5d$ states with a large energy gap ΔE between $(^3F_4, t_{2g})$ and $(^3H_6, t_{2g})$. Other important factors for the observation of emission D are the low phonon energies of the lattices. The present study demonstrates that UC processes are not restricted to $4f$-$4f$ transitions in lanthanides and some special cases of transition metal doped materials.

The efficiency of 11% in $CsCaI_3$:Tm^{2+} at 10 K is impressive, also compared to other very efficient UC materials. First investigations of the $RbCaI_3$:Tm^{2+} compounds reveals that the UC efficiency in this material is even higher than in $CsCaI_3$:Tm^{2+}. A thorough investigation of this compound is the subject of work in progress. The chemical variation of the Tm^{2+} doped materials is a powerful tool by which the spectroscopic and thus UC properties can be influenced. This opens many possibilities for further investigations on Tm^{2+}.

[1] F. Auzel, Chem. Rev. **104**, 139 (2004).
[2] J. F. Suyver, A. Aebischer, D. Biner, P. Gerner, J. Grimm, S. Heer, K. W. Krämer, C. Reinhard, and H. U. Güdel, Opt. Mat. **27**, 1111 (2005).
[3] M. F. Joubert, Opt. Mater. **11**, 181 (1999).
[4] M. L. F. Phillips, M. P. Hehlen, K. Nguyen, J. M. Sheldon, and N. J. Cockroft, Proc. Electrochem. Soc. **99-40**, 123 (2000).
[5] S. Heer, K. Kömpe, H. U. Güdel, and M. Haase, Adv. Mat. **16**, 2102 (2004).
[6] A. Shalav, B. S. Richards, T. Trupke, K. W. Krämer, and H. U. Güdel, Appl. Phys. Lett. **86**, 013505 (2005).
[7] W. J. Schipper, A. Meijerink, and G. Blasse, J. Lumin. **62**, 55 (1994).
[8] C. Wickleder, J. Alloys Comp. **300-301**, 193 (2000).
[9] O. S. Wenger, C. Wickleder, K. W. Krämer, and H. U. Güdel, J. Lumin. **94-95**, 101 (2001).
[10] J. Grimm, J. F. Suyver, E. Beurer, G. Carver, and H. U. Güdel, J. Phys. Chem. B (2005), accepted.
[11] E. Beurer, J. Grimm, P. Gerner, and H. U. Güdel, J. Am. Chem. Soc. (2005), submitted.
[12] J. Eijder, J. Opt. Soc. Am. **59**, 223 (1969).
[13] H.-J. Seifert and U. Langenbach, Z. anorg. allg. Chem.

368, 36 (1969).
[14] H.-J. Seifert and D. Haberhauer, Z. anorg. allg. Chem. **491**, 301 (1982).
[15] Y. Vaills, J. Y. Buzaré, A. Gibaud, and C. Lunay, Solid State Comm. **60**, 139 (1986).
[16] G. Schilling and G. Meyer, Z. anorg. allg. Chem. **622**, 759 (1996).
[17] J. Grimm, E. Beurer, and H. U. Güdel, Inorg. Chem. (2005), submitted.
[18] D. S. McClure and Z. J. Kiss, J. Chem. Phys. **39**, 3251 (1963).
[19] L. van Pieterson, M. F. Reid, R. T. Wegh, S. Soverna, and A. Meijerink, Phys. Rev. B **65**, 045113 (2002).
[20] L. van Pieterson, M. F. Reid, G. W. Burdick, and A. Meijerink, Phys. Rev. B **65**, 045114 (2002).
[21] P. Dorenbos, J. Phys. Cond. Matter **15**, 575 (2003).
[22] P. Dorenbos, J. Phys. Cond. Matter **15**, 6249 (2003).
[23] D. R. Gamelin and H. U. Güdel, *Topics in Current Chemistry*, vol. 214 (Edited by H. Yersin, Springer Verlag Berlin, 2001).
[24] S. Garcia-Revilla, P. Gerner, H. U. Güdel, and R. Valiente, Phys. Rev. B **72**, 125111 (2005).

4*f*-4*f* and 4*f*-5*d* Excited States and Luminescence Properties of Tm^{2+} in CaF$_2$, CaCl$_2$, SrCl$_2$ and BaCl$_2$

Judith Grimm

An overview of the spectroscopic properties of Tm^{2+} doped CaF$_2$, CaCl$_2$, SrCl$_2$ and BaCl$_2$ is presented. The absorption and emission spectra of Tm^{2+} in solids are composed of two types of electronic transitions: weak and sharp-line 4*f*-4*f* transitions below 9500 cm^{-1} and strong broad 4*f*-5*d* transitions at higher energies. The former are easily understood because of their analogy to the transitions in the isoelectronic Yb^{3+} and are observed in all title compounds in absorption and emission. Understanding of the 4*f*-5*d* transitions is more difficult because their position and bandshape is dependent on the crystal field, electron interactions and spin-orbit coupling in the $(4f)^{12}(5d)^1$ electron configuration. The 4*f*-5*d* transitions are very sensitive to the crystalline environment. The present series demonstrates very nicely that in addition to the chemical variation also the site symmetry and the coordination geometry of Tm^{2+} influences the 4*f*-5*d* transitions. 5*d*-4*f* emission is observed in all compounds, including previously unobserved emissions in CaF$_2$:Tm^{2+} and SrCl$_2$:Tm^{2+}.

I. INTRODUCTION

Investigations of the spectroscopic properties of Tm^{2+} are not very abundant [1]. The reason is that the preferred oxidation state of Tm in solids is the trivalent one. Nevertheless, Tm^{2+} can be successfully stabilized in compounds of the heavier halides [2]. The thermodynamic instability of Tm^{2+} in fluorides and oxides prevents the synthesis of pure TmF$_2$ or TmO and compounds thereof [3]. As a consequence, Tm^{3+} is inevitably present in Tm^{2+} doped fluorides and oxides. First investigations of the spectroscopic properties of Tm^{2+} appeared in the 1960's. These studies were done in CaF$_2$, SrF$_2$, BaF$_2$ and SrCl$_2$ [4–8]. Laser action was demonstrated in CaF$_2$:Tm^{2+} [9], and SrCl$_2$:Tm^{2+} was suggested as an infrared quantum counter [10]. Later, McClure and coworkers did a thorough investigation of the photoionization threshold of the Tm^{2+} doped fluorides [11, 12]. In the past ten years, spectroscopic studies on new classes of Tm^{2+} doped compounds appeared. In SrB$_4$O$_7$ [13], SrZnCl$_4$ and BaZnCl$_4$ [14], Tm^{2+} was found to emit not only from the 4*f*-4*f* excited state but also from the first 4*f*-5*d* excited state. The latter emission had not been observed in the Tm^{2+} doped fluorides. Tm^{2+} being a dual emitter prompted an upconversion study in SrCl$_2$:Tm^{2+} [15]. Recently, a systematic investigation on the Tm^{2+} doped CsCaCl$_3$, CsCaBr$_3$ and CsCaI$_3$ series was presented [16]. It was found that Tm^{2+} exhibits up to six different types of emission, the number of emissions being highly dependent on the host lattice. The observation of multiple 5*d*-4*f* emissions is rare. Literature reports on the coexistence of spin-forbidden and spin-allowed emission from the 4*f*-5*d* states in lanthanides with more than a half-filled shell exist [1, 17, 18]. However, the report of higher lying 5*d*-4*f* emission is without precedent. Upconversion involving exclusively the 4*f*-5*d* excited states was thereupon demonstrated for the first time [19].

Here, an overview of the spectroscopic properties of Tm^{2+} in a series of earth alkaline halides is presented. In addition to the chemical variation, also the symmetry of the Tm^{2+} site as well as the coordination geometry is varied along the series. The spectroscopic properties of Tm^{2+} are very sensitive to these variations, especially the 4*f*-5*d* transitions. Two of the title compounds, i.e. CaF$_2$:Tm^{2+} and SrCl$_2$:Tm^{2+}, were subject of previous investigations, see Refs. [4, 6, 15, 20]. Our study revealed the existence of previously unobserved 5*d*-4*f* emissions in these two host lattices. An analysis of the spectroscopic properties of Tm^{2+} doped into CaCl$_2$ and BaCl$_2$ has not been reported so far.

II. EXPERIMENTAL SECTION

A. Synthesis and Crystal Growth

Single crystals of CaF$_2$, CaCl$_2$, SrCl$_2$ and BaCl$_2$ doped with Tm^{2+} were grown by the Bridgman technique. Tm^{2+} was prepared in situ by synproportionation of TmX$_3$ (X=F, Cl) and Tm metal. The use of tantalum rather than the more commonly used silica ampoules was indispensable.

CaF$_2$:Tm^{2+} crystals were obtained from a starting mixture of CsF, CaF$_2$, TmF$_3$ and a 30-fold excess of Tm metal. The synthesis of CaF$_2$:Tm^{2+} was performed under inert atmosphere due to oxygen sensitive Tm metal. In fluorides Tm^{2+} is thermodynamically not stable (see Refs. [2, 3, 21]) and therefore the CaF$_2$:Tm^{2+} crystals contain trace amounts of Tm^{3+}. The CaF$_2$:Tm^{2+} crystals can be handled outside the glove box. No conversion of Tm^{2+} into Tm^{3+} was observed over a range of three years in the fluoride samples.

For the synthesis of the chlorides, MCl$_2$ (M=Ca, Sr, Ba) were mixed with TmCl$_3$ and a twofold excess of Tm metal. Due to the hygroscopic nature of the starting materials and the crystals, their handling occurred under inert atmosphere at all times. The absolute concentration of Tm in the chloride crystals (nominal concentration: 1%) was determined with ICP-OES and is 0.81%, 1.27% and 1.16% in CaCl$_2$, SrCl$_2$ and BaCl$_2$, respectively.

All crystals were checked for purity by X-ray powder diffraction. For absorption measurements the

SrCl$_2$:Tm^{2+} and BaCl$_2$:Tm^{2+} samples were polished. Due to the small size of the CaF$_2$:Tm^{2+} and CaCl$_2$:Tm^{2+} crystals, they could not be polished and all spectroscopic measurements were performed on untreated crystals. For absorption measurements, the samples were enclosed in an air-tight copper cell equipped with quartz windows. For luminescence measurements the chloride samples were sealed into quartz ampoules under partial pressure of He, which serves as an inert atmosphere as well as a heat transmitter.

B. Spectroscopic Measurements

Sample cooling was achieved with a closed-cycle cryostat (Air Products) for absorption and with the He gas flow technique for emission measurements. Absorption spectra were recorded on a Cary 6000i spectrometer (Varian). Emission spectra were excited with the 457.9 nm (21834 cm^{-1}) or 514.5 nm (19436 cm^{-1}) line of an Ar$^+$ laser (Spectra Physics 2060-10 SA). The sample luminescence was dispersed either with a 0.85 m double monochromator (Spex 1402) or a 0.75 m single monochromator (Spex 1702). A PMT (Hamamatsu P3310-01) and a photon counting system (Stanford Research 400) or a Ge detector (ADC 403L and 403HS) interfaced to a lock-in amplifier (Stanford Research 830) were used for detection of the signal in the visible and infrared range, respectively. The luminescence transients were measured with either the Ar$^+$ laser and an acousto-optic modulator (Coherent 305, Stanford Research DS 345 function generator) or the fundamental (1064 nm = 9398 cm^{-1}) or the third harmonic (355 nm = 28169 cm^{-1}) of a pulsed Nd:YAG laser (Quanta Ray DCR 3, 20 Hz). Transient signals were detected as described above using a multichannel scaler (Stanford Research 430) or an oscilloscope (Tektronix TDS 540a). All luminescence spectra are corrected for the sensitivity of the detection system and are displayed as photon counts versus energy.

III. RESULTS AND DISCUSSION

A. Structures and Site Symmetries

CaF$_2$ and SrCl$_2$ crystallize in the fluorite structure in space group *Fm3m* [22]. The Tm^{2+} ions replace Ca^{2+} and Sr^{2+} on site $4(a)$ with O_h point symmetry. The coordination of the Ca^{2+} and Sr^{2+} ion is eightfold, generating a cube around the central cation. The data interpretation of the spectroscopic properties of Tm^{2+} in these two lattices is done in O_h.

CaCl$_2$ crystallizes in the orthorhombic *Pnnm* phase [22]. In this phase Ca^{2+} has site symmetry C_{2h} and is coordinated by six Cl$^-$. The distortion of the octahedron is small. The data interpretation of the spectroscopic properties of Tm^{2+} in this lattice is done in the octahedral approximation because we are not able to assign

TABLE I: Ionic radii of Tm^{2+}, Ca^{2+}, Sr^{2+} and Ba^{2+} in sixfold coordination (values from Ref. [24]).

	Tm^{2+}	Ca^{2+}	Sr^{2+}	Ba^{2+}
Ionic radius [Å]	1.03	1.00	1.18	1.35

any splitting in the spectra to the lowering of the site symmetry from O_h to C_{2h}.

BaCl$_2$ crystallizes in the orthorhombic *Pnma* phase [23]. Ba^{2+} has site symmetry C_s and is coordinated by nine Cl$^-$ ions. It corresponds to an angular distortion of a tricapped trigonal prism. This low symmetry has to be taken into account for the data interpretation of the spectroscopic properties of Tm^{2+} in this lattice.

In Table I the ionic radii of Tm^{2+}, Ca^{2+}, Sr^{2+} and Ba^{2+} are displayed. Upon doping, the Tm^{2+} ion will replace the divalent cation in the crystal structure. From Table I it is seen that the ionic radii of Tm^{2+} and Ca^{2+} match perfectly. The deviation between Tm^{2+} and Sr^{2+} is larger and quite substantial for Tm^{2+} and Ba^{2+}. This will be important for the discussion of the spectroscopic properties of the BaCl$_2$:Tm^{2+} sample.

B. 4*f*-4*f* Transitions

Tm^{2+} has a $(4f)^{13}$ ground state electron configuration, i.e. it corresponds to a one-hole system and is isoelectronic with Yb^{3+}. There are two multiplets arising from the $(4f)^{13}$ electron configuration: $^2F_{7/2}$ and $^2F_{5/2}$. The sharp 4*f*-4*f* transitions are observed in absorption and emission below 9500 cm^{-1}, see Figs. 1–4. The energy of the $^2F_{5/2}$ multiplet is lowered compared to Yb^{3+}, reflecting the smaller spin-orbit-coupling in Tm^{2+} [4, 16].

The absorption and emission spectrum of CaF$_2$:Tm^{2+} (Figs. 1 (a) and (b)) was reported and analyzed before [4]. The assignment in Figs. 1 (a) and (b) is based on Ref. [4], and the electronic transitions are indicated in Fig. 1 (c). Tm^{2+} occupies a centrosymmetric site in CaF$_2$. Therefore the electronic origins arise by a magnetic dipole (MD) mechanism. In the 10 K absorption spectrum in Fig. 1 (a), the $\Gamma_7 \rightarrow \Gamma_7$' origin at 8961 cm^{-1} can be identified. The position of the $\Gamma_7 \rightarrow \Gamma_8$' origin is known from the literature and is located at 9377 cm^{-1} [4]. The $\Gamma_6 \leftrightarrow \Gamma_7$ transition is MD forbidden in O_h symmetry and therefore not observed in the 10 K emission spectrum in Fig. 1 (b). Aside from the sharp origins $\Gamma_7' \rightarrow \Gamma_7$ at 8961 cm^{-1} and $\Gamma_7' \rightarrow \Gamma_8$ at 8404 cm^{-1}, there is some vibronic structure in the emission spectrum. Vibronic intensity in the 4*f*-4*f* transition is often observed in Yb^{3+} and Tm^{2+} spectra [16, 25].

The 10 K absorption spectrum of CaCl$_2$:Tm^{2+} shown in Fig. 2 (a) is dominated by the sharp line at 8799 cm^{-1}. Because of its coincidence with the corresponding cold emission line in Fig. 2 (b), this peak is assigned to the $\Gamma_6 \leftrightarrow \Gamma_8$' electronic origin in O_h symmetry. The Γ_6 to
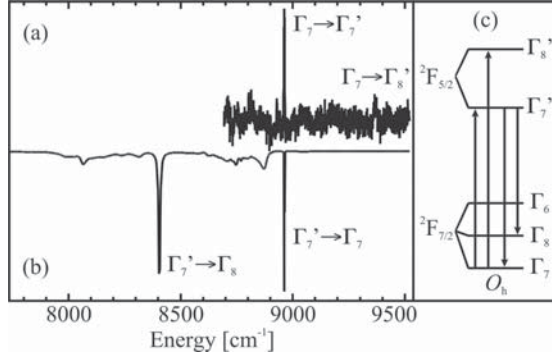
FIG. 1: (a) 10 K single crystal absorption spectrum of the $^2F_{7/2} \rightarrow {}^2F_{5/2}$ transitions of CaF$_2$:Tm^{2+}. The corresponding emission spectrum is shown in (b). The emission was photoexcited at 19436 cm^{-1}. In (c), a schematic energy level diagram for the splitting of the $^2F_{7/2}$ and $^2F_{5/2}$ multiplet in cubal coordination is displayed. The assignment of the bands is given on top of each spectrum and the transitions are indicated by arrows in (c).
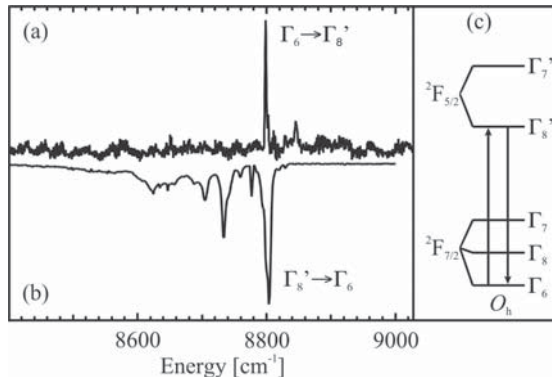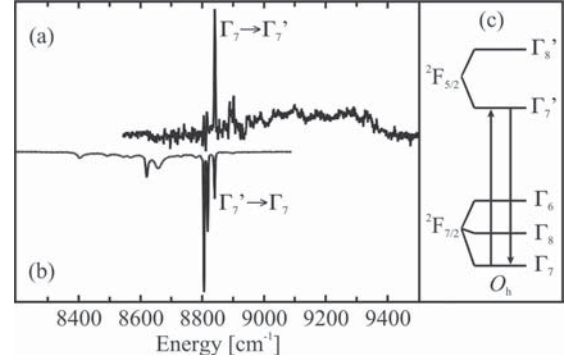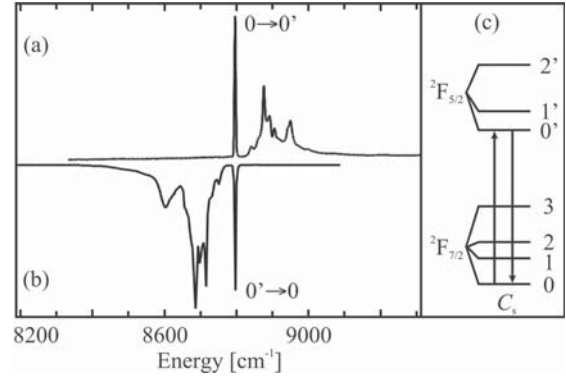

FIG. 3: (a) 10 K single crystal absorption spectrum of the $^2F_{7/2} \rightarrow {}^2F_{5/2}$ transitions of SrCl$_2$:1.27% Tm^{2+}. The corresponding emission spectrum is shown in (b). The emission was photoexcited at 21834 cm^{-1}. In (c), a schematic energy level diagram is displayed. The assignment of the bands is given on top of each spectrum and the transitions are indicated by arrows in (c).

FIG. 2: (a) 10 K single crystal absorption spectrum of the $^2F_{7/2} \rightarrow {}^2F_{5/2}$ transitions of CaCl$_2$:0.81% Tm^{2+}. The corresponding emission spectrum is shown in (b). The emission was photoexcited at 21834 cm^{-1}. In (c), a schematic energy level diagram is displayed. The assignment of the bands is given on top of each spectrum and the transitions are indicated by arrows in (c).

FIG. 4: (a) 10 K single crystal absorption spectrum of the $^2F_{7/2} \rightarrow {}^2F_{5/2}$ transition of BaCl$_2$:1.16% Tm^{2+}. The corresponding emission spectrum is shown in (b). The emission was photoexcited at 19436 cm^{-1}. In (c), a schematic energy level diagram is displayed. The assignment of the bands is given on top of each spectrum and the transitions are indicated by arrows in (c).

Γ_8' transition arises by a magnetic dipole (MD) mechanism. It is not possible to unambiguously assign any other features outside the 8800 cm^{-1} region to other origins in the spectra in Figs. 2 (a) and (b). In emission the origins are most likely hidden in the vibronic structure of the band.

The 10 K absorption and emission spectra of SrCl$_2$:Tm^{2+} are shown in Figs. 3 (a) and (b). The $\Gamma_7 \leftrightarrow \Gamma_7$' origin is assigned on the basis of the exact coincidence of the absorption line at 8840 cm^{-1} with the cold emission line at this energy. Because of the centrosymmetric site of Tm^{2+}, the origins are expected to

gain intensity by a MD mechanism. The $\Gamma_7 \leftrightarrow \Gamma_8$' (in absorption) and the $\Gamma_7' \leftrightarrow \Gamma_8$ (in emission) are hidden in the vibronic structure in the spectra in Figs. 3 (a) and (b). The $\Gamma_7' \leftrightarrow \Gamma_6$ does not have MD intensity in this structure and as a consequence is not observed in Fig. 3 (b).

For BaCl$_2$:Tm^{2+} the absorption and emission spectrum is displayed in Figs. 4 (a) and (b). The absorption spectrum (Fig. 4 (a)) shows a rich structure in contrast to the previously discussed spectra (Figs. 1-3 (a)). In the BaCl$_2$ structure, a center of inversion is absent and therefore the 4f-4f transition is expected to have electric

dipole intensity. Due to the C_s site symmetry of Tm²⁺ in BaCl₂ the electronic origins can no longer be labeled in the O_h notation, see Fig. 4 (c). The $0 \leftrightarrow 0'$ origin is assigned to the line at 8796 cm⁻¹. Further assignment of origins is difficult. Tm²⁺ is much smaller than Ba²⁺ (see Table I) and we cannot exclude the possibility that Tm²⁺ enters the lattice on sites other than the Ba²⁺ site. Thus the spectrum may be composed of lines from multiple sites. This is also suspected from the analysis of the 5d-4f emission spectrum (vide infra).

C. 4f-5d Transitions

4f-5d transitions correspond to the promotion of an electron from a 4f orbital to a 5d orbital. The resulting electron configuration is $(4f)^{n-1}(5d)^1$. The $(4f)^{12}(5d)^1$ electron configuration of Tm²⁺ has a total degeneracy of 910 and is split by the crystal field, electron interactions and spin-orbit coupling. The interactions that can be identified in the 4f-5d spectra of the Tm²⁺ doped title compounds are:

- Crystal field interaction of the 5d electron, denoted as H$_{CF}(d)$

- Coulomb repulsion and spin-orbit coupling within the $(4f)^{12}$ configuration, denoted as H$_{Coul+SO}(f)$

- Coulomb repulsion of the 4f and 5d electrons, denoted as H$_{Coul}(fd)$

H$_{CF}(d)$ splits the fivefold degenerate set of 5d orbitals according to the site symmetry of Tm²⁺. In O_h site symmetry, the crystal field will split the $(5d)^1$ into a t$_{2g}$ and an e$_g$ set of octahedral orbitals, separated by 10 Dq. This applies for CaF₂:Tm²⁺, CaCl₂:Tm²⁺ and SrCl₂:Tm²⁺. In cubal coordination, the e$_g$ will be lower in energy than the t$_{2g}$ (CaF₂:Tm²⁺ and SrCl₂:Tm²⁺) whereas in octahedral coordination the situation is reversed (CaCl₂:Tm²⁺). In BaCl₂:Tm²⁺, the site symmetry is C_s. In this low symmetry the $(5d)^1$ will be split into five sets of orbitals and 10 Dq cannot be assigned anymore.

H$_{Coul+SO}(f)$ splits the $(4f)^{12}$ configuration into $^{2S+1}L_J$ terms which are the well-known Tm³⁺ energy levels found in the Dieke diagram [26]. The energy multiplets of the Tm²⁺ $(4f)^{12}(5d)^1$ configuration are therefore labeled $(^{2S+1}L_J, t_{2g})$ and $(^{2S+1}L_J, e_g)$ in O_h. This situation is schematically depicted in Figure 5. For the low-symmetry case in BaCl₂:Tm²⁺, the energy multiplets are labeled $(^{2S+1}L_J, 5d^1)$.

For Tm²⁺ each of these multiplets is split by H$_{Coul}(fd)$ into a set of high-spin ($S = 3/2$) and a set of low-spin ($S = 1/2$) states. Due to Hund's rule, the former lie at lower energy and, as a consequence transitions from the $^2F_{7/2}$ groundstate to the lowest energy 4f-5d bands, are expected to be spin-forbidden. This is expressed in
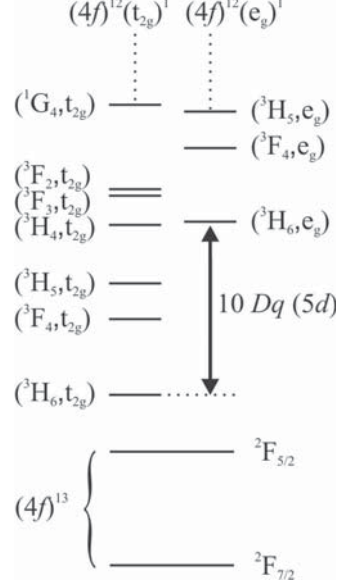
FIG. 5: Schematic energy splittings of the $(4f)^{13}$ and $(4f)^{12}(5d)^1$ electron configurations of Tm²⁺. The $(4f)^{13}$ electron configuration is split into two multiplets by the spin-orbit coupling (lower part of the diagram). For the $(4f)^{12}(5d)^1$ the result of the action of H$_{CF}(d)$ and H$_{Coul+SO}(f)$, as defined in the text, are considered for an octahedral coordination of Tm²⁺. The levels derived from $(4f)^{12}(t_{2g})^1$ and $(4f)^{12}(e_g)^1$ are displayed separately for better distinction. In case of cubal coordination, the t$_{2g}$ and e$_g$ are reversed. The labeling of the transitions corresponds to Fig. 6 and Table II.

weaker oscillator strengths compared to the spin-allowed bands, see Fig. 6 and Refs. [1, 5, 27]. On the basis of this model the assignment of the 4f-5d absorption bands in Fig. 6 is done.

1. 4f-5d Absorption Transitions

Fig. 6 shows the absorption spectra of CaF₂:Tm²⁺ (a), CaCl₂:Tm²⁺ (b), SrCl₂:Tm²⁺ (c) and BaCl₂:Tm²⁺ (d), extending from 13000 cm⁻¹ in the near infrared (NIR) up to 35000 cm⁻¹ in the near-ultraviolet (UV). This is the spectral region of the Tm²⁺ 4f-5d excitations. For the divalent rare earth ions the energy separation between the $(4f)^n$ and $(4f)^{n-1}(5d)^1$ configurations is smaller than for the trivalent rare earth ions. The consequence is that the 4f-5d transitions are shifted into the near-infrared and visible spectral range [5]. These transitions are parity allowed. In the spectra of the rare earth ions they appear as intense and broad bands [5, 27, 28]. The width of the bands is caused by the interaction of the 5d electron with the crystalline environment. As a consequence it is expected that the surrounding ions strongly influence the 4f-5d transitions.

TABLE II: Emission bands, positions, percent of the emission of the total photon flux and the lifetimes at 10 K of CaF$_2$:Tm^{2+}, CaCl$_2$:Tm^{2+}, SrCl$_2$:Tm^{2+} and BaCl$_2$:Tm^{2+}.

Compound	Emission transition	Position [cm^{-1}]	[%] of the total photon flux at 10 K	lifetime [μs]
CaF$_2$:Tm^{2+}	^{2}F$_{5/2}$→^{2}F$_{7/2}$	8961	$-^a$	3600^b
	$(^3$H$_6$,e$_g)S = 3/2$ →^{2}F$_{7/2}$	13720	$-^a$	$-^c$
CaCl$_2$:Tm^{2+}	^{2}F$_{5/2}$→^{2}F$_{7/2}$	8799	0.1	5210
	$(^3$H$_6$,t$_{tg})S = 3/2$ →^{2}F$_{7/2}$	12840	98.66	322
	$(^3$F$_4$,t$_{tg})$→^{2}F$_{7/2}$	20050	1.24	$-^c$
SrCl$_2$:Tm^{2+}	^{2}F$_{5/2}$→^{2}F$_{7/2}$	8840	0.1	4720
	$(^3$H$_6$,e$_g)S = 3/2$ →^{2}F$_{7/2}$	14020	22	222
	$(^3$F$_4$,e$_g)$→^{2}F$_{7/2}$	20740	77.9	21
BaCl$_2$:Tm^{2+}	^{2}F$_{5/2}$→^{2}F$_{7/2}$	8796	66.8	2600
	$(^3$H$_6$,5$d^1)S = 3/2$ →^{2}F$_{7/2}$ (site A)	12250	12.3	340
	$(^3$H$_6$,5$d^1)S = 3/2$ →^{2}F$_{7/2}$ (site B)	13730	20.9	213

^{a}The overview spectrum could not be measured.
^{b}taken from Ref. [4].
^{c}The lifetime is too fast to be determined with our equipment.

The absorption spectra of CaF$_2$:Tm^{2+} and SrCl$_2$:Tm^{2+} (Fig. 6 (a) and (c)) are discussed together because the site symmetry as well as the coordination geometry (cubal) of the Tm^{2+} ion is the same in the two hosts. The onset of the 4f-5d absorption bands is redshifted from CaF$_2$:Tm^{2+} to SrCl$_2$:Tm^{2+} by about 150 cm^{-1} (Fig. 6 (a) and (c)). The spectra of these two samples bear some resemblance at the lowest energies as can be expected because of the isostructural systems. Above the multiplets labeled (^{3}F$_4$, e$_g$), the similarities end. Due to the action of H$_{CF}(d)$, the 5d electron is in the e$_g$ in the lowest absorption band. The lowest two multiplets of the Tm^{3+} staircase in e$_g$ can be identified and are indicated on top of the bands. This is the result of the H$_{Coul+SO}(f)$ interactions. Further Tm^{3+} multiplets are not assigned because of the increasing overlap of bands towards higher energies. Finally, the action of H$_{Coul}(fd)$ is most obvious at the lowest 4f-5d excitations. The first absorption bands which are hardly seen in Fig. 6 (a) and (c) correspond to the spin-forbidden transition indicated by the arrow labeled $S = 3/2$. At higher energies the spectra are dominated by intense broad bands. The onset of the spin-allowed bands is marked by the arrow labeled $S = 1/2$. The spin-forbidden and spin-allowed bands overlap towards higher energies and the spin state of the bands cannot be assigned unambiguously anymore [16, 29]. Also in trivalent rare earth ions it is observed that spin is not a good quantum number anymore towards higher lying 4f-5d bands [30].

In the CaF$_2$:Tm^{2+} spectrum in Fig. 6 (a), the ^{3}H$_6$→^{3}F$_4$ absorption transition of the Tm^{3+} impurity is located just below the onset of the (^{3}H$_6$,e$_g)S = 3/2$ band of Tm^{2+}. The Tm^{3+} bands are not analyzed in detail because up to four different Tm^{3+} sites were identified in CaF$_2$:Tm^{3+} [31].

The 4f-5d absorption spectrum of CaCl$_2$:Tm^{2+} is shown in Fig. 6 (b). The action of H$_{CF}(d)$ causes the 5d electron to be in the t$_{2g}$ in the lowest absorption bands. The action of H$_{Coul+SO}(f)$ is identified at the lowest energies where the (^{3}H$_6$,t$_{2g}$) and the (^{3}F$_4$,t$_{2g}$) are assigned. The spin-forbidden and spin-allowed bands in the region of the (^{3}H$_6$,t$_{2g}$) multiplet in Fig. 6 (b) are the result of the H$_{Coul}(fd)$ interaction.

In BaCl$_2$:Tm^{2+} (Fig. 6 (d)), an identification of the five multiplets caused by H$_{CF}(d)$ is not possible. Similarly, the Tm^{3+} multiplets caused by H$_{Coul+SO}(f)$ are not identified. Therefore, only the (^{3}H$_6$,5d^1) multiplet is labeled in Fig. 6 (d), which corresponds to the lowest 4f-5d absorption transition. It is to be expected that the overlap of multiplets is increased in this sample. The low site symmetry causes large splittings. Further, multiple sites may be present which will cause broadening of the bands as well. However, a distinction between the spin-forbidden and spin-allowed 4f-5d absorption bands caused by the H$_{Coul}(fd)$ interaction can be made at the lowest energies.

A blueshift of the onset of the lowest 4f-5d bands is observed along the chloride series. The location of the lowest absorption band is determined mainly by the splitting of the 5d orbitals and the energy separation between the 4f and the 5d orbitals. The latter separation is decreased due to the increased radius of the earth alkaline host ion (see Table I). The 5d orbital can expand, which reduces the Coulomb repulsion between the 4f and the 5d orbitals of the Tm^{2+} dopant. 10 Dq is expected to decrease between CaCl$_2$:Tm^{2+} and SrCl$_2$:Tm^{2+} by about 1600-2000 cm^{-1}. The overall splitting of the 5d orbitals in BaCl$_2$:Tm^{2+} is most likely larger than the splitting in a O_h Ba site. The combination of the splitting of the 5d orbitals and the energy separation between the 4f and the 5d orbitals results in a blueshift
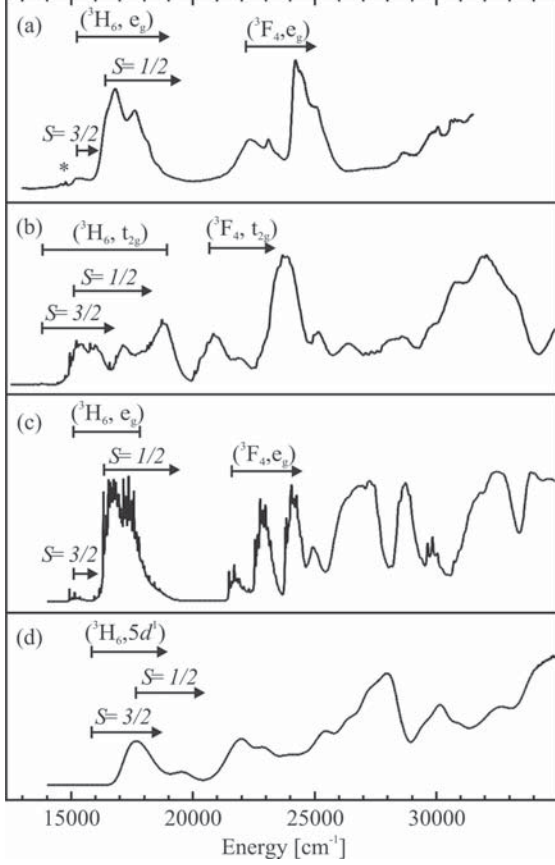
FIG. 6: 10 K absorption spectrum of (a) CaF_2:Tm²⁺, (b) $CaCl_2$:0.81% Tm²⁺, (c) $SrCl_2$:1.27% Tm²⁺, and (d) $BaCl_2$:1.16% Tm²⁺. The absorption transitions in this region are due to the Tm²⁺ $4f$-$5d$ transitions from the $^2F_{7/2}$ ground-state. The assignment of the absorption bands is given on top of each spectrum. The peak in (a) labeled with an asterisk (*) is assigned to the Tm³⁺ $^3H_6 \rightarrow {}^3F_4$ absorption transition.

of about 2200 cm⁻¹ from $CaCl_2$:Tm²⁺ to $BaCl_2$:Tm²⁺. The overall shape of the three chloride spectra does not reflect that Tm²⁺ is doped into a series of compounds as was found for the $CsCaX_3$ (X=Cl, Br, I) series [16, 29]. The chemical as well as the structural variation is responsible for the differences in the splittings of the states.

2.   4f-5d Emission Transitions

In Fig. 7 the spectral range of the $5d$-$4f$ emissions is displayed. In contrast to the $4f$-$4f$ emission in Figs. 1–4, the $5d$-$4f$ emissions are intense broad bands. In all samples, emission from the lowest $4f$-$5d$ absorption band is observed between 11000 cm⁻¹ and 15000 cm⁻¹. This
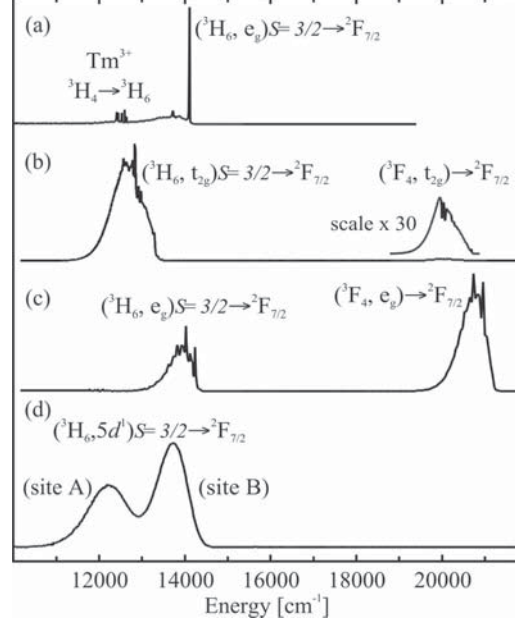
FIG. 7: Overview $5d$-$4f$ emission spectra of CaF_2:Tm²⁺ (a), $CaCl_2$:0.81% Tm²⁺ (b), $SrCl_2$:1.27% Tm²⁺ (c) and $BaCl_2$:1.16% Tm²⁺ (d) at 10 K. Laser excitation occurred at 19436 cm⁻¹ for (a) and at 21839 cm⁻¹ for (b), (c) and (d), respectively. The labeling of the emission bands is given on top of each spectrum. Note the emissions from Tm³⁺ impurities in (a) and the scale change in (b).

$5d$-$4f$ emission originates in the lowest spin-forbidden $4f$-$5d$ absorption band. The spin-forbidden character of the emission is reflected in the lifetime of a few hundred μs, which is rather long for a parity allowed transition (Table II). The measured lifetimes of the spin-forbidden transitions in the title compounds compare well with other Tm²⁺ doped systems [13, 15, 16]. In $CaCl_2$:Tm²⁺ (Fig. 7 (b))and $SrCl_2$:Tm²⁺ (Fig. 7 (c)) an additional $5d$-$4f$ emission is observed at higher energy between 19000 cm⁻¹ and 21500 cm⁻¹. The position as well as measured lifetime of each emission band is given in Table II.

The $(^3H_6,e_g)S = 3/2$ to $^2F_{7/2}$ emission has not been reported before for CaF_2:Tm²⁺ (Fig. 7 (a)). Because of the inevitable presence of Tm³⁺ this emission was most probably quenched. We think that in our sample the emission is observed because a higher percentage of Tm was reduced to Tm²⁺. The chemical production of Tm²⁺ may be beneficial for this, in contrast to the ionization methods applied in earlier investigations [4–6]. The emission spectrum in Fig. 7 (a) is excited at 19436 cm⁻¹. At this excitation energy, Tm²⁺ is selectively excited because no energy level of Tm³⁺ falls in this energy range. Upon excitation at 21834 cm⁻¹ the relative intensity of the Tm²⁺ emission is reduced compared to the Tm³⁺ emission because the excitation energy is almost reso-

nant with the ^{1}G$_4$ state of Tm^{3+}. The lifetime of the $(^3$H$_6$,e$_g)S = 3/2 \rightarrow{}^2F_{7/2}$ emission was too short to be determined in CaF$_2$:Tm^{2+}. This points to a significant quenching of this emission by energy transfer to Tm^{3+} impurities, but also by non-radiative relaxation to the ^{2}F$_{5/2}$ multiplet. The phonon energies are higher in a fluoride than in a chloride, and thus multiphonon relaxation processes will be enhanced compared to the chloride samples. No emission from the higher lying $(^3$F$_4$,e$_g)$ multiplet is observed in CaF$_2$:Tm^{2+}. The two quenching processes discussed before will also dominate the relaxation processes between the higher lying $4f$-$5d$ states.

In CaCl$_2$:Tm^{2+}, two $5d$-$4f$ emission bands are observed, Fig. 7 (b). The spin-forbidden emission $(^3$H$_6$,t$_{2g})S = 3/2 \rightarrow{}^2F_{7/2}$ dominates the spectrum, see also the relative percentages of the emission bands in Table II. The intensity of the $(^3$F$_4$,t$_{2g}) \rightarrow{}^2$F$_{7/2}$ emission in contrast is very low. This is not surprising considering the absorption spectrum of the sample (Fig. 6 (b)). The gap between the highest level of $(^3$H$_6$,t$_{2g})$ and the lowest level of $(^3$F$_4$,t$_{2g})$ is less than 2000 cm^{-1}. Thus, multiphonon relaxation from $(^3$F$_4$,t$_{2g})$ to $(^3$H$_6$,t$_{2g})$ will dominate at all temperatures. The lifetime of the $(^3$F$_4$,t$_{2g}) \rightarrow{}^2$F$_{7/2}$ emission could not be determined with our equipment because it is too fast.

In SrCl$_2$:Tm^{2+} (Fig. 7 (c)), in addition to the previously reported spin-forbidden emission $(^3$H$_6$,e$_g)S = 3/2 \rightarrow{}^2F_{7/2}$, emission from the higher lying $(^3$F$_4$,e$_g)$ is observed. So far, this emission has not been reported for SrCl$_2$:Tm^{2+} [15, 20]. The gap between the highest level of $(^3$H$_6$,e$_g)$ and the lowest level of $(^3$F$_4$,e$_g)$ is around 4200 cm^{-1}. This is the largest gap between these two multiplets among all Tm^{2+} doped systems reported so far [16, 29]. In CsCaCl$_3$:Tm^{2+} the same gap is 2760 cm^{-1} and the percentage of the higher excited state emission from $(^3$F$_4$,t$_{2g})$ is 36.5%. Multiphonon relaxation is thus significantly reduced across the gap in SrCl$_2$:Tm^{2+}, which explains the dominance of the $(^3$F$_4$,e$_g)S = 3/2 \rightarrow{}^2F_{7/2}$ emission at 10 K (see also Table II). The $(^3$H$_6$,e$_g)S = 3/2 \leftrightarrow{}^2F_{7/2}$ and the $(^3$F$_4$,e$_g) \leftrightarrow{}^2$F$_{7/2}$ transitions show considerable fine structure in SrCl$_2$:Tm^{2+}, see Fig. 8 and 9. A detailed analysis of the spectra is planned.

In BaCl$_2$:Tm^{2+} (Fig. 7 (d)) a double emission band is observed from the $(^3$H$_6$,5$d^1)S = 3/2$ absorption multiplet. This points to the existence of two sites in the structure. Accordingly, the emission band centered at 12250 cm^{-1} is labeled $(^3$H$_6$,e$_g)S = 3/2 \rightarrow{}^2F_{7/2}$ (site A) and the one centered at 13730 cm^{-1} is labeled $(^3$H$_6$,e$_g)S = 3/2 \rightarrow{}^2F_{7/2}$ (site B) in Fig. 7 (d) and Table II. The decay curves of these two emission bands are double exponential and the prominent decay time is given in Table II for both bands. Also in the discussion of the $4f$-$4f$ transition (Fig. 4) the possibility of multiple sites was mentioned. This is thus confirmed here. The absence of any large gap at higher energies in the absorption spectrum (Fig. 6 (d)) explains why we only observe emission from the $(^3$H$_6$,5$d^1)S = 3/2$.

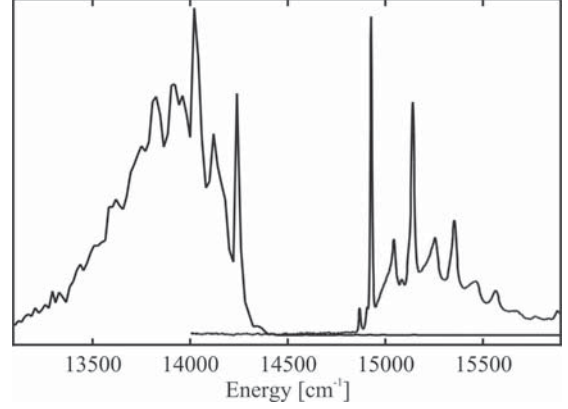FIG. 8: Detail of the $(^3$H$_6$,e$_g)S = 3/2 \leftrightarrow{}^2F_{7/2}$ transition in SrCl$_2$:Tm^{2+}.
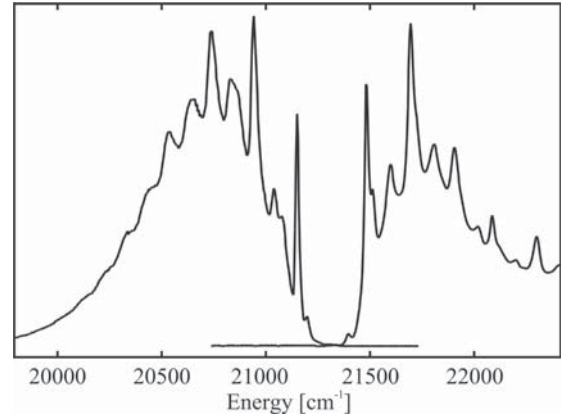
FIG. 9: Detail of the $(^3$F$_4$,e$_g) \leftrightarrow{}^2$F$_{7/2}$ transition in SrCl$_2$:Tm^{2+}.

The relative percentage of the $4f$-$4f$ and the $5d$-$4f$ emissions at 10 K varies along the series, see Table II. For CaF$_2$:Tm^{2+} we assume that the ^{2}F$_{5/2} \rightarrow{}^2$F$_{7/2}$ (Fig. 1) emission is dominant at all temperatures. We were not able to detect the $5d$-$4f$ emission in an attempt to determine the overview spectrum. In CaCl$_2$:Tm^{2+} and SrCl$_2$:Tm^{2+} the percentage of the $4f$-$4f$ transition is low. This is similar to CsCaCl$_3$ (see Ref. [16]) and we conclude that multiphonon relaxation from the $(^3$H$_6$,t$_{2g})S = 3/2$ and $(^3$H$_6$,e$_g)S = 3/2$, respectively, to ^{2}F$_{5/2}$ is very low. It is likely that non-radiative relaxation is inhibited by a spin selection rule [16, 17]. In BaCl$_2$:Tm^{2+} the ^{2}F$_{5/2} \rightarrow{}^2$F$_{7/2}$ emission is the dominant emission already at 10 K, see Table II. Efficient multiphonon relaxation from the lowest component of $(^3$H$_6$,5$d^1)S = 3/2$ to the ^{2}F$_{5/2}$ is therefore present which may also be attributed to the presence of multiple Tm^{2+} sites.

IV.   CONCLUSIONS

The present series of Tm^{2+} doped compounds is a nice example to demonstrate the influence of chemical and structural variation on the spectroscopic properties of Tm^{2+}. The coordinating anion and the site symmetry strongly influences the $4f$-$5d$ transitions. The number as well as the position and relative intensity of the $4f$-$5d$ transitions varies along the series and can be understood from the energy level structure in the $(4f)^{12}(5d)^1$ electron configuration. The most important interactions are presented in order to understand the splittings in this configuration.

The very simple principle of variation proves to be a powerful tool to influence the spectroscopic properties of Tm^{2+}. This is interesting considering potential applications. Laser action on the $^2\mathrm{F}_{7/2} \leftrightarrow {}^2\mathrm{F}_{5/2}$ transition was demonstrated 40 years ago in CaF$_2$:Tm^{2+} [9]. The energy of this transition is in a range where few laser sources are available. Further, the $4f$-$5d$ transitions are ideal to build a tunable solid state laser [32]. In the present contribution we demonstrate that Tm^{2+} can be successfully stabilized in a variety of materials despite its preference for the trivalent oxidation state in solids. This opens the possibility for creating materials with preferred properties.

[1] P. Dorenbos, J. Phys. Condens. Matter **15**, 575 (2003).
[2] G. Meyer, Chem. Rev. **88**, 93 (1988).
[3] O. Greis and T. Petzel, Z. anorg. allg. Chem. **434**, 89 (1977).
[4] Z. J. Kiss, Phys. Rev. **127**, 718 (1962).
[5] D. S. McClure and Z. J. Kiss, J. Chem. Phys. **39**, 3251 (1963).
[6] E. Loh, Phys. Rev. **175**, 533 (1968).
[7] E. S. Sabisky and C. H. Anderson, Phys. Rev. **159**, 234 (1967).
[8] A. A. Kaplyanski and P. P. Feofilov, Opt. Spectry. **13**, 129 (1962).
[9] R. C. Duncan and Z. J. Kiss, Appl. Phys. Lett. **3**, 23 (1963).
[10] R. C. Duncan, IEEE J. Quantum Electron. Suppl. Sec. QE **2**, R52 (1966).
[11] C. Pedrini, D. S. McClure, and C. H. Anderson, J. Phys. Chem. **70**, 4959 (1979).
[12] D. S. McClure and C. Pedrini, Phys. Rev. B **32**, 8465 (1985).
[13] W. J. Schipper, A. Meijerink, and G. Blasse, J. Lumin. **62**, 55 (1994).
[14] C. Wickleder, J. Alloys Comp. **300-301**, 193 (2000).
[15] O. S. Wenger, C. Wickleder, K. W. Krämer, and H. U. Güdel, J. Lumin. **94-95**, 101 (2001).
[16] J. Grimm, J. F. Suyver, E. Beurer, G. Carver, and H. U. Güdel, J. Phys. Chem. B (2005), accepted.
[17] R. T. Wegh and A. Meijerink, Phys. Rev. B **60**, 10820 (1999).
[18] L. van Pieterson, R. T. Wegh, A. Meijerink, and M. F. Reid, J. Chem. Phys. **115**, 9382 (2001).
[19] E. Beurer, J. Grimm, P. Gerner, and H. U. Güdel, submitted to J. Am. Chem. Soc.
[20] R. C. Alig, R. C. Duncan, and B. J. Mokross, J. Chem. Phys **59**, 5837 (1973).
[21] G. Q. Wu and R. Hoppe, Z. anorg. allg. Chem. **514**, 92 (1984).
[22] G. Brauer and O. Müller, Z. anorg. allg. Chem. **295**, 218 (1958).
[23] E. B. Brackett, T. E. Brackett, and R. L. Sass, J. Phys. Chem. **67**, 2132 (1963).
[24] R. D. Shannon, Acta Cryst. A **32**, 751 (1976).
[25] M. P. Hehlen and H. U. Güdel, J. Chem. Phys **98**, 1768 (1993).
[26] G. H. Dieke, *Spectra and Energy Levels of Rare Earth Ions in Crystals* (John Wiley & Sons, 1968).
[27] L. van Pieterson, M. F. Reid, G. W. Burdick, and A. Meijerink, Phys. Rev. B **65**, 045114 (2002).
[28] L. van Pieterson, M. F. Reid, R. T. Wegh, S. Soverna, and A. Meijerink, Phys. Rev. B **65**, 045113 (2002).
[29] J. Grimm, E. Beurer, and H. U. Güdel, submitted to Inorg. Chem.
[30] P. Dorenbos, J. Phys. Condens. Matter **15**, 6249 (2003).
[31] K. Muto, J. Phys. Chem. Solids **34**, 2029 (1973).
[32] S. Kück, Appl.Phys. B **72**, 515 (2001).

3 Upconversion in a Ni^{2+} Doped Fluoride

Broadband green upconversion luminescence of Ni^{2+} in KZnF$_3$

Judith Grimm, Oliver S. Wenger[1], Hans U. Güdel*

Department of Chemistry and Biochemistry, University of Bern, Freiestrasse 3, CH-3000 Bern 9, Switzerland

Abstract

The upconversion properties of divalent nickel doped into KZnF$_3$ are reported. By exciting into the ^{3}T$_{1g}$ (^{3}F) or ^{1}E$_g$ excited state of Ni^{2+} with monochromatic light, a broad green luminescence around 20,000 cm^{-1} is observed that originates in the ^{1}T$_{2g}$ higher excited state. The upconversion is shown to be a single ion process, consisting of a sequential two-photon absorption. The green luminescence is observed at all temperatures between 15 K and room temperature. This is strikingly different from what is observed in Ni^{2+} doped chloride and bromide materials in which the ^{1}T$_{2g}$→^{3}A$_{2g}$ luminescence is located in the red spectral range and is quenched well below room temperature.
© 2002 Elsevier Science B.V. All rights reserved.

Keywords: Upconversion; Ni^{2+}; Fluoride host lattice

1. Introduction

The spectroscopic properties of Ni^{2+} (3d^8) have been the subject of extensive studies in the past [1]. It was found already in the 1970s that octahedrally coordinated Ni^{2+} in halide and oxide lattices exhibits multiple emissions from a higher excited state [2–5]. Luminescence transitions from more than one excited state are a rare phenomenon among transition metal doped materials. Usually non-radiative decays are predominant due to strong electron–phonon coupling. Only a limited number of transition metals has been known up to date, in which radiative processes from higher

excited states compete successfully with non-radiative processes [3,6–8].

The presence of multiple metastable excited states is an important precondition for upconversion (UC) processes [12]. UC is a non-linear optical process that generates short wavelength luminescence upon excitation at longer wavelengths. These processes rely on either absorption or energy transfer (ET) from an intermediate excited state to reach the higher emitting state. The most common processes are denoted GSA/ESA and GSA/ETU. The former consists of a sequence of ground state absorption (GSA) and excited state absorption (ESA) steps on a single ion. The latter is cooperative and requires two interacting ions. Both are initially excited to the intermediate state, and in the subsequent ET step one of the ions is excited to the upper state, while the partner relaxes to the ground state. Both mechanisms lead to the population of a higher

---

*Corresponding author. Fax: +41-31-631-4399.

E-mail address: hans-ulrich.guedel@iac.unibe.ch (H.U. Güdel).

[1] Present address: California Institute of Technology, 1200 East California Boulevard, Pasadena, CA 91125, USA.
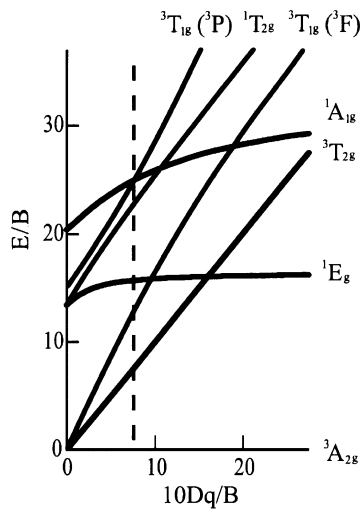
Fig. 1. Tanabe Sugano diagram for the $3d^8$ configuration in an octahedral crystal field plotted for a ration $C/B = 4.2$. The dashed line indicates the situation for $KZnF_3:Ni^{2+}$.

excited state from which radiative emission can occur. The intermediate level, the lifetime of which should not be too short, typically at least 10^{-6} s, serves as an energy reservoir until the second step in the UC process takes place.

The energetic structure of divalent nickel is best illustrated in terms of a Tanabe–Sugano-diagram for d^8 ions that is shown in Fig. 1. The dashed line shows where the ligand field strength of a fluoride host material is. In $KZnF_3$ as well as other fluoride hosts, Ni^{2+} exhibits luminescence from the lowest excited state ($^3T_{2g}$) as well as multiple emissions from the $^1T_{2g}$ to lower lying states [3–5,9]. In $KZnF_3:Ni^{2+}$, three emissions are observed from the $^1T_{2g}$ state: $^1T_{2g} \rightarrow {}^3A_{2g}$, $^3T_{2g}$, $^3T_{1g}$ (^3F) and one transition from $^3T_{2g}$ to $^3A_{2g}$. The emissions from the $^1T_{2g}$ state are not only observed at cryogenic temperatures, they persist up to room temperature, in contrast to Ni^{2+} chloride and bromide crystals, in which the $^1T_{2g}$ emissions are quenched below 200 K [10,11].

2. Experimental

The methods of sample preparation and crystal growth have been described elsewhere [13]. Ab-

sorption spectra were measured on a Cary 5e (Varian) Spectrometer. The samples were cooled using a closed-cycle helium cryostat (Air Products Displex). Continuous-wave luminescence measurements were performed using the 21,008 or 21,839 cm^{-1} line of an Ar$^+$ laser (Spectra Physics). For the UC experiments, a frequency doubled Nd^{3+}:YVO$_4$ laser (Spectra Physics Millenia Xs) pumped Ti^{3+}:sapphire laser (Spectra Physics 3900S) and the 15,454 cm^{-1} line of a Kr$^+$-laser (Innova 300) were used. Wavelength control for the Ti^{3+}:sapphire laser for the UC excitation measurements was achieved with a step-motor-driven birefringent filter and a Burleigh WA 2500 wavemeter. The wavelength dependence of the laser power was measured simultaneously on a powermeter (Coherent Labmaster). The sample luminescence was dispersed by a 0.85 double monochromator (Spex) equipped with a 1200 grooves/nm grating blazed at 500 nm. Ni^{2+} luminescence between 490 and 1000 nm was detected by a cooled photomultiplier tube (Hamamatsu P3310-01) connected to a photon counting system (Stanford Research 400). For short pulse experiments the sample was excited with a frequency doubled pulsed Nd^{3+}:YAG (Quanta-Ray DCR-3, 20 Hz) pumped dye laser (Lambda Physik FL3002, Pyridine I in methanol). The detection system consisted of a $\frac{3}{4}$ m single mono-chromator (Spex 1702) equipped with a 600 grooves/mm grating blazed at 750 nm and a cooled photomultiplier tube (RCA C31034) connected to a photon counting system (Stanford Research 400). The decay curves were recorded on a multi-channel scaler (Stanford Research 430). Sample cooling for all luminescence measurements was achieved with a He gas flow technique. All luminescence spectra were corrected for the wavelength dependence of the detection system and were converted to photon counts versus energy.

3. Results

Fig. 2 shows the 15 K survey absorption spectrum of 3% Ni^{2+}:$KZnF_3$. The Ni^{2+} ion occupies a perfectly octahedral site in the cubic perovskite
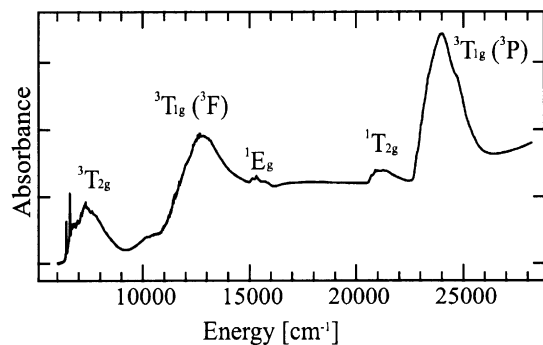
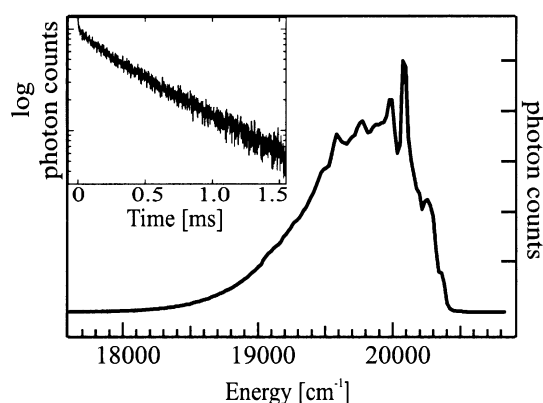Fig. 2. Survey absorption spectrum of KZnF$_3$:Ni^{2+} (3%) at 10 K with assignments of the bands to d–d excitations.

Fig. 3. Green part of the UC luminescence spectrum (15 K) corresponding to the $^1T_{2g} \rightarrow {}^3A_{2g}$ transition obtained under excitation at 14,063 cm^{-1}. The inset shows in a semilogarithmic representation the time dependence of the luminescence intensity measured at 20,000 cm^{-1} after a 10 ns laser pulse at 14,493 cm^{-1}.

Fig. 4. The lower trace is a 15 K excitation spectrum. The Ti^{3+}-sapphire laser was scanned in the region between 13,700 and 14,500 cm^{-1} while the $^1T_{2g} \rightarrow {}^3A_{2g}$ luminescence was monitored at 20,000 cm^{-1}. The upper trace shows the red $^1T_{2g} \rightarrow {}^3T_{2g}$ luminescence spectrum at 15 K.

KZnF$_3$ lattice and the observed bands are readily assigned, see Fig. 1 [13].

The 15 K $^1T_{2g} \rightarrow {}^3A_{2g}$ luminescence band in the green obtained under 14,063 cm^{-1} excitation of a 2% Ni^{2+} doped crystal is shown in Fig. 3. In this UC excitation mode, the first GSA step is into the $^3T_{1g}$ (^3F). The same luminescence can be excited with the 15,454 cm^{-1} Kr$^+$-laser-line (spectrum not shown). In this case, the GSA step is into ^1E_g. The emission in Fig. 3 is broad with some vibrational fine structure and its position and shape matches the one obtained by directly exciting into the $^1T_{2g}$ state (data not shown). In the inset of Fig. 3, the time dependence of the $^1T_{2g} \rightarrow {}^3A_{2g}$ emission intensity of KZnF$_3$:Ni^{2+} (0.5%) at 15 K excited with a 10 ns laser pulse of 14,493 cm^{-1} is shown in a semilog representation. The luminescent transient is a single exponential curve and the decay time extracted from this data is $\tau = 518\,\mu s$.

In Fig. 4 the excitation spectrum of the UC luminescence of KZnF$_3$:Ni (2%) at 15 K is shown as a full line. In this experiment, the laser was scanned in the energy range between 13,700 and 14,500 cm^{-1} while monitoring the $^1T_{2g} \rightarrow {}^3A_{2g}$ luminescence intensity at 20,000 cm^{-1}. The sharp origin observed at 14,063 cm^{-1} is coincident with that of the red $^1T_{2g} \rightarrow {}^3T_{2g}$ luminescence band at 15 K, also shown in this figure as a dotted line.

Fig. 5 shows the integrated intensities of the green $^1T_{2g}$ luminescence as a function of temperature for 15,454 cm^{-1} Kr$^+$-laser excitation. The luminescence persists up to room temperature, where the integrated intensity still amounts to roughly 50% of the one measured at 15 K.
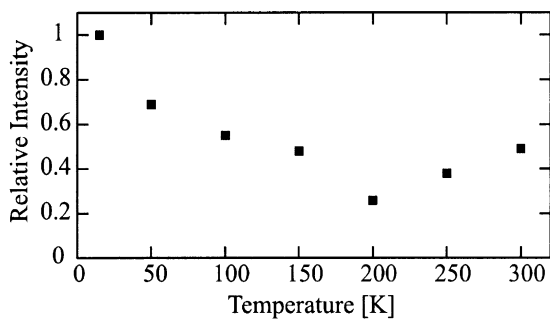
Fig. 5. Temperature dependence of the integrated $^1T_{2g} \rightarrow {}^3A_{2g}$ luminescence intensity under 15,454 cm^{-1} excitation.

4. Discussion

4.1. Mechanism of the upconversion luminescence in KZnF$_3$:Ni^{2+}

We have established fingerprinting techniques for the identification of the UC mechanisms [12]. A GSA/ESA sequence reveals itself in the excitation spectrum of the upconverted luminescence. It is the product of the GSA and ESA spectra and usually contains recognizable features of both. In contrast, the excitation spectrum of a GSA/ETU excited UC luminescence corresponds to the square of the GSA spectrum. A second technique for a clear-cut distinction is by measuring the time evolution of the UC luminescence immediately after a 10 ns excitation pulse. In the case of the GSA/ESA sequence both excitation steps are radiative, and thus both have to occur during the laser pulse. As a consequence the UC transient simply consists of a decay of the upper emitting state. The intermediate state leaves no trace in this measurement. In contrast, in a GSA/ETU process all the excitation is stored in the intermediate state during the laser pulse. Energy-transfer UC then sets in and is followed by the decay of the upper excited state. The UC transient thus exhibits a rise and a decay part. In our KZnF$_3$:Ni^{2+} system we have applied both techniques, and they lead to and unambiguous identification of the mechanism.

The UC transition after a 10 ns pulsed excitation into the $^3T_{2g}$ at 15 K is shown in the inset of Fig. 3. No rise is observed, and the decay time of 518 μs is identical within the experimental error with the

$^1T_{2g}$ lifetime obtained under $^1T_{2g}$ direct excitation (578 μs, transient not shown). This means that the $^1T_{2g}$ is populated within the duration of the laser pulse. In MgF$_2$:Ni^{2+}, Tonucci et al. reported a lifetime of the $^3T_{1g}$ (^{3}F) intermediate state of 12 μs [14]. Since we do not observe any rise in our transient, we conclude that in our system the relaxation from $^3T_{1g}$ (^{3}F) to $^3T_{2g}$ occurs within the laser pulse and a GSA/ESA sequence is responsible for the UC process.

The complete picture for the UC mechanism in KZnF$_3$:Ni^{2+} is obtained with the help of the excitation spectrum shown in Fig. 4. When the laser energy is scanned from 13,700 cm^{-1} to higher energy, UC luminescence intensity is registered starting from 14,063 cm^{-1}. The 14,063 cm^{-1} excitation line is coincident with the sharp origin line of the $^1T_{2g} \rightarrow {}^3T_{2g}$ emission which is also shown in Fig. 5 [15], and which is the reverse of the ESA. We conclude that the second step in the UC process is an ESA transition from $^3T_{2g}$ to $^1T_{2g}$. The UC excitation spectrum corresponds to the product of the GSA and ESA. The GSA in the energy range between 14,000 and 14,500 cm^{-1} is broad and featureless, and therefore the excitation spectrum in Fig. 4 is mainly given by the ESA.

The following mechanism for the UC process, schematically shown in Fig. 6 is thus firmly established. The first photon induces a GSA into the $^3T_{1g}$ (^{3}F) or ^1E_g state. The system relaxes non-radiatively within picoseconds to the $^3T_{2g}$ first excited state. At 10 K this has a lifetime of 9 ms [3].
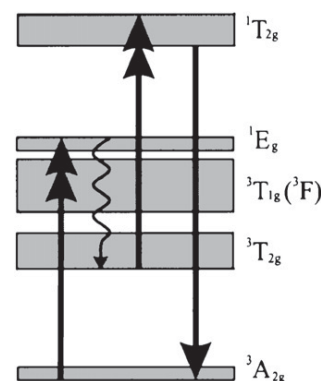

Fig. 6. Schematic representation of the UC mechanism.

By the absorption of a second photon, excitation to $^1T_{2g}$ occurs, followed by the emission of green luminescence. The nature of the UC mechanism can also be understood in terms of energetic considerations: Two quanta of $^3T_{2g}$ excitation at 6418 cm^{-1} are not sufficient to reach the $^1T_{2g}$ state at 21,109 cm^{-1}. This rules out a two-center GSA/ETU process with one color excitation. It would be possible by a rather unlikely three-center GSA/ETU.

4.2. Temperature dependence of the green upconversion luminescence

As seen in Fig. 5, the UC luminescence intensity when excited at 15,454 cm^{-1} decreases between 15 and 200 K, and then increases again up to 300 K. At room temperature its value is about 50% of the 15 K value. The UC process consists of several temperature dependent steps (GSA, multiphonon relaxation, ESA). We have measured the GSA cross-section at 15,454 cm^{-1} as a function of temperature. The GSA cross-section decreases with increasing temperature. Multiphonon relaxation rates usually increase with increasing temperatures. For the ESA cross sections there are no direct measurements available. We consider the temperature dependence to be similar to the GSA into $^1T_{2g}$. At 21,872 cm^{-1} this cross-section first becomes smaller due to the shift of the $^1T_{2g}$ absorption band to lower energies, but it starts increasing around 200 K because the much more intense $^3T_{1g}$ (^3P) band starts moving in. Since the other factors become smaller with increasing temperature we conclude that the observed increase between 200 and 300 K in Fig. 5 is mainly the result of the increasing ESA cross-section at this particular excitation energy.

5. Summary and outlook

In the present study some aspects of the UC properties of Ni^{2+} doped into KZnF$_3$ are shown and interpreted. The experiments performed so far used monochromatic excitation of the Ni^{2+}. This is, however, not the only and by far not the most efficient way to excite UC luminescence in this compound. One of the advantages of the system is that it offers many possibilities to tune UC because of the broad absorption bands. A two-color experiment, in which one excitation source directly populates the $^3T_{2g}$ state and the second one induces a $^3T_{2g} \rightarrow {}^1T_{2g}$ ESA transition is expected to be more efficient by several orders of magnitude. Both of the excitation sources can be sharp line lasers or broadband lamps, and they can both be tuned in the NIR region to increase the efficiency of the UC process. We are also interested to explore multicolor excitation by just using one broadband lamp source. Such a process would be most interesting from point of view of lighting. Present day lamps, and particularly incandescent lamps, have a big part of their output in the near-IR. If part of this could be recycled by broadband NIR absorption followed by UC into VIS, the efficiency of lamps could conceivably be improved.

Fluorides also have an advantage over the other halides from a materials point of view: They are much less air-sensitive, and they are harder. Their handling is therefore much easier because they do not need to be held under inert atmosphere. That makes them more attractive for possible materials applications. In terms of NIR to VIS UC there is also an energetic advantage: The Ni^{2+} luminescence from the $^1T_{2g}$ state in KZnF$_3$ is located in the green, whereas in Ni^{2+} doped chlorides and bromides the same emission is in the red [11].

References

[1] B. Henderson, G.F. Imbusch, Optical Spectroscopy of Inorganic Solids, Oxford Science Publications, Oxford, 1989.
[2] J.E. Ralph, M.G. Townsend, J. Phys. C 3 (1970) 8.
[3] W.E. Vehse, K.H. Lee, S.I. Yun, W.A. Sibley, J. Lumin. 10 (1975) 149.

[4] J. Ferguson, H. Masui, J. Phys. Soc. Japan 42 (5) (1977) 1640.

[5] M.V. Iverson, W.A. Sibley, J. Lumin. 20 (1979) 311.

[6] D.R. Gamelin, H.U. Güdel, J. Am. Chem. Soc. 120 (1998) 12143.

[7] M. Wermuth, H.U. Güdel, Chem. Phys. Lett. 281 (1997) 81.

[8] S.M. Jacobsen, H.U. Güdel, J. Lumin. 43 (1989) 125.

[9] D.R. Gamelin, H.U. Güdel, Acc. Chem. Res. 33 (2000) 235.

[10] P.S. May, H.U. Güdel, Chem. Phys. Lett. 175 (5) (1990) 488.

[11] P.S. May, H.U. Güdel, J. Chem. Phys. 95 (9) (1991) 6343.

[12] O.S. Wenger, S. Bénard, H.U. Güdel, Inorg. Chem. 41 (2002) 5968.

[13] J. Ferguson, H.J. Guggenheim, J. Chem. Phys. 44 (3) (1966) 1095.

[14] R.J. Tonucci, S.M. Jacobson, W.M. Yen, J. Lumin. 46 (1990) 155.

[15] U. Oetliker, M.J. Riley, H.U. Güdel, J. Lumin. 63 (1995) 63.

4 Photoionization in Ce^{3+} Doped Chlorides

On the Determination of Photoionization Thresholds of Ce^{3+} Doped Cs$_3$LuCl$_6$, Cs$_2$LiLuCl$_6$ and Cs$_2$LiYCl$_6$ by Thermoluminescence

Judith Grimm, Karl W. Krämer, Daniel Biner, and Hans U. Güdel*

Department of Chemistry and Biochemistry, University of Bern
Freiestrasse 3, 3012 Bern, Switzerland

Julian Fleniken and Uwe Happek

Department of Physics and Astronomy,
The University of Georgia
30605 Athens, GA, United States

We report on photoionization measurements of three Ce^{3+} doped chlorides: Cs$_3$LuCl$_6$, Cs$_2$LiLuCl$_6$ and Cs$_2$LiYCl$_6$. These chlorides are hygroscopic and must be kept hermetically sealed in quartz vials, complicating the use of standard techniques to determine electron transfer processes. Thus, a solely optical technique, based on thermoluminescence excitation spectroscopy, is applied to detect the photoionization energies of Ce^{3+} in the three compounds.

I. INTRODUCTION

When a rare earth or a transition metal ion is doped into an insulator material, localized energy levels are introduced in the bandgap of the host, leading to new absorption bands. Studies on the optical properties have mainly been concerned with transitions between the localized states of the impurity. Knowledge about transitions from the impurity to the host or vice versa is rather limited. To obtain a complete picture of the optical properties of a material one also has to establish the relationship between the impurity levels and the extended states of the crystal lattice. Understanding these interactions is important to understand the light emission properties of a material. Enhanced, reduced or even inhibited performance of phosphors and scintillators [1] or laser materials [2, 3] has been shown to be due to electron transfer processes.

Techniques to locate the impurity groundstate relative to the host valence (VB) and conduction band (CB) are photoconductivity [1, 2, 4], thermoluminescence (TL) [5, 6] and X-ray photoelectron spectroscopy (XPS) [3]. Since the materials of this study are hygroscopic, precautions on the experimental set-up are required and not all of the above mentioned techniques are readily applicable. Here, a TL technique is introduced that allows measurements on samples sealed in quartz envelopes: We use a form of excitation spectroscopy based on thermally activated luminescence, which is a solely optical technique and gives direct insight in the location of the CB relative to the Ce^{3+} groundstate in the samples of this study.

———

*Electronic address: `guedel@iac.unibe.ch`

II. EXPERIMENTAL SECTION

Single crystals of the Ce^{3+} doped chlorides were grown from the melt by the vertical Bridgman technique as described in Refs. 7–9. The nominal Ce^{3+} concentrations in the crystals of the present study are: Cs$_3$LuCl$_6$: 0.1% Ce^{3+}, Cs$_2$LiLuCl$_6$: 0.5% Ce^{3+} and Cs$_2$LiYCl$_6$: 0.02% Ce^{3+}. Due to their hygroscopic nature, the crystals were handled under inert atmosphere at all times. For the measurements they were sealed in small quartz vials, filled with He gas for thermal coupling.

In order to measure hygroscopic samples sealed in quartz vials, a copper sample holder with spring mounts was designed that accounts for the different thermal expansion coefficients of copper and quartz upon heating or cooling. The sample holder is mounted onto the coldfinger of a temperature variable cryostat. The sample is illuminated at low temperature (typically 140 K) at selected wavelengths between 200 and 350 nm with a 30 W D$_2$ lamp filtered by a 0.125 m monochromator and appropriate bandpass filters (10 nm) to avoid stray light. Illumination times are chosen such that the total amount of photons is constant for all illumination wavelengths. If the energy of the incident photons is sufficient to bridge the gap between the groundstate of Ce^{3+} and the bottom of the CB, electrons are released into the CB. A fraction of the delocalized electrons will be trapped in electron traps at low temperature (see Fig. 1(a)).

After illumination the sample temperature is rapidly raised from the base temperature up to 570 K. As the temperature is increased, the trapped electrons are released back into the CB due to thermal activation. From the CB the electrons can recombine with a Ce^{4+} ion, thus producing a Ce^{3+} ion, which in turn will relax to the groundstate under emission of its ion-specific $5d{\rightarrow}4f$ luminescence (see Fig. 1(b)). The TL signal is recorded as a function of temperature using a cooled EMI PMT equipped with a 400 nm bandpass filter (bandwidth 80 nm) to detect the Ce^{3+} $5d{\rightarrow}4f$ emission intensity, result-
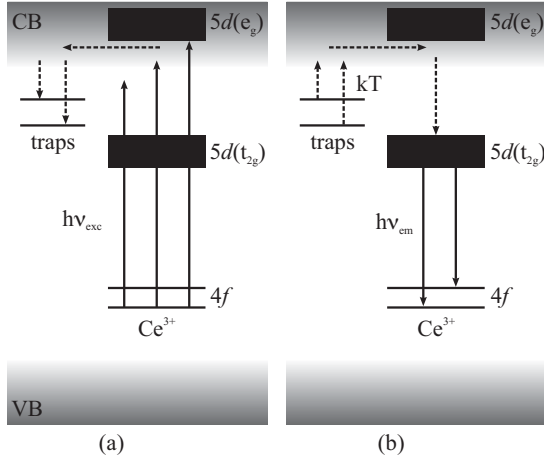
FIG. 1: Principle of thermoluminescence excitation spectroscopy: a) Trap filling process: The sample is irradiated at low temperature at a fixed photon energy. If the photon energy is sufficient to promote electrons to the CB, trap states are filled. b) Trap reading process: The occupation of the traps is monitored by thermally liberating the electrons and detecting the impurity specific luminescence when the electrons recombine with the probe ions.

ing in a so-called glowcurve. For a given excitation energy the integrated glowcurve signal is proportional to the ionization and trapping cross sections. Thus, a plot of the integrated signal as a function of the incident excitation energy will give information about the ionization energy.

III. RESULTS

In Fig. 2, a selection of glowcurves obtained in the thermoluminescence experiment is shown for all three samples for various excitation wavelengths. The peaks in the glowcurves are related to traps of different depths: shallow traps are emptied at low temperature, deeper traps at higher temperature. The peak pattern is characteristic for each sample, indicating that the trap structure is different in the three materials.

A constant glowcurve shape for varying excitation energy is an indication that there is no change in the process of trap filling. In addition to ionization of the impurity other possible electron/hole transfers can be observed in a thermoluminescence experiment: creation of holes in the valence band, electron transfer to defects near the impurity site without involving the extended states of the host and others [10]. If the process changes by varying the excitation wavelength, a change in the glowcurve is expected. For Cs_3LuCl_6 and Cs_2LiYCl_6 the peaks remain at the same position as a function of excitation wavelength. In the case of $Cs_2LiLuCl_6$ we observe changes in the shape of the glowcurves upon variation of

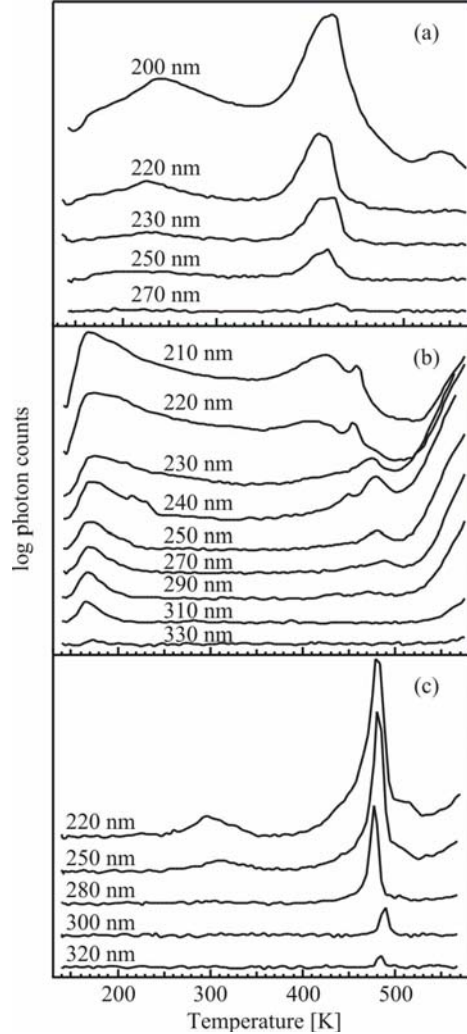FIG. 2: A selection of glowcurves excited at various wavelengths in a semilogarithmic plot for (a) Cs_3LuCl_6, (b) $Cs_2LiLuCl_6$ and (c) Cs_2LiYCl_6 doped with Ce^{3+}. The curves are scaled relative to each other and arbitrarily shifted along the vertical axis.

the excitation wavelength. Up to 230 nm (5.4 eV) the shape stays the same but then the relative peak strength changes, indicating an excitation energy dependence of the trapping probability as will be discussed later. At higher excitation energies the curves are consistent again.

The integrated glowcurve signals as a function of excitation energy for the three compounds are shown in Fig. 3. These are effectively excitation spectra for the promotion of a Ce^{3+} $4f$ electron into the CB.
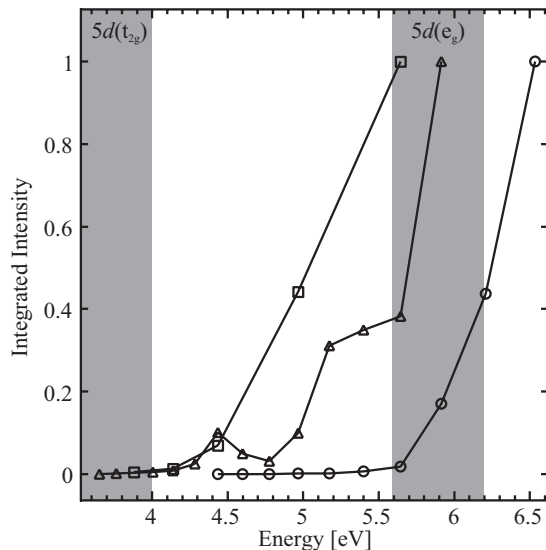
FIG. 3: Integrated spectra of Cs$_3$LuCl$_6$ (circles), Cs$_2$LiLuCl$_6$ (triangles) and Cs$_2$LiYCl$_6$ (squares) doped with Ce^{3+}. The signal is normalized to 1 at the highest excitation wavelength. The straight lines are a guide to the eye. The location of the 5d bands of Ce^{3+} in the three title compounds is indicated by light grey bars for comparison, see Refs. 7–9. Octahedral notation is used to label the 5d states despite the fact that they are Jahn-Teller susceptible and that small deviations from exact octahedral coordination occur in Cs$_3$LuCl$_6$ and Cs$_2$LiLuCl$_6$.

IV. DISCUSSION

In the excitation spectrum of Cs$_3$LuCl$_6$ (circles in Fig. 3) the signal onset is rather weak at low energy (4.4 eV). The signal rises gradually with increasing excitation energy up to 5.6 eV where after a huge signal increase is observed. A comparison with the electronic structure of Ce^{3+} reveals that the increase after 5.6 eV is correlated with the onset of the 5d(e$_g$) band. The position of the 5d bands which is roughly the same in all three samples is given schematically by the shaded areas in Fig. 3. It has been observed before that the ionization process is en-

hanced through the promotion of electrons into the 5d energy levels, followed by ionization of the Ce^{3+} ion [11]. A similar enhancement of the ionization signal is observed in the excitation spectrum of Cs$_2$LiLuCl$_6$ (Fig. 3): The signal rises gradually between 3.6 and 5.6 eV, but then it is more than doubled between 5.6 and 5.9 eV where the ionization is resonant with the Ce^{3+} 5d(e$_g$) band. As mentioned earlier, the glowcurves for the data points at 5.6 and 5.9 eV change shape (Fig. 2(b)). We interpret this as a change in the preferred filling of traps when the excitation energy becomes resonant with the 5d(e$_g$) band. For Cs$_2$LiYCl$_6$ we cannot make the distinction of ionization enhancement via the above discussed process due to insufficient data.

The signal below the 5d(e$_g$) energy levels (i.e. below 5.6 eV) is significant in all samples. We conclude that the ionization energy lies below the 5d(e$_g$) level in all samples. This is compatible with the work of Dorenbos and coworkers who also position the CB below the 5d(e$_g$) in the three samples under investigation (see Refs. 7–9). In our experiments the electronic excitation and thus the trap filling process occurred at 140 K, and we cannot exclude the possibility of phonon assisted ionization processes at this temperature. The gradual onset of the integrated signal in Fig. 3 at low energies is an indication in this direction. This prevents an exact quantitative determination of the ionization energies on the basis of the present data. We plan experiments at lower excitation temperatures.

To summarize, we have used thermoluminescence excitation spectroscopy to measure the photoionization of Ce^{3+} ions in hygroscopic samples hermetically sealed in quartz ampules. Our results show that the ionization energy in Cs$_3$LuCl$_6$, Cs$_2$LiLuCl$_6$ and Cs$_2$LiYCl$_6$ lies below the energy of the Ce^{3+} 5d(e$_g$) excited state.

[1] M. Raukas, S. A. Basun, W. van Schaik, W. M. Yen, and U. Happek, Appl. Phys. Lett. **69**, 3300 (1996).

[2] W. C. Wong, D. S. McClure, S. A. Basun, and M. R. Kokta, Phys. Rev. B **51**, 5682 (1995).

[3] C. W. Thiel, H. Cruegel, H. Wu, Y. Sun, G. J. Lapeyre, R. L. Cone, R. W. Equall, and R. M. Macfarlane, Phys. Rev. B **64**, 085107 (2001).

[4] D. S. McClure and C. Pedrini, Phys. Rev. B **32**, 8465 (1985).

[5] W. C. Wong, D. S. McClure, S. A. Basun, and M. R.

Kokta, Phys. Rev. B **51**, 5693 (1995).

[6] J. Fleniken, J. Wang, J. Grimm, M. J. Weber, and U. Happek, J. Lumin. **94-95**, 465 (2001).

[7] P. Dorenbos, E. V. D. van Loef, C. W. E. van Eijk, K. W. Krämer, and H.U.Güdel, Phys. Rev. B **68**, 125108 (2003).

[8] A. Bessière, P. Dorenbos, C. W. E. van Eijk, L. Pidol, K. W. Krämer, and H. U. Güdel, J. Phys. C **16**, 1887 (2004).

[9] A. Bessière, P. Dorenbos, C. W. E. van Eijk, K. W.

Krämer, H. U. Güdel, and A. Galtayries, J. Lumin. **117**, 187 (2006).

[10] R. Chen and S. W. S. McKeever, *Theory of Thermoluminescence and Related Phenomena* (World Scientific

Publishing Co. Pte. Ltd, Singapore, 1997).

[11] J. Fleniken, Ph.D. thesis, The University of Georgia, Athens, USA (2004).

5 Summary and Outlook

This thesis covers investigations on the spectroscopic properties of a variety of transition metal and rare earth doped systems. Excited states, luminescent properties, upconversion (UC) as well as photoionization processes have been the field of interest. In the following, a short summary of the research is presented as well as an outlook on further investigations on the respective projects.

5.1 Spectroscopy of Tm^{2+} Doped Halides

Chapter two provides a systematic investigation of Tm^{2+} doped halide compounds (CaF$_2$, CaCl$_2$, SrCl$_2$, BaCl$_2$, CsCaCl$_3$, CsCaBr$_3$ and CsCaI$_3$). Prior to this investigation only a handful of compounds had been studied. We found that Tm^{2+} can be successfully incorporated into crystals of the heavier halides without the presence of Tm^{3+} impurities. From the synthesis of many different compounds we conclude that it is not possible to stabilize Tm exclusively in its divalent oxidation state in fluorides. In terms of possible applications this is a serious drawback because hygroscopic materials (chlorides, bromides and iodides) are not as easy to handle as air-stable compounds (fluorides and oxides).

The investigation of the spectroscopic properties of these Tm^{2+} doped halides proved to be a challenging but very rewarding task. The spectra of Tm^{2+} in solids are composed of two types of electronic transitions: weak sharp-line $4f$-$4f$ transitions and strong broad $4f$-$5d$ transitions at higher energies. The former are easily understood because of their analogy to the transitions in the isoelectronic Yb^{3+}. Understanding of the $4f$-$5d$ transitions is more difficult because of the simultaneous action of the crystal field, Coulomb interactions and spin-orbit coupling. Investigations of these transitions started in the 1960's and much of today's understanding builds upon this work. For the interpretation of the Tm^{2+} $4f$-$5d$ spectra we developed a simple picture to explain the energy level structure. The energy level structure of the $(4f)^{12}(5d)^1$ can be understood by coupling the crystal field split $5d$ orbitals to the $(4f)^{12}$ core terms of Tm^{3+}. Further splitting of the multiplets into high-spin and low-spin sets is observed. With this picture we have been able to interpret the spectra of all compounds, at least to a certain extent. A complete assignment of all observed bands from the $(4f)^{12}(5d)^1$ electron configuration is not possible - contrary to our initial ambitions. The $(4f)^{12}(5d)^1$ electron configuration is 910-fold degenerate and the aforementioned interactions are but the most important that lead to a splitting of the $4f$-$5d$ excited states. In recent years there has been a renewed interest in the $4f$-$5d$ transitions of lanthanides. The investigation of these transitions in trivalent lanthanides has been mainly driven by the search for new phosphors for future solid state lighting devices. A systematic study of the high energy $4f$-$5d$ transitions of trivalent lanthanides was performed [1, 2]. This has prompted theoretical work on this type of transitions, not only for trivalent but also for divalent rare earth ions [3, 4, 5]. We started a collaboration with Prof. M. Reid from the University of Canterbury (New Zealand) which aims at the modeling of the $4f$-$5d$ excited states of Tm^{2+}. However, at the time of writing this thesis we are not able to present results yet.

The investigation of the luminescent properties of Tm^{2+} revealed the presence of unexpected and previously not observed emissions. All the compounds investigated during the course of this thesis exhibit sharp-line $4f$-$4f$ emission from the $^2F_{5/2}$ state as well as spin-forbidden emission from the lowest $4f$-$5d$ state. The observation of the latter emission in CaF_2:Tm^{2+} is a surprising novelty. Spin-allowed $4f$-$5d$ emission is observed in $CsCaBr_3$:Tm^{2+} and $CsCaI_3$:Tm^{2+}, which is attributed to the lower phonon energies in these materials compared to chlorides and fluorides. In Tm^{2+} doped $CsCaCl_3$, $CsCaBr_3$, $CsCaI_3$, $CaCl_2$ and $SrCl_2$, emission from a higher lying $4f$-$5d$ state is observed. The observation of spin-allowed and higher excited emission is without precedent for Tm^{2+} doped materials. Higher excited emission has not been reported in the entire literature on $4f$-$5d$ transitions in rare earth ions. As a general trend, the number of $4f$-$5d$ emission transitions increases towards the heavier halides which is mainly attributed to the lower phonon energies of these materials.

The observation of multiple emissions makes Tm^{2+} an ion suitable for UC. We were able to demonstrate UC involving exclusively the $4f$-$5d$ excited states. This is a completely new type of UC and the high efficiency in $CsCaI_3$:Tm^{2+} compared to $CsCaBr_3$:Tm^{2+} and $CsCaCl_3$:Tm^{2+} is a surprising result. $SrCl_2$:Tm^{2+} is a promising candidate for future investigations on this type of UC. We also tried to induce UC by first populating the $^2F_{5/2}$ multiplet and subsequent UC to the $4f$-$5d$ excited states as was demonstrated in $SrCl_2$:Tm^{2+} [6]. However, the experiments on $CsCaCl_3$:Tm^{2+}, $CsCaBr_3$:Tm^{2+} and $CsCaI_3$:Tm^{2+} yielded no measurable UC emission. For reasons that are not entirely clear we may simply have not been able to create a high enough population in the $^2F_{5/2}$ excited state to induce UC. This shows that there are limitations to induce UC from the first excited $4f$-$4f$ state to higher lying $4f$-$5d$ states.

A class of materials that are less hygroscopic than the heavier halides and where Tm^{2+} can potentially be stabilized are mixed halides. The existence of TmFCl, TmFBr and TmFI is reported in the literature [7]. These materials crystallize in the tetragonal PbFCl structure (space group P4/nmm) where the divalent cation is located on site $2c$ with symmetry C_{4v}. This could be an attractive class of materials for further investigation. It would be interesting to find out what types of $5d$-$4f$ emission can be observed from mixed halide type compounds.

Laser action was demonstrated on the $4f$-$4f$ transition in CaF_2:Tm^{2+} 40 years ago [8]. The energy of this transition (between 8800 cm^{-1} and 9000 cm^{-1}) is in a range where few laser sources are available. Additionally, Tm^{2+} doped materials are also considered as potential tunable solid state laser materials because of the broad $4f$-$5d$ transitions [9]. Excited state absorption measurements are needed to assess the laser potential of the Tm^{2+} doped systems.

The Tm^{2+} doped compounds are ideal for photoionization studies. During a stay at the lab of Prof. U. Happek, first photoionization studies were undertaken for $SrCl_2$:Tm^{2+}. However the data is not sufficient to make a clear assignment of the photoionization threshold. The investigation of the isostructural perovskite series is interesting because it is expected that the photoionization threshold decreases along the series. Divalent lanthanides have the advantage that the photoionization experiments can be done using visible radiation. Therefore experiments are easier to perform as compared to trivalent ions where often the use of vacuum UV set-ups is the only way to measure photoionization.
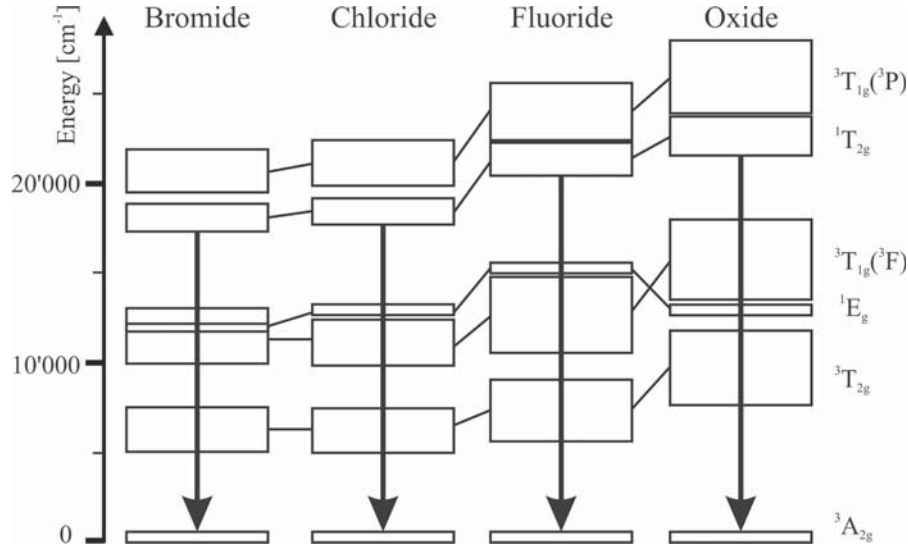
Figure 1: *General trend of the shift of the Ni^{2+} excited state energies upon doping in different crystalline environments. From bromides to oxides, the crystal field as well as the Racah parameters are enhanced. As a consequence, a blueshift of the excited states is observed. The blueshift from bromides to oxides is made clear by the increasing length of the $^1T_{2g} \rightarrow ^3A_{2g}$ emission arrow. The phonon energies are also increased, which makes multiphonon relaxation increasingly more likely along the series.*

5.2 Upconversion in a Ni^{2+} Doped Fluoride

In chapter three the UC properties of Ni^{2+} in a fluoride host lattice are presented. Most of the previous Ni^{2+} UC studies had been performed on chlorides and bromides. The observation of UC from a transition metal incorporated in halides, and especially in a fluoride, is amazing. Generally it is expected that multiphonon relaxation will be the dominant relaxation process between the higher excited states. In KZnF$_3$:Ni^{2+} the energy level structure makes emission from the higher excited $^1T_{2g}$ to the $^3A_{2g}$ groundstate possible. The $^1T_{2g} \rightarrow ^3A_{2g}$ emission is at higher energies than in chlorides and bromides (see Fig. 1) and persists up to room temperature. The crystal field and the Racah parameters are increased in fluorides compared to heavier halides and cause a blueshift of the absorption and emission bands. The trend is continued towards oxides, see Ref. [10] and Fig. 1. From energy considerations it is thus attractive to dope Ni^{2+} into fluorides and oxides. Additionally, these materials have the advantage that they are not air-sensitive. The investigation could have been extended to other fluoride host lattices and also to oxides. However, the existing literature on Ni^{2+} doped fluorides and oxides is very broad and extensive. These materials were already intensively studied 20-30 years ago.

Wenger et al. demonstrated that Ni^{2+}-Cl$^-$-Mn^{2+} superexchange interactions lead to enhancement of the Ni^{2+} $^3A_{2g} \rightarrow ^1E_g$ spin-flip transition. As a consequence the UC luminescence was increased by more than an order of magnitude in RbMnCl$_3$ compared to CsCdCl$_3$:Ni^{2+} [11]. Additionally, it was observed that in CsMnCl$_3$:Ni^{2+} the excitation energy was transferred from Ni^{2+} to Mn^{2+}. Upon excitation into the ^1E_g state of Ni^{2+}, the

Mn^{2+} $^4T_{1g} \rightarrow ^6A_{1g}$ emission was observed which resulted in a very efficient UC process [11]. From energy considerations it is expected that a Ni^{2+}-F^--Mn^{2+} superexchange could also be possible in the $KZnF_3$:Ni^{2+} system upon codoping it with Mn^{2+}. Some preliminary investigations were therefore performed on a $KZnF_3$:Ni^{2+},Mn^{2+} crystal. However we did not find any enhancement of the ^1E_g transition. The conclusion is that the effect in the codoped fluoride is either absent or too weak to be detected. Perhaps a $RbMnF_3$ crystal doped with Ni^{2+} would be a suitable material to induce superexchange interactions.

The investigation of higher emissions from transition metal doped halides is a rather new research field, and of interest both from a fundamental and an applied perspective. With regard to possible applications the $KZnF_3$:Ni^{2+} is an interesting material because it is stable in air. A green Ni^{2+} laser could possibly be built on the $^1T_{2g} \rightarrow ^3A_{2g}$ transition in $KZnF_3$:Ni^{2+}, see Fig. 1 [12].

5.3 Determination of the Photoionization Threshold in Ce^{3+} Doped Chlorides

In chapter four the photoionization studies of Ce^{3+} doped Cs_3LuCl_6, $Cs_2LiLuCl_6$ and Cs_2LiYCl_6 are discussed. The aim of these studies is to get information about the location of the rare earth ion states relative to the conduction (CB) and valence band (VB) of the host material. By measuring the photoionization threshold, the location of the rare earth states relative to the CB is determined. In all chloride samples we were able to measure photoionization by applying the thermoluminescence technique. It was not a priori clear that it would be possible to measure thermally stimulated luminescence (TSL) from these samples as the hygroscopic nature of the chlorides requires additional precautions on the experimental set-up. Except for one report in the literature [13], all photoionization studies were performed on samples that can be handled in air. TSL was chosen as experimental technique because it is very versatile. Our investigations prove that TSL is a suitable technique to study hygroscopic samples. This opens the field to a whole new class of compounds that were hardly ever considered for photoionization studies so far.

The results on Ce^{3+} doped Cs_3LuCl_6, $Cs_2LiLuCl_6$ and Cs_2LiYCl_6 suggest that further and more detailed work is needed to clarify the issue of the location of the CB of the host material relative to the groundstate of the Ce^{3+} ion. TSL experiments are planned in the Happek group, including cooling the samples to lower temperatures during the irradiation process. That will significantly reduce thermally assisted photoionization processes. Further, it is desirable to perform several different measurements on the same sample, such as thermoluminescence, photoconductivity, X-ray photoelectron spectroscopy (XPS) and others. XPS measurements were performed by Bessière and coworkers on $Cs_2LiLuCl_6$:0.5% Ce^{3+} [14]. However, their results are contradictive to both, the model that was derived from the luminescence study (see Ref. [14]) as well as our TSL measurements. We also attempted to do photoconductivity measurements on Ce^{3+} doped Cs_3LuCl_6, $Cs_2LiLuCl_6$ and Cs_2LiYCl_6 crystals. For photoconductivity measurements the crystals need to be polished to thin disks with a diameter of more than 0.5 cm. This is not an easy task considering the softness and brittleness of these crystals. First measurements

performed by Dr. E. van der Kolk from the Technische Universiteit Delft (The Netherlands) on Cs_2LiYCl_6:0.02% Ce^{3+} did not yield any interpretable results, most likely due to the low Ce^{3+} concentration in the sample.

In conclusion, to answer the question of where the states of a rare earth ion are located relative to the CB and VB is not easy. Further input is needed, also from a theoretical point of view.

References

[1] L. van Pieterson, M. F. Reid, R. T. Wegh, S. Soverna, A. Meijerink, Phys. Rev. B 65 (2002) 045113.

[2] L. van Pieterson, M. F. Reid, G. W. Burdick, A. Meijerink, Phys. Rev. B 65 (2002) 045114.

[3] L. van Pieterson, R. T. Wegh, A. Meijerink, M. F. Reid, J. Chem. Phys. 115 (2001) 9382.

[4] P. Dorenbos, J. Phys. Cond. Matt. 15 (2003) 575.

[5] C. K. Duan, M. F. Reid, J. Solid State Chem. 171 (2003) 299.

[6] O. S. Wenger, C. Wickleder, K. W. Krämer, H. U. Güdel, J. Lumin. 94-95 (2001) 101.

[7] H. P. Beck, J. Solid State Chem. 23 (1978) 213.

[8] R. C. Duncan, Z. J. Kiss, Appl. Phys. Lett. 3 (1963) 23.

[9] S. Kück, Appl. Phys. B 72 (2001) 515.

[10] W. E. Vehse, K. H. Lee, S. J. Yun, W. A. Sibley, J. Lumin. 10 (1975) 149.

[11] O. S. Wenger, H. U. Güdel, Inorg. Chem. 40 (2001) 157.

[12] M. Pollnau, private communication.

[13] B. R. Soller, M. Voda, D. S. McClure, J. Lumin. 24/25 (1981) 201.

[14] A. Bessière, P. Dorenbos, C. W. E. van Eijk, K. W. Krämer, H. U. Güdel, A. Galtayries, J. Lumin. 117 (2006) 187.

Publication List

1. Judith Grimm, Oliver S. Wenger and Hans U. Güdel

   Broadband Green Upconversion Luminescence of Ni^{2+} in KZnF$_3$

   Journal of Luminescence, 102-103 (2003) 380-385.

2. Judith Grimm and Hans U. Güdel

   Five Different Types of Spontaneous Emission Simultaneously Observed in Tm^{2+} Doped CsCaBr$_3$

   Chemical Physics Letters, 404 (2005) 40-43.

3. J. Freek Suyver, Annina Aebischer, Daniel A. Biner, Pascal Gerner, Judith Grimm, Stephan Heer, Karl W. Krämer, Christine Reinhard and Hans U. Güdel

   Novel Materials Doped with Trivalent Lanthanides and Transition Metal Ions Showing Near-Infrared to Visible Photon Upconversion

   Optical Materials, 27 (2005) 1111-1130.

4. J. Freek Suyver, Judith Grimm, Karl W. Krämer and Hans U. Güdel

   Highly Efficient Near-Infrared to Visible Up-conversion Process in NaYF$_4$:Er^{3+}, Yb^{3+}

   Journal of Luminescence, 114 (2005) 53-59.

5. J. Freek Suyver, Judith Grimm, Marieke K. van Veen, Daniel A. Biner, Karl W. Krämer and Hans U. Güdel

   Upconversion Spectroscopy and Properties of NaYF$_4$ Doped with Er^{3+},Tm^{3+} and/or Yb^{3+}

   Journal of Luminescence, 117 (2006) 1-12.

6. Judith Grimm, Julian Fleniken, Karl W. Krämer, Daniel Biner, Uwe Happek and Hans U. Güdel

   On the Determination of Photoionization Thresholds of Ce^{3+} Doped Cs$_3$LuCl$_6$, Cs$_2$LiLuCl$_6$ and Cs$_2$LiYCl$_6$ by Thermoluminescence

   Journal of Luminescence, accepted.

7. Judith Grimm, J. Freek Suyver, Eva Beurer, Graham Carver and Hans U. Güdel

   Light Emission and Excited State Dynamics in Tm^{2+} Doped $CsCaCl_3$, $CsCaBr_3$ and $CsCaI_3$

   Journal of Physical Chemistry B, accepted.

8. Eva Beurer, Judith Grimm, Pascal Gerner and Hans U. Güdel

   New Type of Near Infrared to Visible Photon Upconversion in Tm^{2+} Doped $CsCaI_3$

   Journal of the American Chemical Society, submitted.

9. Judith Grimm, Eva Beurer and Hans U. Güdel

   Crystal Absorption Spectra in the Region of $4f\text{-}4f$ and $4f\text{-}5d$ Excitations in Tm^{2+} Doped $CsCaCl_3$, $CsCaBr_3$ and $CsCaI_3$

   Inorganic Chemistry, submitted.

Attended Conferences and Schools

1. **International Conference on Luminescence (ICL'02)**; August 24–29, 2002; Budapest (Hungary).

   Oral Presentation: *Broadband Green Upconversion of Ni^{2+} Doped Fluorides.*

2. **Séminaire Hors-Ville (3ème Cycle) en Chimie Physique: Excitation Migration and Transfer in Organized Media**; September 15–20, 2002; Champéry VS (Switzerland).

   Poster Presentation: *Broadband Green Upconversion of Ni^{2+} in $KZnF_3$.*

3. **Hole Burning, Single Molecule and Related Spectroscopies Conference (HBSM)**; July 27–31, 2003; Bozeman, MT (USA).

   Poster Presentation: *Synthesis, Spectroscopy and Near-Infrared to Visible Upconversion of Tm^{2+} Doped Halide Crystals.*

4. **Fourth Stokes Summer School**; June 18–22, 2004; Skreen (Ireland).

   Oral Presentation: *Determination of Photoionization Thresholds in Ce^{3+} Doped Chlorides.*

5. **Güdel-Meijerink Group Meeting**; August 25–26, 2004; Simplon VS (Switzerland).

   Oral Presentation: *Luminescent Properties of Tm^{2+} in $CsCaCl_3$ and $CsCaBr_3$.*

6. **NRP 47 Spring School on Supramolecular Chemistry**; April 11–15, 2005; Murten FR (Switzerland).

   Poster Presentation: *New Light Emitting Materials: Tm^{2+} Doped Crystals of $CsCaCl_3$ and $CsCaBr_3$.*

7. **International Conference on Luminescence (ICL'05)**; July 25–19, 2005; Beijing (China).

   Oral Presentation: *On the Determination of the Photoionization Thresholds of Ce^{3+} Doped Cs_3LuCl_6, $Cs_2LiLuCl_6$ and Cs_2LiYCl_6 by Thermoluminescence.*

8. **Séminaire Hors-Ville (3ème Cycle) en Chimie Physique: Advanced Materials**; September 18–22, 2005; Villars-sur Ollon VS (Switzerland).

Research Stays and Supervision

1. **Research Stay: Determination of the Photoionization Threshold in Ce^{3+} Doped Chlorides**

   July–September 2003; Prof. U. Happek, Department of Physics and Astronomy, The University of Georgia, Athens, GA (United States).

2. **Research Stay: Determination of the High-Energy Levels of Rare Earth Doped $NaYF_4$**

   February 23–26, 2004; in collaboration with Dr. P. Dorenbos and Dr. E. van der Kolk (Technische Universiteit Delft, The Netherlands), Synchrotronstrahlungslabor HASYLAB at the Deutsche Elektronen-Synchrotron DESY, Hamburg (Germany).

3. **Supervision of a Diploma Thesis: "Synthesis and Optical Light Absorption and Emission Properties of Tm^{2+} Doped $CsCaI_3$ and $RbCaI_3$ Crystals" by Eva Beurer**

   April–November 2005; Department of Chemistry and Biochemistry, University of Bern (Switzerland).

Acknowledgments

At the end of my dissertation it is a pleasure to mention the people who have contributed in different ways to my thesis. This thesis would not have been possible without the support of many who shared their time and knowledge.

First, I would like to thank Prof. Hansueli Güdel for the opportunity to do a Ph.D. thesis in his group. I have greatly benefited from his vast knowledge in luminescent research and he has taught me a lot about science and the value of scientific concepts. The past four years have greatly widened my horizon, not just science-wise, which I consider to be very valuable for my future.

Furthermore, I would like to thank Prof. Cees Ronda for accepting to be the co-referee of my thesis. His insights and interests have had a positive influence these past years. Prof. Silvio Decurtins is gratefully acknowledged for being the co-examiner of this thesis.

Prof. Uwe Happek is acknowledged for giving me the opportunity to spend three months at his lab at the University of Georgia, Athens (United States). His creative way of doing research will always be inspiring to me. I would like to thank him and Dr. Jay Fleniken for introducing me to the secrets of the thermoluminescence technique. The entire Happek group is acknowledged for the pleasant atmosphere. I enjoyed coming back to the good old south and besides research it was great to meet many friends from before.

I would like to thank Dr. Freek Suyver for his many ideas, in particular on the simulation of the temperature dependence of the Tm^{2+} emissions. He helped me to overcome many hurdles and the continued support after he left the group was very valuable to me. Further, I would like to thank him for proofreading my thesis. It has been of great value for me to spend my thesis time together with Annina Aebischer. I would like to thank her for the many scientific and non-scientific discussions and support as well as our joint music sessions. I still hope that we will be able to play the Bach sonatas sometime. Furthermore, I would like to thank her for proofreading my thesis. Dr. Pascal Gerner is acknowledged for his support on many occasions and for the effort that he put into the Tm^{2+} upconversion project during his post-doc. I would like to thank Dr. Karl Krämer and Daniel Biner for their technical support concerning synthesis and crystal growth as well as for the help in the optics lab (K. Krämer). Eva Beurer is acknowledged for being an active and interested diploma student on the Tm^{2+} project. I would like to thank Dr. Christine Reinhard for her support and scientific discussions on many topics. Dr. Oliver Wenger is acknowledged for sharing many of his ideas at the beginning of this thesis.

Curriculum Vitae

Personal

Surname: Grimm

First Name: Judith

Nationality: Swiss

Date of Birth: September, 4th 1976

Place of Origin: Langnau i. E. BE, Switzerland

Civil Status: Single

Education

1983 – 1987   Primary School in Hasle b. B., Switzerland.

1987 – 1992   Secondary School in Hasle-Rüegsau, Switzerland.

1992 – 1996   High School (Typus D), Gymnasium Burgdorf, Switzerland.

1996 – 2000   Studies in Chemistry at the University of Bern, Switzerland.

1999   Research Stay at the Katholieke Universiteit Leuven, Belgium as part of the European Erasmus Exchange Program.
                    Supervisors: Prof. C. Görller-Walrand and Dr. K. Binnemans

2000   Diploma Thesis in Environmental Chemistry at the University of Bern, Switzerland.
                    Supervisor: Prof. U. Krähenbühl

2001   Research Assistant at the Department of Physics and Astronomy, The University of Georgia, Athens, GA, United States.
                    Supervisor: Prof. U. Happek

                    Internship at GE Global Research, Niskayuna, NY, United States.
                    Supervisor: Dr. A. M. Srivastava

2002 – 2006   Ph.D. Thesis in Inorganic Chemistry at the University of Bern, Switzerland.
                    Supervisor: Prof. H. U. Güdel